UNIVERSITY OF CALIFORNIA

Santa Barbara

Rainfall Variability and Change in Central and Southern Peruvian Andes

A dissertation submitted in partial satisfaction of the

requirements for the degree Doctor of Philosophy

in Geography

by

Haline Heidinger Abadía

Committee in charge:

Professor Leila Carvalho, Chair

Professor Charles Jones

Dr. Christopher Funk, Researcher

Dr. Roberto Quiroz, International Potato Center

September 2017

The dissertation of Haline Heidinger Abadía is approved.

_____

Charles Jones

_____

Christopher Funk

_____

Roberto Quiroz

_____

Leila Carvalho, Committee Chair

July 2017

Rainfall Variability and Change in Central and Southern Peruvian Andes

ACKNOWLEDGEMENTS

I acknowledge the Consultative Group for International Agricultural Research (CGIAR) Research Program on Climate Change, Agriculture and Food Security (CCAFS) for funding this research.

I acknowledge the *Consejo Nacional de Ciencia, Tecnología e Innovación Tecnológica* (CONCYTEC) for partially funding my doctoral studies at UCSB.

I acknowledge my family and friends for their invaluable support.

DEDICATION

I dedicate this manuscript to my parents.

VITA OF HALINE HEIDINGER ABADIA

July 2017

EDUCATION

PhD Geography, 2017 (expected)
University of California, Santa Barbara, USA

MSc Applied Ecology, 2009
Universidad Nacional Agraria La Molina, Lima, Peru

BSc Environmental Engineering, 2005
Universidad Nacional Agraria La Molina, Lima, Peru

PROFESSIONAL EMPLOYMENT

Teaching Assistant, 2016 – 2017
Department of Geography, University of California, Santa Barbara, USA

Research Assistant, 2012 – 2016
Earth Research Institute, University of California, Santa Barbara, USA

Research Assistant, 2007 – 2012
International Potato Center, Lima, Peru

Undergraduate and graduate Student, 2005 – 2007
International Potato Center, Lima, Peru

PUBLICATIONS

Heidinger. H., Carvalho, L., Jones, C., Posadas, A., and Quiroz, R. 2017. A new assessment in total and extreme rainfall trends over Central and Southern Peruvian Andes during 1965-2010. Manuscript submitted to *International Journal of Climatology* (in revision).

Heidinger. H., Jones, C., Carvalho, L., Posadas, A., and Quiroz, R. 2017. Evaluation of MJO-ENSO influence on rainfall over Central and Southern Peruvian Andes during 1979-2010 wet seasons. In preparation.

Posadas, A. Duffaut Espinosa, L. A., Yarlequé, C., Carbajal, M., Heidinger, H., Carvalho, L., Jones, C., and Quiroz, R. 2015. Spatial random downscaling of rainfall signals in Andean heterogeneous terrain. *Nonlinear Processes in Geophysics, 22(4), 383.402*.

Heidinger, H., Yarlequé, C., Posadas, A., and Quiroz, R. (2012). TRMM rainfall correction over the Andean Plateau using wavelet multi-resolution analysis. *International Journal of Remote Sensing*, *33*(14), 4583-4602.

ABSTRACT

Rainfall Variability and Change in Central and Southern Peruvian Andes

by

Haline Heidinger Abadía

Understanding the spatiotemporal variability of rainfall over mountainous regions such as the Andes is crucial for the maintenance of water resources and ecosystems. Rainfall variability and change in the Central and Southern Peruvian Andes (CSPA) and their relationship with large-scale atmospheric dynamics is not fully understood. This study examines observed intraseasonal-to-interannual variability and long-term rainfall changes in CSPA.

Chapter 1 describes the motivation, research questions, hypotheses and objectives of this study.

Chapter 2 explains observed regional rainfall features over CSPA during 1965-2010. A regionalization of stations was performed using principal component and clustering analyses of forty-seven daily gauged time-series. Four major homogeneous regions are identified: Amazon, Central Pacific, Southern Pacific and Titicaca. The total and extreme rainfall indices proposed by the Expert Team on Climate Change Detection and Indices (ETCCDI) were calculated for each station. Rainfall indices and geographic features are similar among stations of the same region. Furthermore, this chapter investigates the effect of El Niño Southern Oscillation (ENSO) and the Pacific Decadal Oscillation (PDO) on rainfall indices. ENSO and PDO influences on rainfall are regionally dependent. Most stations in CSPA exhibit positive

(negative) anomaly in total and extreme rainfall indices (consecutive dry days) during La Niña (El Niño) years of 1965-2010. Nevertheless, these rainfall patterns are decade-dependent. Positive (negative) PDO is associated with positive (negative) anomalies of annual total rainfall in Titicaca basin, and with positive (negative) anomalies of consecutive dry days in Amazon, Southern Pacific and Titicaca basins.

Chapter 3 provides a comprehensive analysis of the signal, statistical significance and spatial pattern of rainfall trends from 1965 to 2010 in CSPA. Trends were examined with Mann-Kendall test and Sen's slope estimator applied to yearly rainfall indices following the hydrologic calendar. Significant regional patterns of changes in rainfall extremes were investigated and compared with previous studies. The drying signal within the southern Peruvian Andes is more complex than pointed out in previous studies. Here, statistically significant trends observed in about 30% of stations in each CSPA region is described. The annual total rainfall has decreased in the Amazon basin, despite the increase in the number of rainy days and some extreme rainfall indices. Decrease in one-day and five-day yearly maximum rainfall is observed in Central Pacific, along with an increase in the number of wet days. Positive trends in indices related to the intensity of very strong daily rainfall are evident in Southern Pacific. Titicaca basin shows an increase in the intensity of rainfall extremes. The ENSO-PDO low-frequency conditions seem to influence the complex and mostly non-statistically significant long-term trends in CSPA.

Chapter 4 examines the Madden-Julian Oscillation (MJO) and ENSO combined influence on rainfall during November-March 1979-2010 in CSPA. Positive standardized rainfall anomalies and a higher frequency of extreme rainfall events occurs during active MJO than during inactive MJO phases. This pattern is enhanced (suppressed) during La Niña (El

Niño). MJO-ENSO modulation of rainfall varies according to the location of the stations. During ENSO-neutral conditions, enhanced rainfall in the upper Amazon and Central Pacific basins is evident during MJO phases 4 and 5, whereas MJO phase 2 (phases 6, 7 and 8) enhances rainfall in Southern Pacific (Titicaca) basin. During La Niña, enhanced rainfall occurs during MJO phases 5, 6 and 8 in the Amazon and Central Pacific basins, whereas MJO phases 1, 3 and 6 (phases 2, 4, 7 and 8) enhance rainfall in Southern Pacific (Titicaca) basin. During El Niño, suppressed rainfall occurs during MJO phases 1, 2, 5 and 8 in the Amazon basin, during MJO phase 4 in the Central Pacific basin, during MJO phase 8 in the Southern Pacific basin, and during MJO phases 1, 3 and 5 in the Titicaca basin. Certain MJO-ENSO conditions related with positive and negative anomalies of rainfall show different spatially-coherent statistically significant moisture flux anomalies in each CSPA region.

Chapter 5 presents the final conclusions of this study and proposes some recommendations for future research.

TABLE OF CONTENTS

LIST OF FIGURES

Figure 2.9. Mean (dash) and standard deviation (error bar) of (a) latitude and longitude, (b) altitude, (c) slope and, (d) aspect from all stations in each major Central and Southern Peruvian Andes region. The major regions are: A (Amazon Basin), B (Central Pacific Basin), C (Southern Pacific Basin), and D (Titicaca Basin). Note: The aspect corresponds to a surface facing North (0° - 22.5°), Northeast (22.5° - 67.5°), East (67.5° - 112.5°), Southeast (112.5° - 157.5°), South (157.5° - 202.5°), Southwest (202.5° - 247.5°), West (247.5° - 292.5°), Northwest (292.5° - 337.5°), and North (337.5° - 360°).

Figure 2.10. As in Figure 2.9, but for the fourteen Central and Southern Peruvian Andes subregions.

Figure 2.11. Mean (dash) and standard deviation (error bar) of (a) wet-days annual rainfall (PRCPTOT), (b) percentage of wet days (Wdays), (c) consecutive dry days (CDD), and (d) very wet day rainfall (R95p) of the fourteen Central and Southern Peruvian Andes subregions.

Figure 2.12. Mean (cross) and standard deviation (error bar) of (a) wet-days annual rainfall (PRCPTOT), (b) percentage of wet days (Wdays), (c) consecutive dry days (CDD), and (d) very wet day rainfall (R95p) anomalies of the four Central and Southern Peruvian Andes regions (A, B, C and D) during El Niño (EN) and La Niña (LN) events of 1965-2009. Regions (letters) accompanied by an asterisk (*) represent statistically significant difference in the means of rainfall indices during EN compared to LN years, based on a *z* test with 95% level of confidence and independent number of events.

Figure 2.13. As in Figure 2.12, but for positive (PDO +) and negative (PDO -) PDO phases.

Figure 2.14. Standardized anomalies of wet-days annual rainfall (PRCPTOT) and very wet day rainfall (R95p) of each region of Central and Southern Peruvian Andes stations: (a) A (Amazon basin), (b) B (Central Pacific basin), (c) C (Southern Pacific basin), and (d) D (Titicaca basin). The Pacific Decal Oscillation (PDO) index is shown in gray.

LIST OF TABLES

Table 3.3. Stations with statistically significant trends in total and extreme rainfall indices over Central and Southern Peruvian Andes during 1965-2009 hydrologic years. Rainfall indices are denoted as: wet-days annual rainfall (PRCPTOT), simple daily rainfall intensity (SDII), consecutive dry days (CDD), consecutive wet days (CWD), number of heavy rainfall days (R10) and number of very heavy rainfall days (R20).

Table 3.4. As Table 3.3, but for very wet day rainfall (R95p), extremely wet day rainfall (R99p), maximum 1-day rainfall (RX1day), maximum 5-day rainfall (RX5day), very wet day proportion (R95pTOT), extremely wet day proportion (R99pTOT), percentage of wet days (Wdays), twenty-fifth percentile of daily rainfall (p25th) and seventy-fifth percentile of daily rainfall (p75th).

Table 3.5. Comparison between sign and statistical significance of trends obtained for some rainfall indices at common stations analyzed in Haylock *et al*. (2006), Skansi *et al*. (2013) and the present study over Central and Southern Peruvian Andes. The rainfall indices compared are: wet-days annual rainfall (PRCPTOT), consecutive dry days (CDD), very wet day rainfall (R95p), extremely wet day rainfall (R99p), maximum 1-day rainfall (RX1day) and maximum 5-day rainfall (RX5day). The sign and the statistical significance of trends are expressed as: NSNEG (non-statistically significant negative), SNEG (statistically significant negative), NSPOS (non-statistically significant positive), and SPOS (statistically significant positive).

Table 4.1. Percentage of MJO days from the entire period analyzed (Nov-Mar 1979-2010, 4689 days) and percentage of El Niño (EN), La Niña (LN) and ENSO-neutral (NT) days for each MJO phase. MJO activity refers to inactive (INA) and active (MJO) MJO conditions.

Table 4.2. Prevailing directions of statistically significant moisture flux anomalies during MJO active phases (1 to 8) and different ENSO conditions (EN, LN and NT) of the period Nov-Mar 1979-2010 over each Central and Southern Peruvian Andes (CSPA) region. CSPA regions are A (Amazon basin), B (Central Pacific basin), C (Southern Pacific basin) and D (Titicaca basin). The directions of anomalies are northerly (↓), easterly (←), southerly (↑), westerly (→), northeasterly (↙), northwesterly (↘) and southeasterly (↖).

Table 4.3. As Table 4.2, but over two contrasting locations in South America: western Amazon and east of the Andes.

Table 4.4. Summary of suppressed rainfall (SupR), enhanced rainfall (EnhR), enhanced frequencies of extreme rainfall events (FrqEx) and direction of statistically significant moisture flux anomalies (Mflux) during different MJO-ENSO conditions for each CSPA region. SupR, EnhR and FrqEx show an 'X' ('-') when more (less) than 55% of stations per each region reported suppressed rainfall, enhanced rainfall and enhanced rainfall extremes, respectively. Mflux shows the direction of spatially coherent moisture flux anomalies: northerly (↓), easterly (←), southerly (↑), westerly (→), northeasterly (↙), northwesterly (↘) and southeasterly (↖). 'X' is colored in red (blue) to highlight the MJO-ENSO conditions when rainfall is suppressed (enhanced) and a spatially coherent moisture flux in the region is present.

CHAPTER I: Introduction

The Andes Cordillera divides Peru in three broad regions: The Pacific Coast to the west, the Highlands or Sierra in the middle and the Amazon forest to the east. The Andes orographic rainfall is considered the most important source of fresh water that sustains the population, and maintains hydropower and agriculture (ANA 2015). Most of the Peruvian population lives in the semiarid Pacific Coast, around Lake Titicaca, and in the Andean zones of the Amazon basin, where the availability of freshwater resources is scarce (Lavado *et al.*, 2012). The combination of a unique physiography, lithology, land use, steep slope and distinctive pattern of orographic rainfall result in great susceptibility of the Andean population to floods, landslides and droughts (MINAM 2011). Despite the importance of understanding rainfall variability and change in this mountainous region, there are few published scientific researches about these topics most likely due to the limited access to observational datasets. These antecedents motivated this study to further explore variability and changes of total and extreme rainfall over the Peruvian Andes based on gauged rainfall datasets recently made available by the Peruvian National Water Authority (*Autoridad Nacional del Agua* or ANA).

This study focused on Central and Southern Peruvian Andes (CSPA) which extends from 9°-18°S and 68°- 78°W, and has elevations greater than 1500 m.a.s.l. CSPA covers three major basins delimited by ANA: Pacific, Amazon and Titicaca. The Pacific basin demands 58% of the water for agriculture, 33% for energy generation and 8% for household purposes, while the Amazon basin demands 73% of water for energy production, 18% for agriculture and 2% for household purposes. The water demand for agriculture is even larger in the Titicaca basin (95%), where only 4% of the demand is for household purposes (ANA 2015). Thus,

agriculture is by far the most important activity requiring water in the Pacific and the Titicaca basins, the two basins that reported water scarcity problems in CSPA.

CSPA is located in the tropics and rainfall variability is influenced by large-scale coupled modes on intraseasonal-to-decadal scales (e.g. ENSO, PDO and MJO). Locally, rainfall variability depends on the complex terrain, which significantly modify dynamical and thermodynamical conditions at local scales. This study investigates how common regional patterns of observed rainfall variability and long-term trends in total and extreme rainfall arise based common characteristics of basins or subregions within these basins. To improve our understanding about rainfall variability and trends in the CSPA, this study investigates the following fundamental questions: *Are there regions with similar rainfall regimes and geographic characteristics in the CSPA? What are the main mechanisms modulating rainfall on intraseasonal-to-interannual time-scales in the CSPA? Are there long-term trends in total and extreme rainfall in the CSPA? Are the intraseasonal-to interannual rainfall variability and rainfall trends regionally dependent?* To answer these general questions, the most complete gauged rainfall dataset was gathered for CSPA and the most appropriate methods were chosen to evaluate rainfall variability and trends, which is the general objective of this study. The specific objectives of this study are: (1) to describe regional patterns of total and extreme rainfall indices during different conditions of ENSO and PDO, (2) to assess long-term trends in total and extreme rainfall indices, and (3) to evaluate the effects of MJO-ENSO in rainfall anomalies and extremes and potentially explain them based on moisture flux dynamics. Each of these objectives were thoroughly examined and addressed in Chapters II, III and IV of this dissertation, respectively.

CHAPTER II: Regional Geographic and Rainfall Characteristics

A. Background

The spatiotemporal variability of rainfall in the Central and Southern Peruvian Andes results from the interactions of complex processes occurring on a broad range of temporal scales. For instance, the diurnal cycle of convective activity is characterized by enhanced convection during the afternoon at high elevations in CSPA (Giovannettone and Barros, 2009; Romatschke and Houze, 2010, 2013), whereas heavy rainfall occurs mainly at night over the Vilcanota cordillera, which is located in the southeastern Peruvian Andes (Perry *et al.*, 2014).

Most of the rainfall is concentrated during the austral summer (Garreaud, 2009) in association with the South American Monsoon System (SAMS). At upper levels, SAMS is characterized by an anticyclonic circulation located approximately at the Bolivian Altiplano, named Bolivian High and a trough over the tropical and sub-tropical southern Atlantic Ocean, also known as the "northeast trough". At low-levels SAMS main features are a thermal low (known as the Chaco low) centered over northern Argentina, the South Atlantic Convergence Zone (SACZ) (Carvalho *et al.*, 2004), and the South American Low-Level Jet (SALLJ) east of the Andes (Marengo *et al.*, 2012; Vera *et al.*, 2006).

SAMS exhibits variations on intraseasonal timescales characterized by long periods of enhanced convective activity (active phase) and periods of persistent suppression of convection (break phases). Carvalho *et al.* (2002) showed that active (break) phases of SAMS are associated with westerly (easterly) intraseasonal anomalies in the low-level winds dominating tropical South America. In CSPA, enhanced convection is observed during break phases of SAMS in association with the strengthening easterly winds (Carvalho *et al.*, 2002). The Madden-Julian Oscillation (MJO) is considered the most important source of intraseasonal

variability affecting circulation and rainfall in South America (Liebmann and Mechoso, 2011). The extratropical response of the MJO and resulting propagation of wave-trains equatorward along eastern South America modulates convection and circulation from the subtropics to the tropics, influencing the position and convective activity in the SACZ (Carvalho *et al.*, 2011b, 2004) and in the Intertropical Convergence Zone (ITCZ) (Tomaziello *et al.*, 2015).

Other meteorological phenomenon affecting extreme rainfall in the Peruvian Andes is the east coast trough regime proposed by Romatschke and Houze (2010). This synoptic condition is characterized by the northward displacement of the SALLJ, accompanied by the displacement of the trough toward the east coast of South America and a build-up of surface high pressure over the La Plata Basin. These conditions promote moisture transport from the Amazon Basin to CSPA. Over this region, the maximum wide convective cores occur at night, the maximum rainfall is evident from midnight to noon, and the broad stratiform formations occur during the morning (Romatschke and Houze, 2010, 2013).

The El Niño Southern Oscillation (ENSO) is the most important tropical coupled mode of variability that modulates rainfall in the Andes on interannual time-scales. The warm (cold) phase of ENSO is generally associated with below (above) average rainfall over tropical South America (Garreaud, 2009) and the Altiplano (Vuille *et al.*, 2000). In general, easterly (westerly) upper level winds are related to enhanced (suppressed) rainfall on interannual time-scales in the Altiplano resulting from the increased (reduced) moisture influx from east of the Andes (Garreaud and Aceituno, 2001; Vuille, 1999). Furthermore, there is spatially different responses in the central Peruvian Andes (Garreaud *et al.*, 2003) and southern Peruvian Andes (Perry *et al.*, 2014; Vuille and Keimig, 2004). Lagos *et al.* (2008) found weakly positive, neutral and moderately negative correlation coefficients between sea surface temperature

(SST) anomaly in the Niño 3.4 region (5°N-5°S, 120°-170°W) and rainfall in the northern, central and southern Peru, respectively. Lavado and Espinoza (2014) described the spatial variability of rainfall impacts of ENSO in Peru. They showed increased rainfall during strong El Niño in the northern Pacific basin, decreased (increased) rainfall during strong El Niño (La Niña) in the Southern Pacific basin and decreased rainfall during strong El Niño in the Titicaca basin. ENSO impacts on rainfall depend not only on location, but also on the period of analysis. Bourrel *et al*. (2014) evaluated the impacts of ENSO on rainfall during 1964-1975, 1977-1999, and 2001-2011 over the central and northern Peruvian Pacific coast. They found that, without considering the strong ENSO events of 1982/1983 and 1997/1998, the region experienced increased (decreased) rainfall during El Niño events of the period 1964-1999 (2000-2011).

The Pacific Decadal Oscillation (PDO) is the leading mode of monthly sea surface temperature anomalies in the Pacific Ocean north of 20°N, that exhibits a decadal oscillation between warm (positive) and cold (negative) phases (Newman *et al.*, 2016; Seiler *et al.*, 2013). Previous studies have shown that the PDO affects the South American climate on decadal time-scales (Mantua and Hare, 2002). Garreaud *et al.* (2009) showed negative (positive) correlations between rainfall anomalies and PDO in some parts of South America, mainly north (south) of ~10°S. Total annual rainfall and number of extreme events in the Bolivian lowlands are higher during positive PDO phase (Seiler *et al.*, 2013). Furthermore, some authors have related rainfall trends in South America with changes in PDO. Marengo *et al.* (2004) associated the shift from negative to positive rainfall anomalies over the southern Amazon of Brazil in the 1970s with the switch of the PDO from cold to warm phase in 1976/77. Carvalho *et al.* (2011a) showed that the amplitude of SAMS increased after the 1976/77 climate shift with impacts on rainfall. Seiler *et al.* (2013) showed that monthly and annual standardized rainfall anomalies

increased from ~1965 to 1984 and decreased from ~1985 to 2004, following the basic structure of the PDO index. They also found that up to 15% of the 68 stations analyzed in Bolivia have increased (decreased) total and extreme rainfall during 1965-84 (1985-2009).

The climate setting of CSPA (described in the former paragraphs of this subsection) gives a general idea of the main atmospheric factors affecting the spatiotemporal variability of rainfall in the region. Nevertheless, a better understanding of this variability is expected to be aided by using observed data. In this chapter, long-term daily rainfall data gauged in CSPA is examined to describe regional rainfall and geographic patterns, and decadal-dependent rainfall responses to ENSO and PDO.

B. Data

1. Gauged stations

This study relied on daily rainfall data from forty-seven rain-gauge stations located in CSPA (Figure 2.1) from 1965-2010 calendar years. Eight stations are in the Amazon Basin, eleven in the Titicaca Basin, and twenty-eight in the Pacific Basin. The dataset was provided by the Peruvian National Meteorological and Hydrological Service (SENAMHI or *Servicio Nacional de Meteorología e Hidrología*) through the National Water Authority (ANA or *Autoridad Nacional del Agua*) website (www.ana.gob.pe). Information about location, altitude, slope, aspect, and time-series completeness for each station is listed in Table 2.1. The location and altitude were provided by SENAMHI, while the slope and the aspect of each station were calculated based on the 90-meters resolution Shuttle Radar Topography Mission (SRTM) dataset (Farr *et al.*, 2007). All stations have more than thirty valid years, where a valid year is considered as the one having less than fifteen days of missing values (as in Donat *et al.*, 2013).

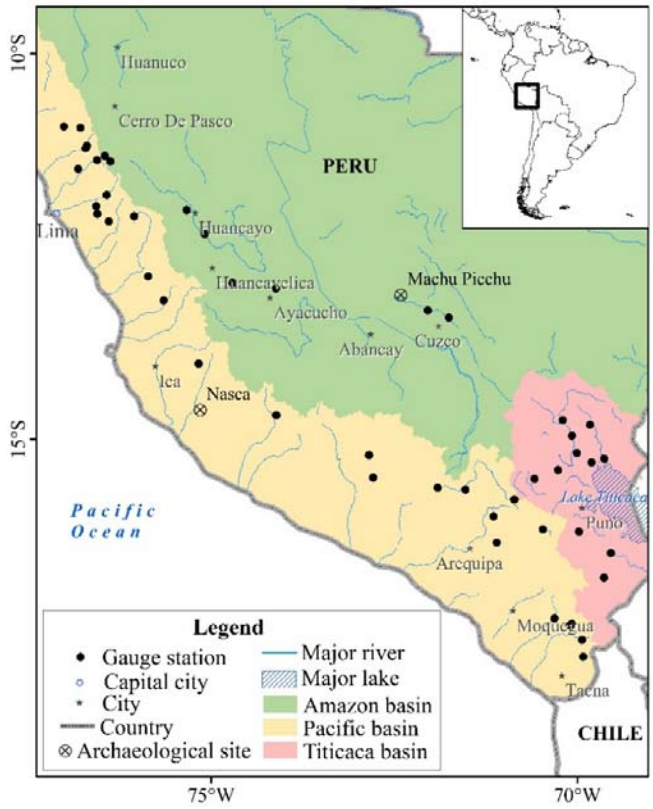

Figure 2.1. Location of the forty-seven rainfall stations analyzed over Central and Southern Peruvian Andes. The delineation of major basins performed by the Peruvian National Water Authority is shown only for the Peruvian territory.

A quality control procedure was performed for all stations investigated here. The software RHtest was used to identify inhomogeneities in the datasets at daily and monthly time-scales. This software runs a test based on the penalized maximal *T* test (Wang *et al.*, 2007) and the penalized maximal *F* test (Wang 2008a), which are embedded in a recursive testing algorithm (Wang 2008b). Stations with non-climate related inhomogeneities were excluded from the analysis of trends. Additionally, a visual inspection was performed to identify climate-related inhomogeneities (e.g. that may occur during very strong La Niña) to avoid discarding any station because of a natural inhomogeneity in the time-series. For instance, if an inhomogeneity was evident in one or more neighbor stations during a climate-related event such as ENSO, then the inhomogeneity identified was considered as climate-related and the station was maintained.

Table 2.1. Description of the stations analyzed in this study. The column *Region* refers to the regionalization of the stations. The *Aspect* is denoted as: North (N), Northeast (NE), East (E), Southeast (SE), South (S), Southwest (SW), West (W), and Northwest (NW). The column *Years* refers to the number of valid hydrologic years analyzed here, where a valid year is considered as the one having less than fifteen days of missing values.

Region	Station	Latitude (°)	Longitude (°)	Altitude (m)	Slope (°)	Aspect	Years
A-1	Marcapomacocha	-11.4	-76.3	4479	3.6	SW	33
	Tanta	-12.1	-76.0	4323	29.4	E	39
	Yantac	-11.3	-76.4	4600	6.8	W	37
A-2	Huayao	-12.0	-75.3	3308	1.0	SE	31
	La Quinua	-13.1	-74.1	3260	5.8	S	36
	Lircay	-13.0	-74.7	3150	15.1	N	40
	Pilchaca	-12.4	-75.1	3570	12.6	NE	37
A-3	Pisac	-13.4	-71.8	2950	29.3	S	34
	Urubamba	-13.3	-72.1	2863	8.8	E	36
B-4	Huamantanga	-11.5	-76.8	3392	7.1	SW	38
	Paccho	-11.0	-76.9	3250	26.6	N	39
B-5	Pariacancha	-11.4	-76.5	3800	21.5	SW	40
	Parquin	-11.0	-76.7	3590	18.8	W	38
	Pirca	-11.2	-76.7	3255	24.1	SW	41
	Santa Cruz	-11.2	-76.6	3700	8.9	W	37
B-6	Antioquia	-12.1	-76.5	1839	35.0	SW	43
	Huangascar	-12.9	-75.8	2533	14.1	N	39
	Matucana	-11.8	-76.4	2479	5.4	SE	32
	San Juan De Castrovirreyna	-13.2	-75.6	1810	9.4	NE	34
	San Lazaro De Escomarca	-12.2	-76.4	3600	16.0	N	42
	Santiago De Tuna	-12.0	-76.5	2921	26.5	NW	38
B-7	Cordova	-14.0	-75.2	3240	15.3	SW	40
	Puquio	-14.7	-74.1	3215	1.1	E	36
C-8	Cabanaconde	-15.6	-72.0	3379	5.9	W	36
	Chivay	-15.6	-71.6	3633	11.7	W	34
	Cotahuasi	-15.2	-72.9	2683	6.3	NW	31
	Salamanca	-15.5	-72.8	3203	35.2	S	45
C-9	Las Salinas	-16.3	-71.2	4310	14.1	SE	41
	Pillones	-16.0	-71.2	4360	0.4	NE	41
C-10	Crucero Alto	-15.8	-70.9	4470	3.2	N	39
	Ichuna	-16.1	-70.6	3800	11.2	SW	40
C-11	Cairani	-17.3	-70.4	3443	14.8	W	38
	Palca	-17.8	-70.0	3100	16.2	S	33
	Sitajara	-17.4	-70.2	3166	11.2	SW	39
	Susapaya	-17.4	-70.1	3309	4.5	SE	36
	Talabaya	-17.6	-70.0	3409	7.4	N	40
D-12	Arapa	-15.1	-70.1	3830	7.3	SE	41
	Azangaro	-14.9	-70.2	3863	0.5	N	32
	Huancane	-15.2	-69.8	3890	11.2	S	43
	Munani	-14.8	-70.0	3948	3.4	W	37
	Progreso	-14.7	-70.3	3980	0.1	NE	37
	Taraco	-15.3	-69.9	3820	0.5	N	43
D-13	Lampa	-15.4	-70.4	3892	1.0	NE	41
	Laraqueri	-16.2	-70.1	3900	1.3	SE	37
	Pampahuta	-15.5	-70.7	4400	1.4	SE	39
D-14	Chilligua	-16.4	-69.6	4100	3.1	SW	38
	Mazo Cruz	-16.7	-69.7	4003	0.6	NE	38

The mean annual cycle of rainfall calculated for forty-seven CSPA rainfall stations (Figure 2.2) shows that the hydrologic year of CSPA starts on September 1st and ends on August 31st (for most CSPA stations). Although few CSPA stations, mainly located in the Amazon and Titicaca basin, report rainfall as early as August 1st; this study adopted the hydrological year calculated from September to August as suggested by SENAMHI.

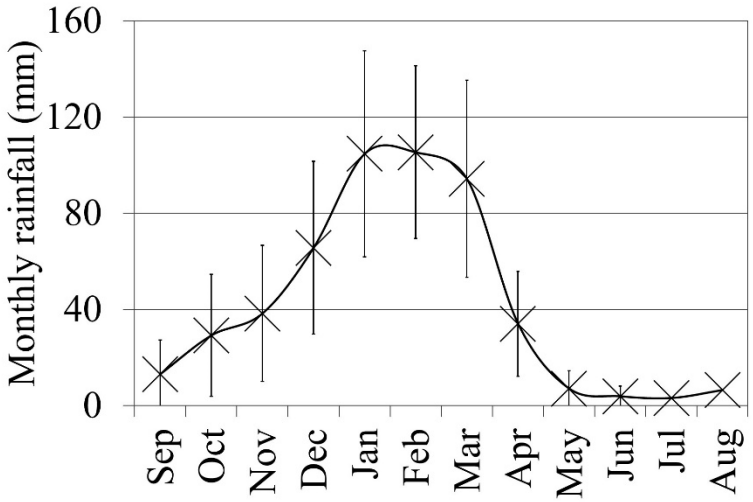

Figure 2.2. Mean (cross) and standard deviation (error bar) of gauged 1965-2010 monthly rainfall of the forty-seven central and southern Peruvian Andean stations analyzed in this study.

2. ENSO and PDO indices

ENSO conditions were defined using the Oceanic Niño Index (ONI) provided by the Climate Prediction Center (CPC) / National Oceanic and Atmospheric Administration (NOAA). ONI is defined as the 3-month running mean of Extended Reconstructed Sea Surface Temperature (ERSST) anomalies in the Niño 3.4 region based on centered 30-year base periods updated every 5 years. Events are defined as 5 consecutive overlapping 3-month periods at or above the +0.5º anomaly for warm (El Niño) events and at or below the -0.5 anomaly for cold (La Niña) events. Seventeen El Niño and fourteen La Niña years occurred

during 1965-2010 (Figure 2.3). Rainfall patterns during El Niño and La Niña conditions of the periods 1965-1976, 1977-1999 and 2000-2010 were evaluated (as in Bourrel *et al*. 2014).

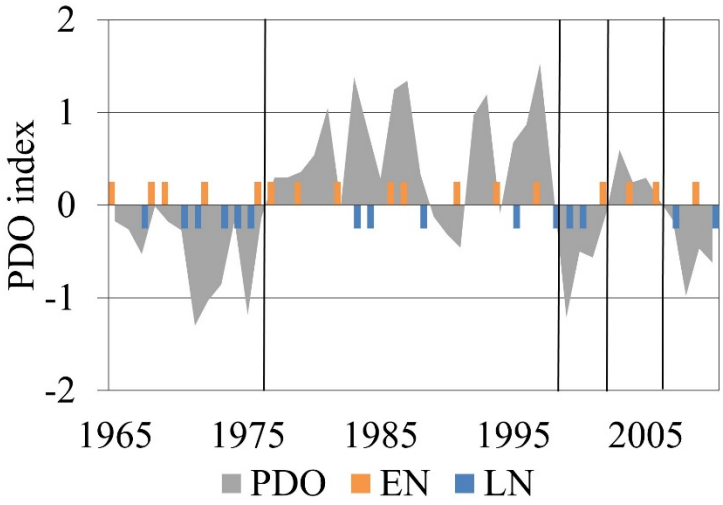

Figure 2.3. Pacific Decadal Oscillation (PDO) index and El Niño Southern Oscillation (ENSO) - El Niño (EN) and La Niña (LN) - conditions during 1965 - 2009. Vertical black lines represent PDO change periods.

The PDO Index is defined as the leading principal component of North Pacific monthly sea surface temperature variability (Zhang *et al.*, 1997), and it was obtained from http://research.jisao.-washington.edu/pdo/ . During the period evaluated in the present study, the PDO index exhibits positive (negative) phases during 1977-1997 and 2002-2006 (1965-1976, 1998-2001 and 2007-2010), as seen in Figure 2.3. CSPA rainfall indices during the two positive and three negative PDO phases were evaluated.

C. Methods

1. Regionalization of stations

To regionalize the stations a combination of principal component analysis (PCA) and cluster analysis was performed based on complete daily rainfall time-series from the forty-seven CSPA quality-controlled stations. The PCA was performed using a correlation matrix

obtained from the forty-seven gauged daily rainfall time-series (after removing the mean annual cycle) to calculate the eigenvalues and eigenvectors that maximize rainfall variance (as in Comrie and Glenn 1998). Figure 2.4 shows the percentage of variability explained by the first four principal components (PCs). The first two PCs explained about 30%, while the first three PCs explained about 37% of the total rainfall variance. The separation of the PCs was evaluated by plotting the respective eigenvalues and eigenvalues errors (Figure 2.4, see the right vertical axis). The eigenvalue error was calculated by multiplying the eigenvalue by the squared root of $2/n'$ (North *et al.*, 1982), where n' is the number of independent events ($n' = n * \frac{1-r1}{1+r1}$), n is the total number of days in the time series (non-missing days) and $r1$ is the lag-1 autocorrelation. According to this method, the first four principal components are separable because their eigenvalues and respective errors did not overlap.

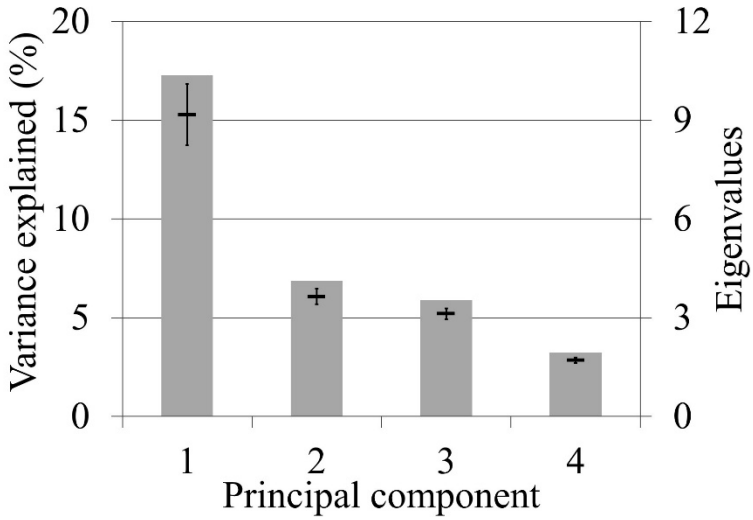

Figure 2.4. Principal component analysis of 1965-2010 daily rainfall of the central and southern Peruvian Andean stations; where the left vertical axis is, the variance explained by the principal components (PCs), and the right vertical axis represents the separability between PCs indicated by eigenvalues (dash) and respective eigenvalues error bars.

The regionalization of stations was finally performed by applying a nonhierarchical clustering method (K-mean) to the PCA loadings obtained based on the gauged daily time series. Many trials of clustering were carried out by using varying number of PCs loadings and increasing number of clusters. To decide on the appropriate number of regions, the Silhouette method was applied. Rousseeuw (1987) defined the Silhouette (s) as:

$$s(i) = \begin{cases} 1 - \frac{a(i)}{b(i)}, & if\ a(i) < b(i) \\ 0, & if\ a(i) = b(i) \\ \frac{b(i)}{a(i)} - 1, & if\ a(i) > b(i) \end{cases} \qquad (2.1)$$

Where i represents each element in a cluster; $a(i)$ is the average dissimilarity of i with respect to all other data within the same cluster; $b(i)$ is the lowest average dissimilarity of i in any other cluster of which i is not a member satisfying the condition that $-1 \leq s(i) \leq 1$. The mean $s(i)$ of the entire dataset is a measure of how appropriately the data has been clustered (Rousseeuw 1987), therefore the closer the value of the mean Silhouette is to one the better the clustering of elements.

Figure 2.5 shows the mean Silhouette values calculated after performing the K-means clustering technique with two, three and four PCs loadings and different number of clusters (from two to sixteen). The maximum mean Silhouette is evident when using the two first principal components and four clusters. The second maximum mean Silhouette is found using the first two PCs and fourteen clusters. The resulting four and fourteen clusters of stations were considered the regionalization of CSPA stations on four major regions and fourteen subregions, respectively. The location and geographic features (latitude, longitude, altitude, slope and aspect) of these major regions and subregions are described in section D.

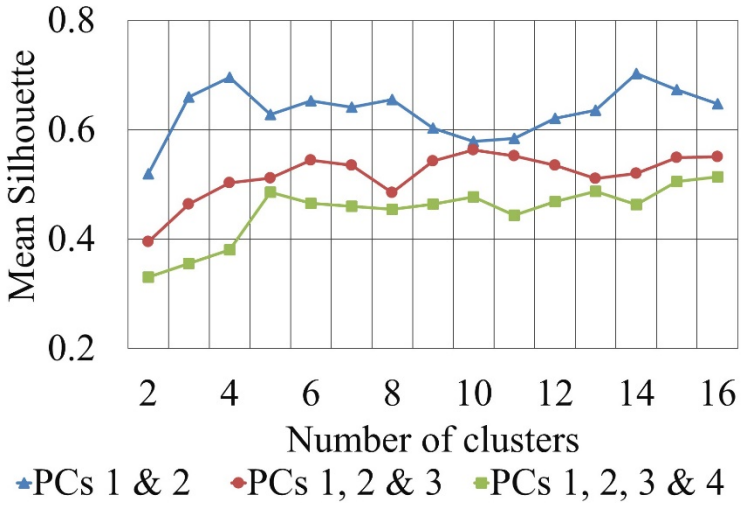

Figure 2.5. Cluster analysis mean Silhouette values after using different number of principal components (PC) loadings and increasing number of clusters.

2. Rainfall indices

The intensity and frequency of rainfall in CSPA were evaluated based on the twelve ETCCDI (Expert Team on Climate Change Detection and Indices) indices and three complementary annual rainfall statistics using quality-controlled daily gauged rainfall data. The ETCCDI indices were proposed by a joint project between the World Meteorological Organization Commission for Climatology (CCI) and the World Climate Research Program Climate Variability and Predictability (CLIVAR) program (Haylock *et al.*, 2006; Zhang *et al.*, 2011). These indices were developed to be non-region-specific and independent (Folland *et al.* 1999; Nicholls and Murray 1999).

The ETCCDI indices are: wet-days annual rainfall (PRCPTOT), simple daily rainfall intensity (SDII), consecutive dry days (CDD), consecutive wet days (CWD), number of heavy rainfall days (R10), number of very heavy rainfall days (R20), very wet day rainfall (R95p), extremely wet day rainfall (R99p), maximum 1-day rainfall (RX1day), maximum 5-day rainfall (RX5day), very wet day proportion (R95pTOT), and extremely wet day proportion

(R99pTOT). The complementary yearly rainfall statistics are: percentage of wet days (Wdays), twenty-fifth percentile of daily rainfall (p25th) and seventy-fifth percentile of daily rainfall (p75th). The calculation of each index is explained in Table 2.2. Only years with less than 15 days of missing data were selected, and the indices were calculated using Western and hydrologic calendars.

3. ENSO and PDO

To evaluate the effect of ENSO on rainfall indices in CSPA, the anomalies of ETCCDI indices during El Niño and La Niña of the period 1965-2010 for each CSPA region of stations were calculated. Anomalies were calculated both including and excluding the strong El Niño's of 1982-1983 and 1997-1998. The significance of the anomalies was found based on a *z* test with 95% level of confidence and seventeen (fourteen) independent El Niño (La Niña) events that occurred during 1965-2010. Furthermore, to assess if the relationship between ENSO and rainfall indices was persistent in time; the anomalies of rainfall indices during the periods 1965 - 1976 (P1), 1977-1999 (P2), and 2000-2010 (P3) separately (excluding the strong El Niño's of 1982-1983 and 1997-1998) were evaluated and the percentage of stations with different anomalies per each CSPA region were calculated. P1, P2 and P3 were the same periods evaluated in Bourrel *et al*. (2014).

To evaluate the effect of PDO on rainfall indices in CSPA, the anomalies of ETCCDI indices during positive and negative PDO phases of the period 1965-2010 for each CSPA region of stations were calculated. The significance of the anomalies was found based on a *z* test with 95% level of confidence and two (three) positive (negative) independent PDO events that occurred during 1965-2010. Finally, the standardized anomalies of rainfall indices were

plotted along with the PDO index to potentially explain any relationship between these time-series.

Table 2.2. Definition of total and extreme rainfall indices proposed by the Expert Team on Climate Change Detection and Indices (ETCCDI). Wet (dry) day is defined when daily rainfall is greater or equal to (less than) 1 mm. The complementary statistics (Wdays, p25th and p75th) used in this study are also defined.

Index	Definition	Units
Wet-days annual rainfall (PRCPTOT)	Annual total rainfall from wet days.	mm
Simple daily rainfall intensity (SDII)	Annual total rainfall divided by the number of wet days in the year.	mm/day
Consecutive dry days (CDD)	Annual maximum number of consecutive dry days.	days
Consecutive wet days (CWD)	Annual maximum number of consecutive wet days.	days
Number of heavy rainfall days (R10)	Annual count of days when daily rainfall is greater or equal than 10 mm.	days
Number of very heavy rainfall days (R20)	Annual count of days when daily rainfall is greater or equal than 20 mm.	days
Very wet day rainfall (R95p)	Annual total rainfall when daily rainfall is greater than the 95th percentile of the reference period (1971-2000).	mm
Extremely wet day rainfall (R99p)	Annual total rainfall when daily rainfall is greater than the 99th percentile of the reference period (1971-2000).	mm
Maximum 1-day rainfall (RX1day)	Annual maximum 1-day rainfall.	mm
Maximum 5-day rainfall (RX5day)	Annual maximum consecutive 5-day rainfall.	mm
Very wet day proportion (R95pTOT)	Percentage of annual total rainfall from days with daily rainfall greater than the 95th percentile of 1971-2000.	%
Extremely wet day proportion (R99pTOT)	Percentage of annual total rainfall from days with daily rainfall greater than the 99th percentile of 1971-2000.	%
Percentage of wet days (Wdays)	Annual number of wet days in the year divided by 365.	%
Twenty-fifth percentile (p25th)	Annual twenty-fifth percentile of daily rainfall.	mm
Seventy-fifth percentile (p75th)	Annual seventy-fifth percentile of daily rainfall.	mm

D. Results

1. Regional geographic and rainfall features

The regionalization of stations described in section C.1 generated four major regions (denoted by the letters A, B, C and D) and fourteen subregions (denoted by the numbers 1 to 14) mapped in Figure 2.6. Fourteen subregions are embedded into the four major regions: subregions 1, 2 and 3 are embedded in region A; subregions 4, 5, 6 and 7, in region B; subregions 8, 9, 10 and 11, in region C; and subregion 12, 13 and 14, in region D. Regions A, B, C and D contain nine, fourteen, thirteen and eleven stations, respectively. Stations regionalized in region A are in the Andean-Amazon-Basin (Amazon Basin for simplification); region B and region C, in the Andean-Pacific-Basin boundary (Pacific Basin for simplification); and region D in the Titicaca Basin. The only exception is Tanta station which has been regionalized in region A (Amazon Basin), but it is located at a very high altitude in the Pacific Basin. That is, the regionalization process indicated that Tanta station shares common rainfall characteristics with the high-elevation stations Marcapomacocha and Yantac located in region A (which are influenced by the South American Monsoon), rather than with other stations influenced by climatic drivers affecting the Pacific Basin. Thus, in this regionalization process the proximity of stations is not necessarily the dominant factor to cluster stations; rather, stations are clustered according to common rainfall patterns independently of the location. Furthermore, altitude does play an important role in the shared rainfall characteristics among stations. Elevation also seems crucial in the regionalization of stations located over the entire Peruvian Pacific basin performed by Rau *et al*. (2016), who applied the K-means clustering followed by the Regional Vector Method (RVM) to gauged monthly rainfall during 1964-2011.

The mean annual rainfall cycle of the four regions and the fourteen subregions of CSPA rainfall stations are shown in Figure 2.7 and Figure 2.8, respectively. Regions A and D shows greater mean monthly rainfall during September to March than regions B and C. Among the stations located in region A (Amazon basin), subregion A-1 is the one with greater amounts of monthly rainfall than regions A-2 and A-3 which are located at lower altitudes. In region B (Central Pacific basin), the subregion B-5, which has the same latitude as A-1 but it is located at the western side of the Andes, showed greater monthly rainfall than the other subregions in region B. Similarly, in region C the subregion with greater mean monthly rainfall is the one with highest altitudes (C-10). Finally, subregions D-12 and D-13 had more rainfall than subregion D-14 during October and November, while subregions D-13 and D-14 showed more rainfall than subregion D-12 during January to March.

Here, each region was characterized regarding basic geographic features (latitude, longitude, altitude, slope, and aspect), and rainfall patterns (mean yearly total and extreme rainfall). Figure 2.9 shows the mean and the standard deviation of latitude, longitude, altitude, slope and aspect between stations in each of the four major regions. It is noticeable that the latitude and longitude of stations in region A (C) are similar to the ones in the region C (D). Nevertheless, the latitude and longitude of regions A and B greatly differ from that of regions C and D. The ranges of altitude, slope and aspect are similar among stations of the four groups; only region D (Titicaca) shows a slightly greater altitude and flatter conditions because of stations located over the High-Andean plateau or *Altiplano*.

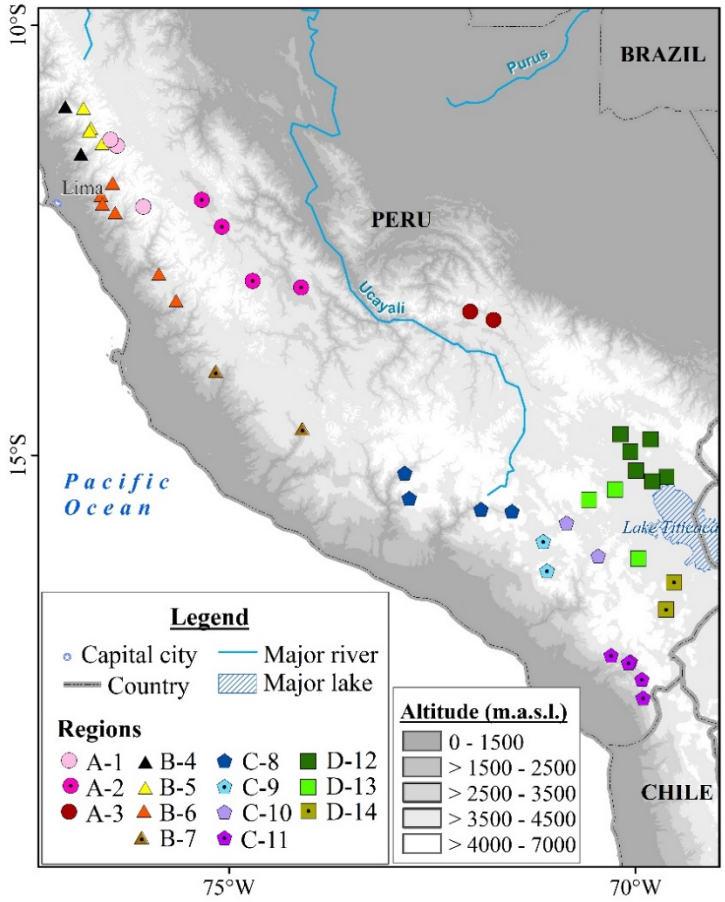

Figure 2.6. Regionalization of stations based on principal component analysis and cluster analysis of gauged rainfall. The major regions are referred by letters (A, B, C or D), while the subregions are denoted by numbers (1 to 14).

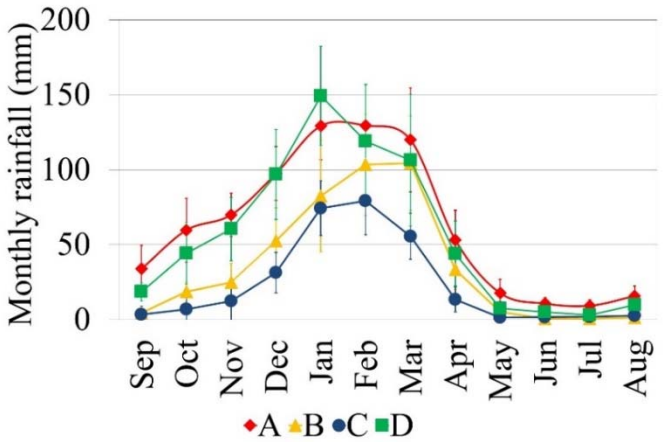

Figure 2.7. As in Figure 2.2, but for each region of the central and southern Peruvian Andean stations: A (Amazon basin), B (Central Pacific basin), C (Southern Pacific basin), and D (Titicaca basin).

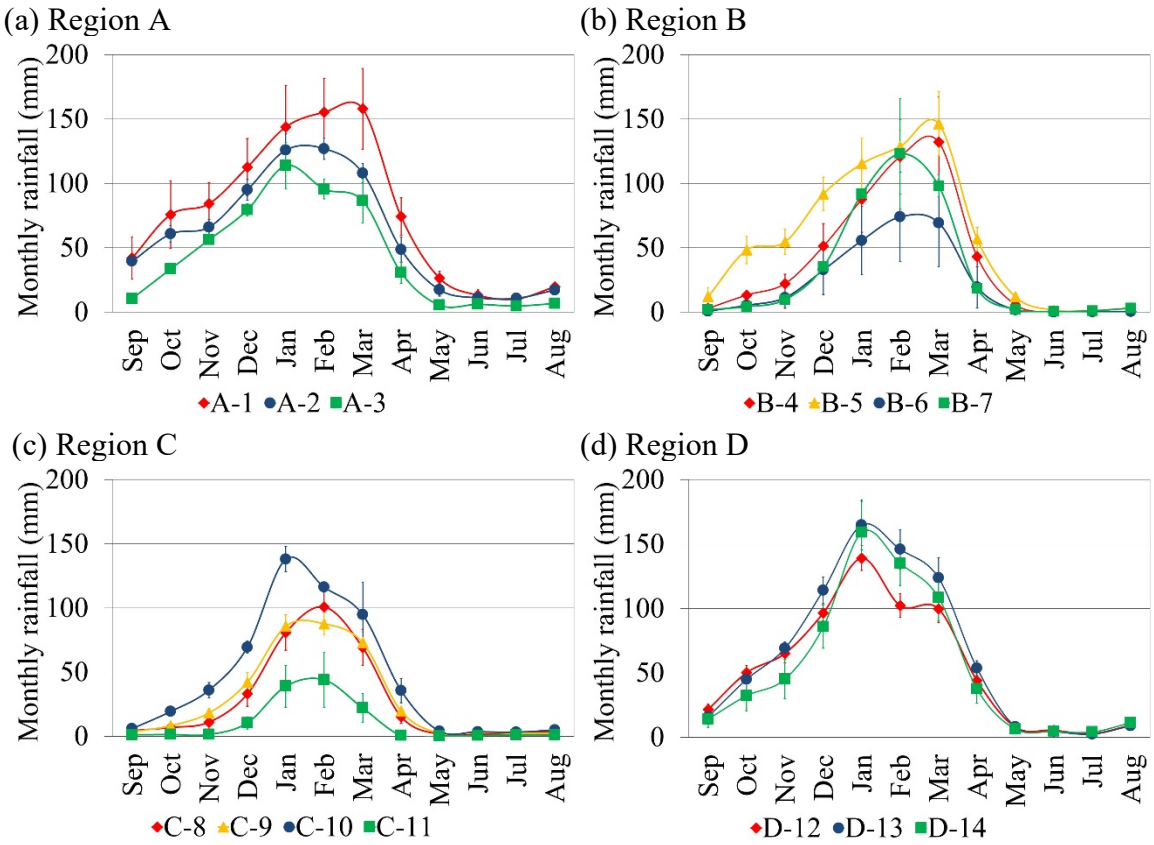

Figure 2.8. As in Figure 2.2, but for each subregion of the central and southern Peruvian Andean stations located in regions: (a) A (Amazon basin), (b) B (Central Pacific basin), (c) C (Southern Pacific basin), and (d) D (Titicaca basin).

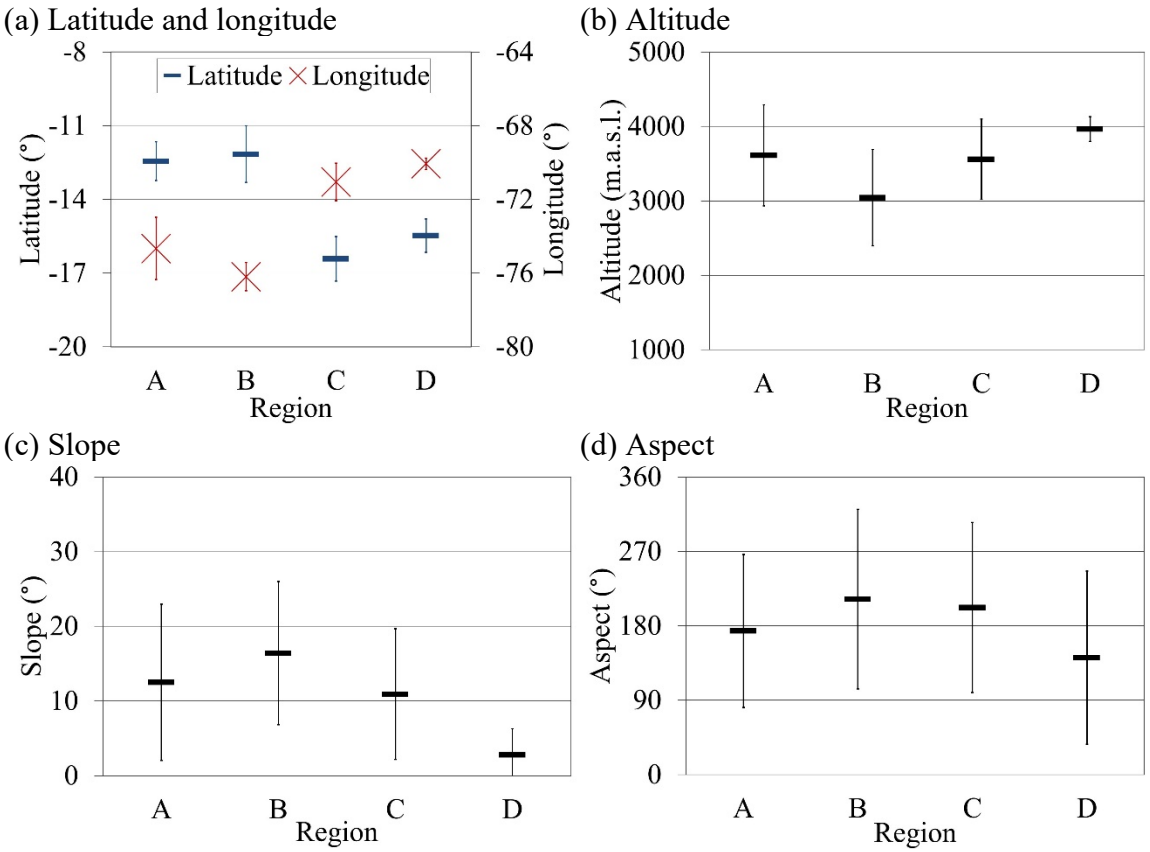

Figure 2.9. Mean (dash) and standard deviation (error bar) of (a) latitude and longitude, (b) altitude, (c) slope and, (d) aspect from all stations in each major Central and Southern Peruvian Andes region. The major regions are: A (Amazon Basin), B (Central Pacific Basin), C (Southern Pacific Basin), and D (Titicaca Basin). Note: The aspect corresponds to a surface facing North (0° - 22.5°), Northeast (22.5° - 67.5°), East (67.5° - 112.5°), Southeast (112.5° - 157.5°), South (157.5° - 202.5°), Southwest (202.5° - 247.5°), West (247.5° - 292.5°), Northwest (292.5° - 337.5°), and North (337.5° - 360°).

Figure 2.10 shows the same characterization, but for the fourteen sub-regions. Although the regionalization method was based solely on rainfall data, it is worth noticing that the geographical characteristics of the regions and subregions (Figure 2.9 and Figure 2.10, respectively) indicate that location and altitude are the dominant factors for different rainfall regimes in the Andes and that the method can capture these differences. The fourteen subregions have different mean latitude, longitude and altitude and smaller standard deviation among stations (Figure 2.10) compared to the four major regions (Figure 2.9). Each of the fourteen subregions is characterized by a unique combination of latitude and longitude (Figure 2.10 a), and altitude (Figure 2.10 b) ranges. Altitude varies greatly among subregions (Figure 2.10 b). For instance, subregion 1 has the greatest altitude in region A; subregion 5, in region B; and subregion 10, in region C. The slope (Figure 2.10 c) is more variable mainly in subregions located over the Amazon Basin (1 to 3) and the Pacific Basin (4 to 11), comparatively to the subregions located in the Titicaca Basin (12 to 14). The aspect (Figure 2.10 d) varies greatly among stations of the same subregion, except for the subregion 3 and 13 (5 and 8) which have most stations facing east (west).

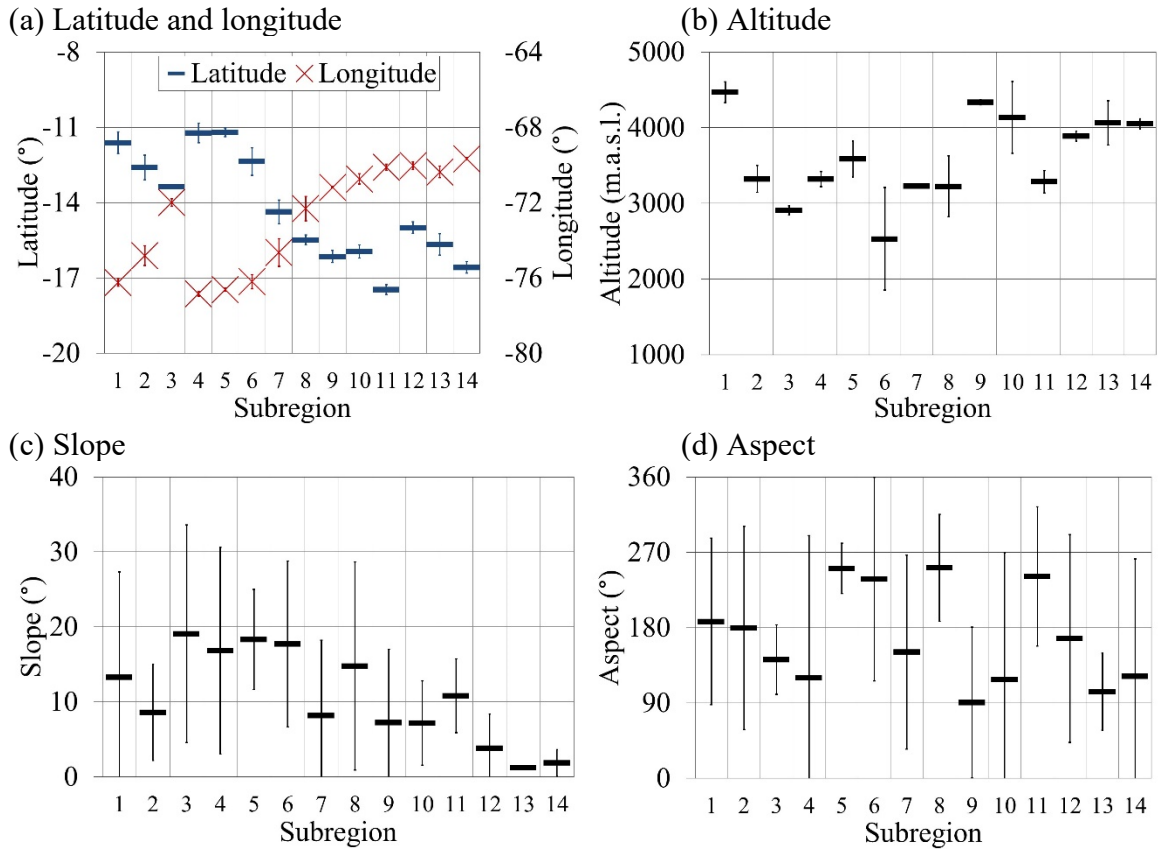

Figure 2.10. As in Figure 2.9, but for the fourteen central and southern Peruvian Andean subregions.

Total and extreme rainfall indices calculated using the hydrologic calendar exhibited differences among subregions of stations. Figure 2.11 shows the mean and standard deviation of some rainfall indices such as the wet-days annual rainfall (PRCPTOT), percentage of wet days (Wdays), consecutive dry days (CDD), and very wet day rainfall (R95p). Greatest amounts of PRCPTOT are evident in the subregions 1, 5, 10 and 13, which expectedly also showed large Wdays and R95p but low CDD. Conversely, the smallest amounts of PRCTOT observed in subregions 6, 7, 8, 9 and 11 are also related to comparatively low Wdays and R95p, and great CDD.

Interestingly, subregions with the highest altitudes (such as subregions 1, 5, 10, 12, 13, 14) showed the greatest amounts of PRCPTOT, Wdays and R95p. These relationship between altitude and rainfall over CSPA differs from the patterns obtained in Lavado *et al.* (2012), who described a decrease of monthly rainfall with altitude in the Titicaca and the Amazon basins, and no evident changes in rainfall with altitude in the Pacific basin.

Furthermore, stations facing east have greater amounts of rainfall as a result of the enhanced transport of moisture east of the Andes (Garreaud, 2009). This is evident in subregion 13 whose stations face east and consequently exhibited the greatest PRCPTOT among all other subregions embedded in region D (Titicaca Basin).

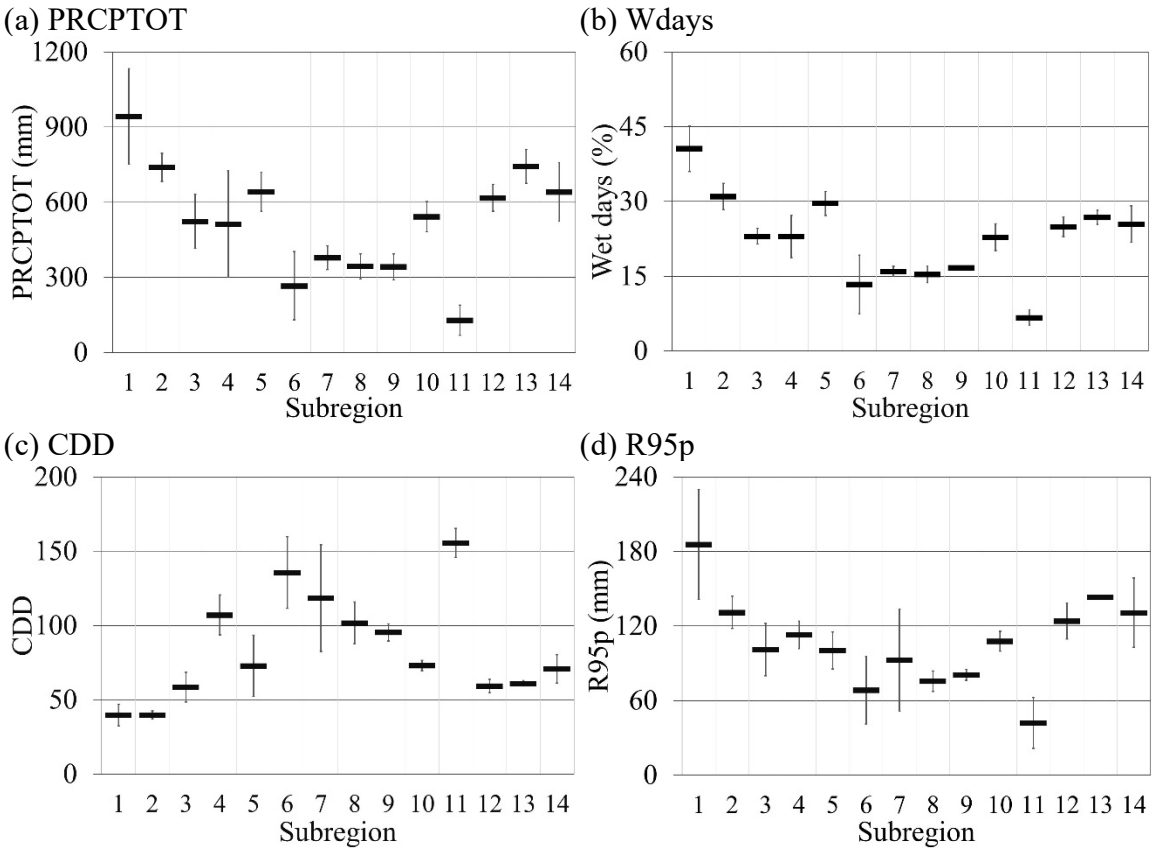

Figure 2.11. Mean (dash) and standard deviation (error bar) of (a) wet-days annual rainfall (PRCPTOT), (b) percentage of wet days (Wdays), (c) consecutive dry days (CDD), and (d) very wet day rainfall (R95p) of the fourteen central and southern Peruvian Andean subregions.

2. Regional ENSO and PDO effects on rainfall

While ENSO played a significant role in the interannual variability of some of the indices calculated for the CSPA, the magnitude of this effect depends on the region and on the period considered. Figure 2.12 shows PRCPTOT, Wdays, CDD, and R95p anomalies during El Niño and La Niña events of 1965-2009 (excluding the strong El Niño's of 1982-1983 and 1997-1998). During La Niña (El Niño) years, positive (negative) anomalies of PRCPTOT, Wdays, and R95p in all CSPA regions were evident, despite the large variability of R95p in regions A and B where the difference in mean anomalies were not statistically significant. Accordingly, positive (negative) anomalies of CDD occurred during El Niño (La Niña) years

in all CSPA regions. The rainfall indices anomalies calculated during 1965-2010 including the strong El Niño's of 1982-1983 and 1997-1998 (not shown) were slightly greater in magnitude due to the enhanced rainfall signal during strong ENSO events.

Table 2.3 shows the percentage of stations in each CSPA region with positive anomalies of PRCPTOT, Wdays, CDD, and R95p during El Niño (EN) and La Niña (LN) years during the periods 1965 - 1976 (P1), 1977 - 1999 (P2), and 2000 - 2010 (P3). It is noteworthy that the strong 1982-1983 and 1997-1998 El Niño events were not included in these statistics. Interestingly, the influence of ENSO on the calculated indices is not uniform throughout time. Greater (fewer) number of stations in regions A and D had PRCPTOT, Wdays and R95p (CDD) positive anomalies during EN events of the period P3 than those of P1 and P2. Greater number of stations in regions B and C had PRCPTOT, Wdays and R95p positive anomalies during LN events of the period P2 and P3 than those of P1. Our results for region B and D corroborates to some extent to the results in Bourrel *et al.* (2014) and Vuille *et al.* (2000). Bourrel *et al.* (2014) described an increased rainfall pattern during EN of the period 1964-1999 compared to 2000-2011, and our results shows that ~60 % (~40%) of the stations in region B had positive rainfall anomalies during EN of the period 1965-1976 (2000-2010). Vuille *et al.* (2000) found below average rainfall during 1965-1990 in southern Peruvian Andes during EN, while our results show that less than half the stations in region D had a positive rainfall anomalies during 1965-1999 and that this number of stations slightly increases in 2000-2010. Notice that ENSO conditions are defined in this study using ONI and does not account for different ENSO regimes (as defined in Takahashi *et al.* 2011), which could eventually result in regional differences.

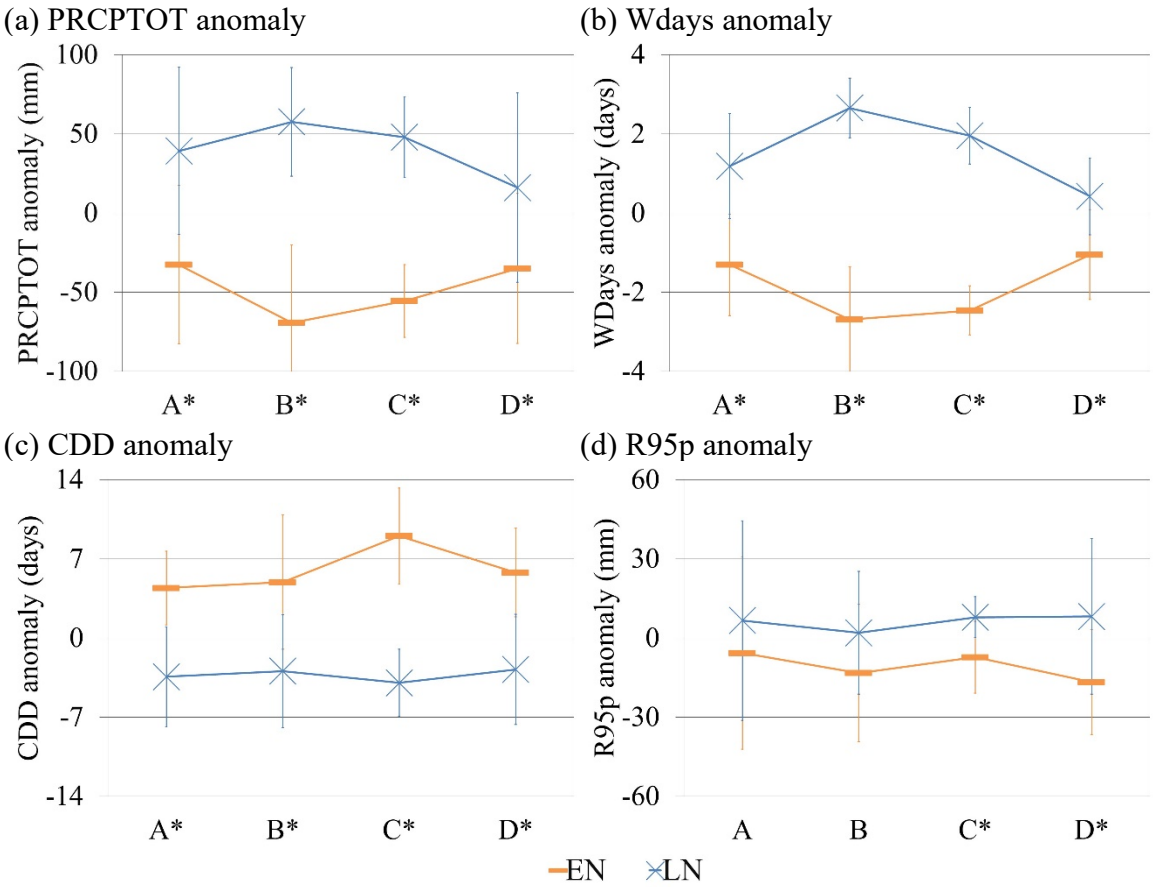

Figure 2.12. Mean (cross) and standard deviation (error bar) of (a) wet-days annual rainfall (PRCPTOT), (b) percentage of wet days (Wdays), (c) consecutive dry days (CDD), and (d) very wet day rainfall (R95p) anomalies of the four central and southern Peruvian Andean regions (A, B, C and D) during El Niño (EN) and La Niña (LN) events of 1965-2009. Regions (letters) accompanied by an asterisk (*) represent statistically significant difference in the means of rainfall indices during EN compared to LN years, based on a *z* test with 95% level of confidence and independent number of events.

Table 2.3. Percentage of stations in Central and Southern Peruvian Andes regions (A, B, C and D) with positive anomalies of wet-days annual rainfall (PRCPTOT), percentage of wet days (Wdays), consecutive dry days (CDD), and very wet day rainfall (R95p) during El Niño (EN) and La Niña (LN) years of the periods: 1965 -1976 (P1), 1977-1999 (P2), and 2000-2010 (P3).

Index	ENSO	Period	A	B	C	D
PRCPTOT	EN	P1	44	57	69	9
		P2	22	0	0	45
		P3	67	36	0	55
	LN	P1	89	43	77	36
		P2	56	100	100	64
		P3	33	93	69	55
Wdays	EN	P1	33	36	46	27
		P2	0	0	0	18
		P3	78	50	8	73
	LN	P1	78	57	77	73
		P2	78	100	100	45
		P3	67	100	77	64
CDD	EN	P1	67	50	92	64
		P2	78	86	92	100
		P3	56	71	62	64
	LN	P1	33	50	38	55
		P2	44	21	31	18
		P3	22	50	38	36
R95p	EN	P1	56	43	54	9
		P2	44	21	23	36
		P3	67	21	0	45
	LN	P1	67	50	38	36
		P2	44	50	54	64
		P3	33	36	69	36

PDO contrasting phases resulted in statistically significant differences in mean anomalies of PRCPTOT in region D, and CDD in regions A, C and D (Figure 2.13). The restrictive *z* test applied here only considered the 2 (3) independent events of positive (negative) PDO conditions during 1965-2009. Positive (negative) anomalies of PRCPTOT in regions D were evident during positive (negative) PDO. Positive (negative) anomalies in CDD were observed in regions A, C and D during positive (negative) PDO. The positive anomalies of total annual rainfall in region D (Titicaca basin or Altiplano) during positive PDO agrees with previous studies by Garreaud *et al.* (2009) and Seiler *et al.* (2013).

Similar results discussed in Figure 2.13 were found after removing the 1982-1983 and 1997-1998 strong El Niño events (not shown). Without considering these years, CSPA stations showed non-statistically significant rainfall trends during 1965-1976 (negative PDO) and 1977-1997 (positive PDO). During 1965-1976, 44 %, 50 %, 62 % and 73 % (44 %, 50 %, 31 % and 27 %) of stations in regions A, B, C and D, respectively; had positive (negative) trends in PRCPTOT. During 1977-1997, 22 %, 36 %, 85 % and 9 % (78 %, 64 %, 15 % and 91 %) of stations in regions A, B, C and D, respectively exhibit positive (negative) trend in PRCPTOT. It is noticeable that the region that showed greater dependence on PDO phase is region D (Titicaca basin). Even though this region showed positive (negative) PRCPTOT anomalies during positive (negative) PDO (Figure 2.13) most stations experienced negative (positive) trend during the period 1977-1997 (1965-1976) which corresponds to a positive (negative) PDO phase.

Figure 2.14 show a 1965-2009 time-series of the PDO index and standardized anomalies of PRCPTOT and R95p in each CSPA region. In general, these rainfall indices were poorly correlated with the PDO index, except for the weak anti-correlation in the first two

decades of the period analyzed. Positive standardized anomalies of PRCPTOT in region A and C (region D) were predominant during negative (positive) PDO phase that occurred from 1965 to 1976 (1977 to 1997). Similar patterns were observed using Wdays (not shown). The interannual variability largely dominated by ENSO events may have obscured the real effect of the PDO on rainfall, as in Seiler *et al.* (2013). Further studies are necessary to examine mechanisms connecting coupled modes of interannual-to-decadal timescales in the Pacific and Atlantic to variations in rainfall in the CSPA.

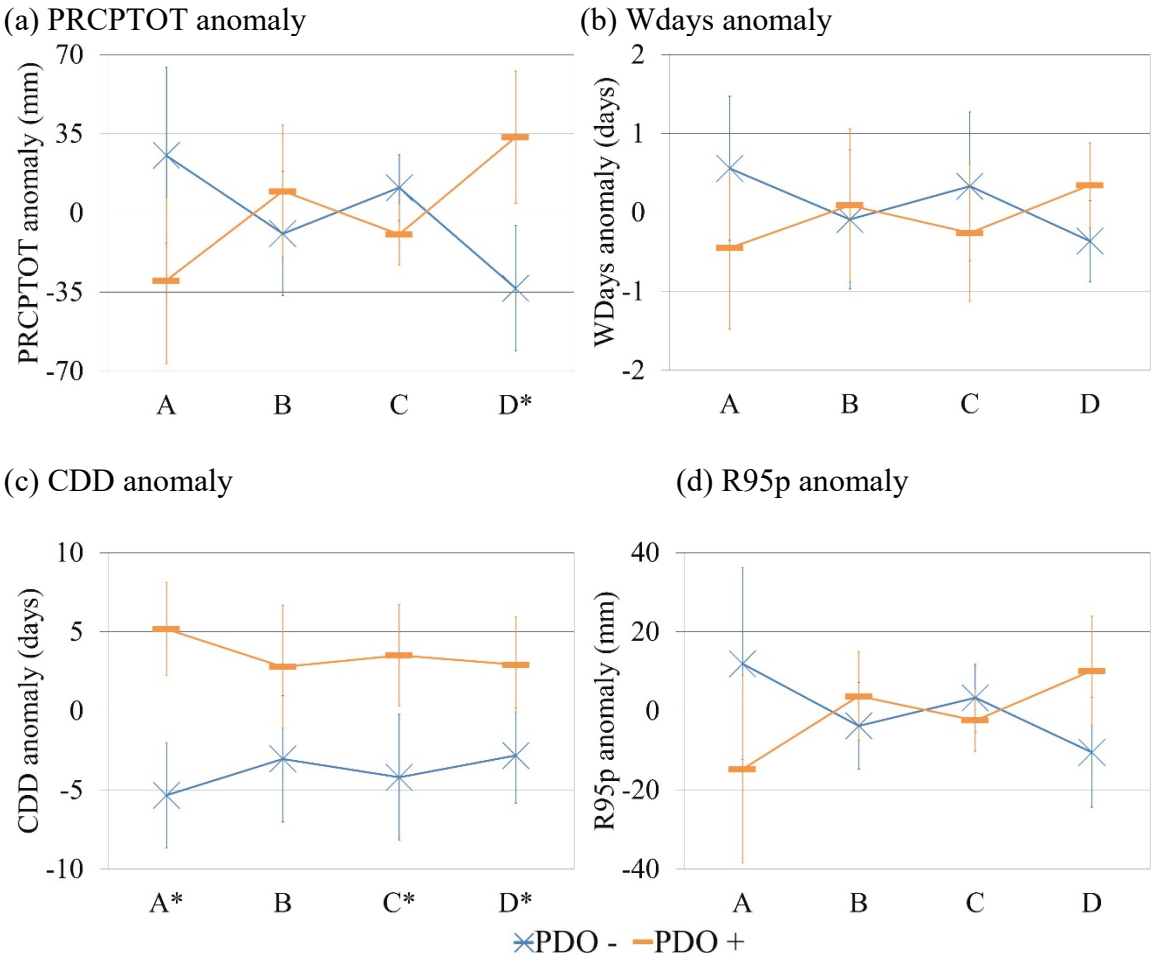

Figure 2.13. As in Figure 2.12, but for positive (PDO +) and negative (PDO -) PDO phases.

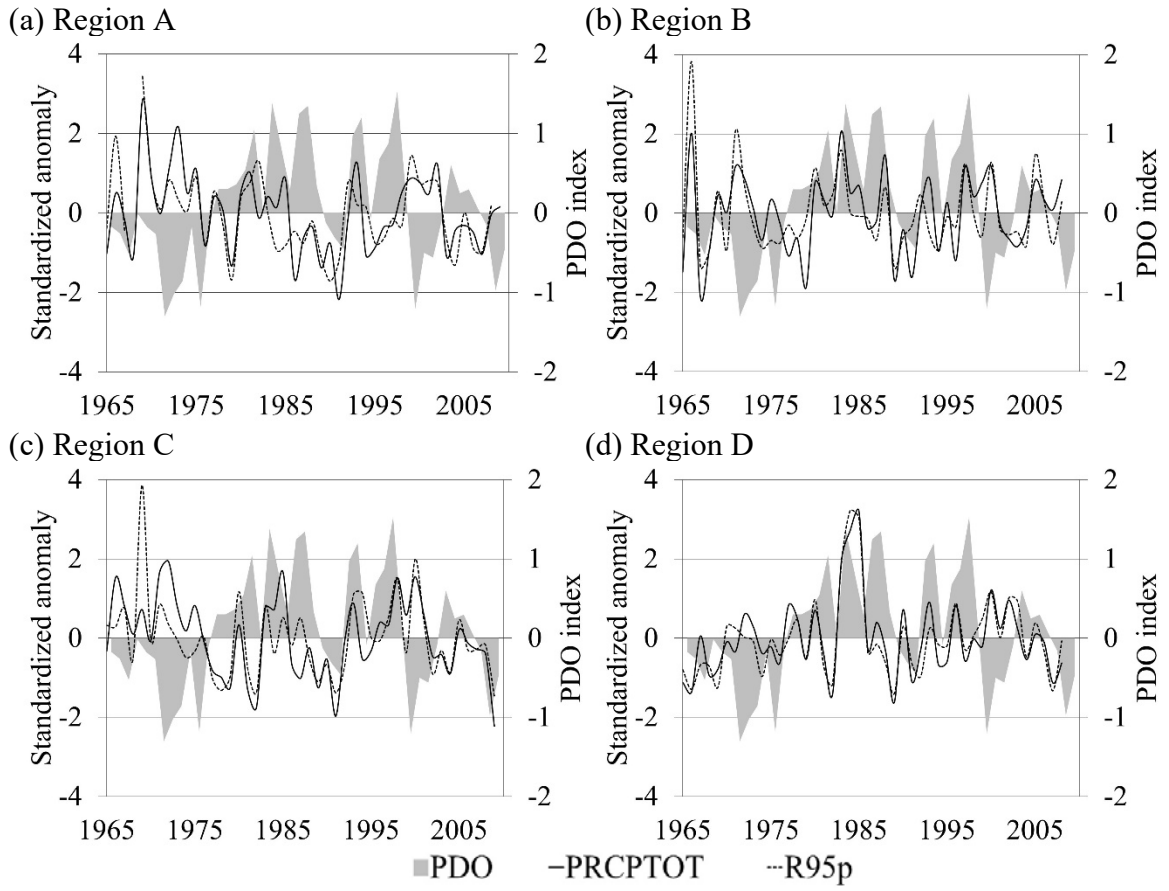

Figure 2.14. Standardized anomalies of wet-days annual rainfall (PRCPTOT) and very wet day rainfall (R95p) of each region of the central and southern Peruvian Andean stations: (a) A (Amazon basin), (b) B (Central Pacific basin), (c) C (Southern Pacific basin), and (d) D (Titicaca basin). The Pacific Decal Oscillation (PDO) index is shown in gray.

E. Conclusions

Total and extreme yearly rainfall indices characterizing the intensity and frequency of rainfall were calculated using daily rainfall from forty-seven quality-controlled stations located in Central and Southern Peruvian Andes (CSPA). Given the influences of the complex terrain on the orographic rainfall, a new method to regionalize stations according to their rainfall characteristics was proposed. The regionalization of stations was based on principal component analysis and cluster analysis of the gauged time series that efficiently separated the stations into four major regions and fourteen subregions. The major regions of stations identified were region A (Amazon basin), region B (Central Pacific basin), region C (Southern Pacific basin) and region D (Titicaca basin). These regions showed consistent differences in latitude, longitude, altitude, and, in some cases, slope. These geographical features also affected the existence of common features in the total and extreme rainfall indices among stations of the same subregion.

During 1965-2009 hydrologic years, the four CSPA regions showed consistent positive (negative) anomalies of total and extreme rainfall indices (consecutive dry days) during La Niña (El Niño) years. Positive (negative) anomalies of total annual rainfall were evident in region D during positive (negative) PDO. Positive (negative) anomalies of consecutive dry days were seen in regions A, C and D during positive (negative) PDO. These ENSO-PDO rainfall patterns showed variable behavior during the different decades evaluated.

CHAPTER III: Trends in Total and Extreme Rainfall

A. Introduction

Tropical South America has significantly warmed in recent decades (Carvalho and Jones, 2013) with impacts on rainfall that are difficult to assess, particularly in areas with complex terrain and a limited availability of gauge stations such as the Andes. Evaluating trends in rainfall and its extremes is crucial to identify areas that are more susceptible to the impacts of climate change. A few studies have examined trends in the Peruvian Andes but only with a limited number of gauge stations. A comprehensive analysis of rainfall trends -based on an adequate density of stations with long periods of observation- is essential to assess climate impacts, vulnerabilities and risks, and to provide the scientific basis for the formulation of adaptation policies for the population living in these regions (Huggel *et al.*, 2015).

A long-term negative rainfall trend in the central and southern Peruvian Andes has been documented using observed rainfall, paleoclimate data and global climate models (Neukom *et al.*, 2015; Minvielle and Garreaud, 2011). These studies associated this trend with a strengthening of the upper-tropospheric westerly winds. Segura *et al.* (2016) found that the easterly (westerly) wind anomalies, which are related to enhanced (suppressed) rainfall over southern Peruvian Andes, are associated with variations in SST over central-western tropical Pacific SST on decadal-to-interdecadal time-scales. Some other potential causes of negative rainfall trends in the Andean-Amazon region have been related to the warming of the North Tropical Atlantic Ocean (Espinoza *et al.*, 2011; Marengo *et al.*, 2011; Yoon and Zeng, 2010) and shortening of the South American Monsoon in recent decades, according to some authors (Arias *et al.*, 2015). However, it is worth mentioning that the length of the monsoon depends on the adopted metric, and there is no general consensus in the literature regarding the observed

changes in SAMS duration in recent decades (e.g. Carvalho and Cavalcanti, 2016; Carvalho *et al.*, 2011a; Jones and Carvalho, 2013).

The most appropriate way to detect changes in climate extremes is by using a set of indices that are statistically robust, cover a variety of climates, and minimize observation noise (Zhang *et al.*, 2011). This chapter provides a comprehensive analysis of rainfall trends in the Peruvian Andes by examining temporal changes in the twelve ETCCDI indices and three complementary basic yearly rainfall statistics (defined in Table 2.2), based on the largest quality-controlled number of stations available in the region. These results are further compared with previous studies that used similar indices but shorter time series and/or fewer stations to examine trends in extreme rainfall in the region.

Rainfall trends have been investigated in parts of the Peruvian Andes using point-wise (gauge stations) data and gridded data obtained by interpolating stations data. Studies that used gridded data to evaluate rainfall trends, including the Peruvian Andes, are described hereafter. Alexander *et al.* (2006) used available daily rainfall from stations worldwide to calculate ten yearly indices that were gridded at 3.75°x 2.5° longitude-latitude resolution. They showed a decrease in the number of heavy rainfall days (R10) but no trends in very wet day rainfall (R95p), consecutive dry days (CDD), simple daily rainfall intensity (SDII), and seasonal maximum 5-day rainfall (RX5day) in Central and Southern Peruvian Andes (CSPA) during 1951-2003. Morin (2011) analyzed the 0.5-deg monthly dataset developed by Beck *et al.* (2005), the Variability Analyses of Surface Climate Observations *(VASClimO*), based on the *Global Precipitation Climatology Centre (GPCC)*. He found a statistically significant negative trend in the total annual rainfall over CSPA during 1951-2000. Donat *et al*. (2013) compiled daily temperature and rainfall from many countries and generated global gridded monthly and

annual indices at a 3.75x2.5-deg resolution, named Hadley Centre Global Climate Extremes Index 2 (HadEX2). They found no trends in the number of heavy rainfall days (R10), very wet day proportion (R95pTOT), consecutive dry days (CDD) and simple daily rainfall intensity (SDII) over the Andes during 1951-2010. Lastly, Donat *et al*. (2014) performed an inter-comparison of multiple global gridded observational and reanalysis datasets of rainfall extremes and showed a decrease in the HadEX2 observed maximum 5-day rainfall (RX5day) over central Peru during 1979-2008.

Observed trends based on gauged station data can show in detail the spatial variability of local rainfall changes in regions with complex terrain such as the Peruvian Andes. Studies that used gauged data, at monthly and daily time-scales, to evaluate rainfall trends in the Peruvian Andes are described hereafter. Lavado *et al*. (2013) investigated monthly rainfall rain gauge data and reported spatially variable trends in fifty-eight Andean and Peruvian Amazon stations during 1965-2007 and a statistically significant decrease (increase) of monthly rainfall in only four (three) stations. At daily time-scales, four studies described trends in the ETCCDI total and extreme indices in some stations located in the Peruvian Andes. Vuille *et al*. (2003) focused on trends in the Peruvian and Bolivian Andes; and Haylock *et al*. (2006), Marengo *et al*. (2009), and Skansi *et al*. (2013), over the entire South America. Data and methods of these four studies are compared in Table 3.1. They used a variable number of gauge stations over CSPA, different periods of analysis, ETCCDI rainfall-indices calculated using Western calendar years only, and similar trend-analysis methods.

Results from previous studies that used point-wise data at daily time-scales to calculate ETCCDI indices to ascertain rainfall trends over CSPA are summarized here chronologically. Vuille *et al*. (2003) found a significant increase of total annual rainfall at some stations in

central Andes and a non-significant decrease of total annual rainfall in the southern Peruvian Andes. Haylock *et al*. (2006) found a significant increase of consecutive dry days in the southern Andes and a non-significant decrease of total and extreme rainfall in the central and southern Andes. Marengo *et al*. (2009) found a non-significant trend in the number of days with rainfall greater than 10 mm over central and southern Andes and a significant increase of dry consecutive days in the southern Andes. Skansi *et al*. (2013) found (a) a non-significant negative trend of total annual rainfall over the central Andes, (b) non-significant mixed trends (positive and negative trends without a spatial coherence) in total annual rainfall in the southern Andes, (c) significant drier conditions and a non-significant increase of extreme rainfall over the southern Andes, and (d) a decrease of extreme rainfall in the central Andes. In conclusion, these studies found non-significant trends in the total annual rainfall and in the intensity of extremes, but a prominent increase of dry conditions over the southern Andes.

Table 3.1. Summary of data and methods used in previous studies to describe trends in total and extreme rainfall indices of gauged stations located over Central and Southern Peruvian Andes (CSPA). The Expert Team on Climate Change Detection and Indices (ETCCDI) rainfall indices are: wet-days annual rainfall (PRCPTOT), simple daily rainfall intensity (SDII), consecutive dry days (CDD), consecutive wet days (CWD), number of heavy rainfall days (R10), number of very heavy rainfall days (R20), very wet day rainfall (R95p), extremely wet day rainfall (R99p), maximum 1-day rainfall (RX1day), maximum 5-day rainfall (RX5day), very wet day proportion (R95pTOT), and extremely wet day proportion (R99pTOT).

Study	**Data**			**Method**	
	Study region	**Stations in CSPA**	**Calendar years**	**Rainfall indices**	**Trend analysis**
Vuille *et al.* 2003	Central Andes	9	1950–1994	Annual total rainfall (similar to PRCPTOT)	Least squares regression trend considering the autocorrelation effect.
Haylock *et al.* 2006	South America	2	1960-2000	PRCPTOT, SDII, CDD, CWD, R10, R20, R95p, R99p, RX1day, RX5day, R95pTOT, R99pTOT	Kendall's tau based slope estimation.
Marengo *et al.* 2009	South America	2	1960-2000	R10, CDD	Kendall's tau based slope estimation considering the autocorrelation effect.
Skansi *et al.* 2013	South America	11	1969-2009	PRCPTOT, SDII, CDD, CWD, R20, R95p, R99p, RX1day, RX5day	Adaptation of Sen's slope considering the serial correlation effect.

These previous studies suggested that the most consistent trend in rainfall is likely the intensification of dry conditions over the southern Andes. However, these previous studies also revealed a large degree of spatial and temporal variability of rainfall in the Peruvian Andes and how these results are subject to the number of stations, spatial resolution of the data, and method applied to identify trends. The present chapter revisits these previous studies and complements them in many ways. To better characterize rainfall changes over CSPA, a greater number of quality-controlled stations (forty-seven stations over the Peruvian Andes during 1965-2009 water years) was used and a robust trend detection method that takes into consideration hydrologic years and serial correlation effects was applied. The focus was on trends in total and extreme rainfall indices. The importance of using the hydrologic year instead of the calendar year to define annual rainfall, and its effect on the calculation of rainfall indices and the estimation of trends were also investigated. Furthermore, rainfall indices and estimates of respective trends over homogeneous regions to assess the influence of geographic features on the observed trends were evaluated.

B. Data and Methods

Trends were examined using daily rainfall data from forty-seven rain-gauge stations located in CSPA (Figure 2.1) from 1965-2010, which consist on the same dataset used in Chapter 2. A combined Mann-Kendall test (Kendall, 1975; Mann, 1945) and Sen' slope (Sen, 1968) approach (e.g. Zilli *et al.*, 2016) were applied to the fifteen yearly rainfall indices, using both calendars (Western and hydrologic). The Western calendar year started on January 1st of the year "y" and ended on December 31st of the year "y" and the hydrological year started on September 1st of the year "y" and ended on August 31st of the year "y+1" (which was defined based on the mean annual rainfall cycle shown in Figure 2.7).

The non-parametric Mann-Kendall test can be used with a time series without assuming any particular distribution. The null hypothesis for this test is that the data were independent and randomly ordered, instead of having any trend. The statistic *S* (Kendall, 1975; Mann, 1945) is defined as:

$$S = \sum_{i=1}^{n-1} \sum_{j=i+1}^{n} sgn(x_j - x_i) \tag{3.1}$$

Where x_i and x_j are the sequential data, n is the total number of data in the time series and

$$sgn(\Delta x) = \begin{cases} 1, \Delta x > 0 \\ 0, \Delta x = 0 \\ -1, \Delta x < 0 \end{cases} \tag{3.2}$$

A positive (negative) value of S indicates a positive (negative) trend. For $n \geq 8$, the statistic S is approximately normally distributed with a mean $E(S) = 0$ and variance (Wilks, 2011):

$$Var(S) = \frac{n(n-1)(2n+5) - \sum_{i=1}^{m} t_i \, (t_i - 1)(2t_i + 5)}{18} \tag{3.3}$$

Where *n* is the number of data points, *m* is the number of tied groups and t_i denotes the number of ties of extent *i*. A tied group is a set of sample data having the same value. In cases where the sample size *n >10*, the standard normal test statistic *Z* is (Wilks, 2011):

$$Z = \begin{cases} \frac{S-1}{\sqrt{Var(S)}}, S > 0 \\ 0, \qquad S = 0 \\ \frac{S+1}{\sqrt{Var(S)}}, S < 0 \end{cases} \tag{3.4}$$

At a significance level $\propto$, the null hypothesis of no trend is rejected if the absolute value of *Z* is greater than the theoretical value $Z_{1-\propto_{L/2}}$, which is obtained from the standard normal

distribution table. In this study, a significance level $\alpha = 0.05$ was used. Thus, the null hypothesis of no trend was rejected if $|Z| > 1.96$.

The Mann-Kendall test is affected by serial correlation. Positive serial correlation in the time series leads to an underestimation of the sampling variance. As a consequence, the statistic Z (Equation 3.4) increases in absolute value, yielding a smaller p values and falsely rejecting the null hypothesis (Wilks, 2011). There are various approaches to adjust the test to avoid the first type error caused by autocorrelation effects: (a) pre-whitening, (b) trend-free pre-whitening, (c) variance correction and (d) block resampling techniques. In this study, the variance correction approach proposed by Hamed and Rao (1998) and Hamed and Rao (2004) was used. Therefore, the variance of this test statistic S was corrected by using an effective sample size. The modified variance of the Mann-Kendall test statistic is given by:

$$Var^*(S) = Var(S) * CF \tag{3.5}$$

Where $Var(S)$ is the variance of the Mann-Kendall test statistic S for the original sample data and CF is a correction factor (Yue and Wang, 2004) calculated as:

$$CF = 1 + 2 \sum_{k=1}^{n-1} \frac{r_k(1-k)}{n} \tag{3.6}$$

Where r_k is the lag-k serial correlation coefficient of data. In this study, it is assumed that the time series was adequately described by an autoregressive process of order one. Then, the corrected variance is:

$$Var^*(S) = Var(S) \frac{(1 + r_1)}{(1 - r_1)} \tag{3.7}$$

Where r_1 is the autocorrelation of the detrended time series (Wilks, 2011). The lag-1 serial correlation coefficient (r_1) was computed as:

$$r_1 = \frac{\frac{1}{n-1}\sum_{i=1}^{n-1}(x_i - E(x_i))(x_{i+1} - E(x_i))}{\frac{i}{n}\sum_{i=1}^{n}(x_i - E(x_i))^2} \quad (3.8)$$

Where $E(x_i)$ is the mean of sample data and n is the sample size. To test the significance of the autocorrelation, a one-tailed test (alternative hypothesis is that true r_1 is greater than zero) was used and the critical value of r_1 for a 5% significance level was computed as:

$$r_1' = \frac{-1 + 1.645\sqrt{n-2}}{n-1} \quad (3.9)$$

Once a statistically significant autocorrelation of the time series was found, *Var*(S)* was used instead of *Var(S)* in Equation 3.4 to estimate *Z*. By doing that, the influence of serial correlation in the test's statistics was removed.

Additionally, the trend slope was calculated using the method of Sen (1968). The magnitude of the slope of the trend was estimated as (Gocic and Trajkovic, 2013):

$$Q_o = \frac{x_j - x_i}{j - i} \quad for\ o = 1, \dots, N \quad (3.10)$$

Where x_i and x_j are data at time i and j $(j>i)$, respectively. If there are n values in the time series, then $N=n(n-1)/2$ slope estimates are possible. Then, the N values of Q_o are ranked from smallest to largest and the median of slope or Sen's slope estimator is:

$$Q_{med} = \begin{cases} Q_{[(N+1)/2]}, if\ N\ is\ odd \\ \frac{Q_{N/2} + Q_{\left[\frac{N+2}{2}\right]}}{2}, if\ N\ is\ even \end{cases} \quad (3.11)$$

The Q_{med} sign reflects the data trend, while its value indicates the steepness of the trend. To determine whether the median slope is statistically different from zero, one should obtain the confidence interval of Q_{med} at a specific probability (Gilbert, 1987; Hollander and Wolfe, 1973) as:

$$C_\propto = Z_{1-\propto/2}\sqrt{Var(S)} \quad (3.12)$$

Where *Var(S)* is defined in Equation 3.3 or *Var*(S)* if the time series is statistically significant auto-correlated, and $Z_{1-\alpha/2}$ is obtained from the standard normal distribution table. Then, $M_1=(N-C_\alpha)/2$ and $M_2=(N+C_\alpha)/2$ are computed. The lower and upper limits of confidence interval, Q_{min} and Q_{max}, are the M_1^{th} largest and $(M_2+1)^{th}$ largest of the N ordered slope estimates. The slope Q_{med} is statistically different than zero if the two limits (Q_{min} and Q_{max}) have similar sign. To conclude that a time-series has a statistically significant trend, both the MK test and the Q_{med} Sen's slope have to be statistically significant; then the sign and slope of that trend is given by Sen's slope calculations.

C. Results

To evaluate the effect of using a specific calendar on the trend analysis of rainfall indices, I calculated the percentage of stations that exhibited different trends (either the signal, the statistical significance or both) when the hydrologic year was used instead of the Western calendar (Table 3.2). The indices that were most sensitive to the use of hydrologic year calendar were the consecutive dry days (CDD) and the extremely wet day rainfall (R99p) as 41.5% and 34% of stations exhibited different trends, respectively. The least sensitive index was the number of very heavy rainfall days (R20), the wet-day annual rainfall (PRCPTOT) and the annual percentage of wet days (Wdays), with only 9.4%, 15.1% and 11.3% of stations, respectively, exhibiting a different trend after using hydrologic years.

Stations that showed statistically significant trends in rainfall indices analyzed here and separated according to the four major regions in CSPA are displayed in Table 3.3 (PRCPTOT, SDII, CDD, CWD, R10 and R20) and Table 3.4 (R95p, R99p, RX1day, RX5day, R95pTOT, R99pTOT, Wdays, p25th and p75th). In region A (the Amazon basin), approximately ~20-

40% out of a total of nine stations exhibited negative trend in PRCPTOT, SDII, CWD, R10, RX1day, RX5day and Wdays; positive trends were observed for R95pTOT, R99pTOT and Wdays. In region B (the Central Pacific basin), about 30-40% out of fourteen stations indicated negative trends in SDII, CDD, RX1day and RX5day whereas ~20% of stations showed a positive trend in Wdays. In region C (the Southern Pacific basin), ~20% of the thirteen stations showed a negative trend in CDD and a positive trend in RX1day. In region D (the Titicaca basin), ~30% of the eleven stations exhibited a positive trend in RX1day. In general, statistically significant trends in the indices are consistent among indices for most stations.

Table 3.2. Percentage of stations over Central and Southern Peruvian Andes with different trends when using the hydrologic calendar rather than the Western calendar years for the calculation of rainfall indices during 1965-2009 hydrologic years.

Index	Stations (%)
Wet-days annual rainfall (PRCPTOT)	15.1
Simple daily rainfall intensity (SDII)	20.8
Consecutive dry days (CDD)	41.5
Consecutive wet days (CWD)	20.8
Number of heavy rainfall days (R10)	20.8
Number of very heavy rainfall days (R20)	9.4
Very wet day rainfall (R95p)	32.1
Extremely wet day rainfall (R99p)	34.0
Maximum 1-day rainfall (RX1day)	24.5
Maximum 5-day rainfall (RX5day)	17.0
Very wet day proportion (R95pTOT)	26.4
Extremely wet day proportion (R99pTOT)	24.5
Percentage of wet days (Wdays)	11.3
Twenty-fifth percentile (p25th)	15.1
Seventy-fifth percentile (p75th)	20.8

Table 3.3. Stations with statistically significant trends in total and extreme rainfall indices over Central and Southern Peruvian Andes during 1965-2009 hydrologic years. Rainfall indices are denoted as: wet-days annual rainfall (PRCPTOT), simple daily rainfall intensity (SDII), consecutive dry days (CDD), consecutive wet days (CWD), number of heavy rainfall days (R10) and number of very heavy rainfall days (R20).

Index	Region A: Amazon basin		Region B: Central Pacific basin		Region C: Southern Pacific basin		Region D: Titicaca basin	
	Negative trend	Positive trend	Negative trend	Positive trend	Negative trend	Positive trend	Negative trend	Positive trend
PRCPTOT	Huayao, Marcapomacocha	-	-	Parquin	-	-	-	-
SDII	Huayao, La Quinua, Marcapomacocha, Pisac	Pilchaca	Antioquia, Huangascar, Pariacancha, San Lazaro De Escomarca, Santiago De Tuna	Huamantanga, Parquin	-	Chivay	Laraqueri	Lampa, Progreso
CDD	-	Pilchaca	Antioquia, Cordova, Huamantanga, Matucana, Pirca, Santiago De Tuna	Paccho	Sitajara, Susapaya, Talabaya	-	Chilligua	-
CWD	Huayao, Marcapomacocha	Urubamba	Huangascar, Pirca	Parquin, San Lazaro De Escomarca	-	Sitajara	Chilligua	-
R10	Huayao, La Quinua, Marcapomacocha, Pisac	-	Pariacancha	Huamantanga, Parquin	Crucero Alto	Chivay	Laraqueri	Chilligua, Progreso
R20	Huayao	-	Pariacancha, Santiago De Tuna	Paccho	Ichuna	-	-	Chilligua

Table 3.4. As Table 3.3, but for very wet day rainfall (R95p), extremely wet day rainfall (R99p), maximum 1-day rainfall (RX1day), maximum 5-day rainfall (RX5day), very wet day proportion (R95pTOT), extremely wet day proportion (R99pTOT), percentage of wet days (Wdays), twenty-fifth percentile of daily rainfall (p25th) and seventy-fifth percentile of daily rainfall (p75th).

Index	Region A: Amazon basin		Region B: Central Pacific basin		Region C: Southern Pacific basin		Region D: Titicaca basin	
	Negative trend	Positive trend	Negative trend	Positive trend	Negative trend	Positive trend	Negative trend	Positive trend
R95p, R99p	Huayao	Tanta	Antioquia, Pariacancha	-	Cairani	Las Salinas, Talabaya	-	Chilligua
RX1day	Huayao, Marcapomacocha	Pisac	Antioquia, Pariacancha, Puquio, Santiago De Tuna	Huamantanga, Pirca	Ichuna	Chivay, Las Salinas, Talabaya	-	Chilligua, Pampahuta, Taraco
RX5day	Huayao, Marcapomacocha, Pisac	-	Antioquia, Huangascar, Pariacancha, Santiago De Tuna	Huamantanga, Parquin	-	Chivay, Las Salinas	Huancane	Chilligua
R95pTOT, R99pTOT	Tanta	Huayao, Marcapomacocha	Parquin, Santiago De Tuna	-	-	-	-	-
WDays	Marcapomacocha, Pilchaca	La Quinua, Tanta, Urubamba,Yantac	-	Pirca, San Lazaro De Escomarca, Santiago De Tuna	-	-	Progreso	-
p25th	Huayao, La Quinua, Pisac	-	Huamantanga, Huangascar, Paccho, Pirca, San Lazaro De Escomarca, Santa Cruz	Parquin	Crucero Alto, Talabaya	-	Laraqueri, Munani	Azangaro, Progreso
p75th	Huayao, La Quinua, Marcapomacocha, Pisac	-	Huangascar, Pirca, San Lazaro De Escomarca, Santiago De Tuna	Huamantanga	Talabaya	Chivay	Laraqueri	Chilligua, Lampa, Progreso

The spatial variability of the signal along with the statistical significance of trends of eight rainfall indices are shown in Figure 3.1 (PRCPTOT, CDD, R95p and RX1day) and Figure 3.2 (RX5day, Wdays, p25th and p75th). Trends exhibited a large degree of variability over the CSPA stations, and trends in most stations were not statistically significant. Notice that stations within the same major region or even within the same subregion may show different trends. Coherent spatial trends were only observed in certain subregions and for some indices as, for instance, a decrease in PRCPTOT over subregion 2, an increase of RX1day over subregion 4, and a decrease of RX5day over subregion 6. The possible reasons for these discrepancies could be related to the interaction of different atmospheric forcings with the complex orography of the study region, resulting in a large spatial variability of rainfall and rainfall trends. Nevertheless, the existence or not of statically significant trends should be interpreted with caution given the period of data availability. For instance, Morin (2011) found that annual rainfall trends over the tropics have a tendency to be undetectable because of high rainfall means and variability. In that study, the author investigated rainfall trends in central Peruvian Andes during 1951-2000 and showed that that trends in the eastern (western) side of the central Peruvian Andes were detected only where there was a change of about 20 to 40% (40 to 75%) of the annual rainfall with respect to the mean annual rainfall in the same period. These conditions are rarely observed for the stations evaluated over CSPA.

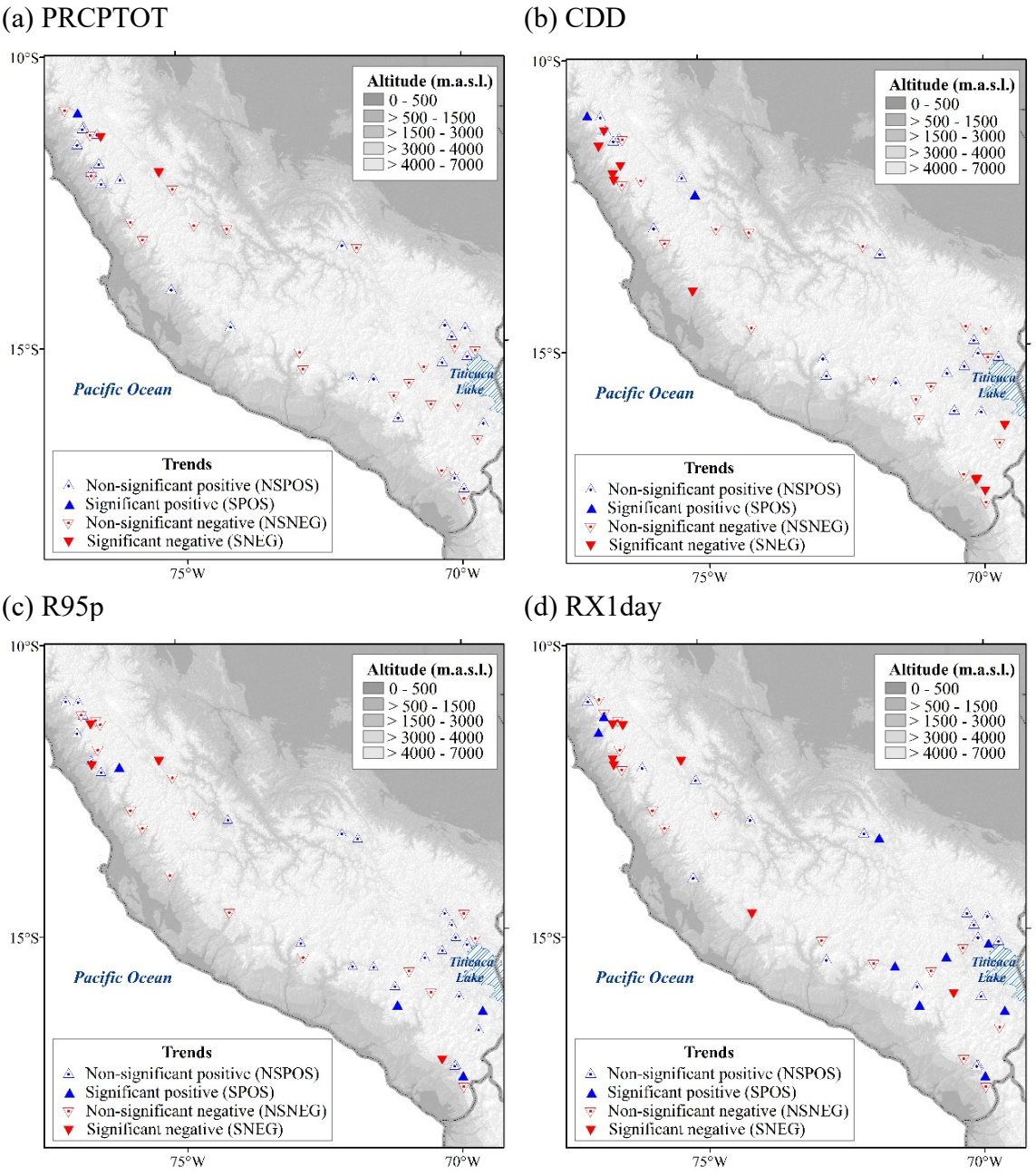

Figure 3.1. Trends in total and extreme rainfall indices over Central and Southern Peruvian Andes during 1965-2009 water years: (a) wet-days annual rainfall (PRCPTOT), (b) consecutive dry days (CDD), (c) very wet day rainfall (R95p), and (d) maximum 1-day rainfall (RX1day).

(a) RX5day

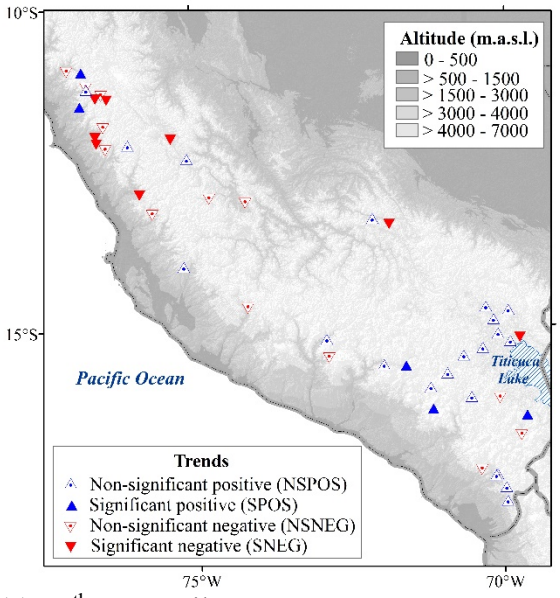

(b) Wdays

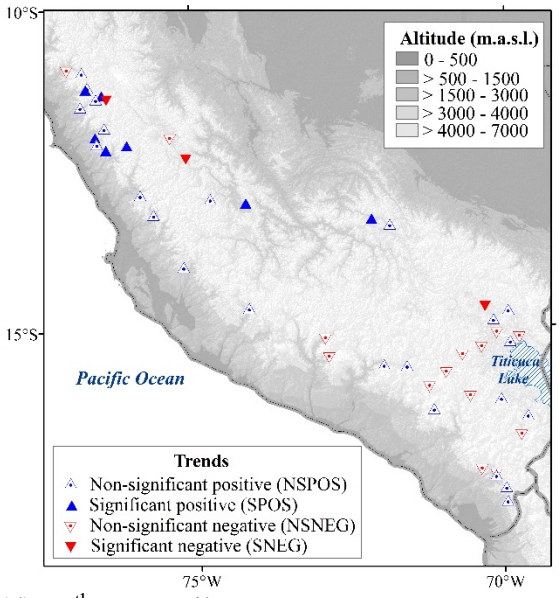

(c) 25th percentile

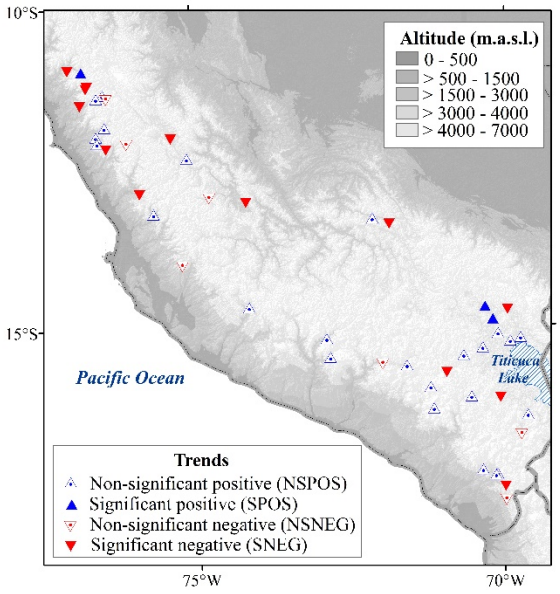

(d) 75th percentile

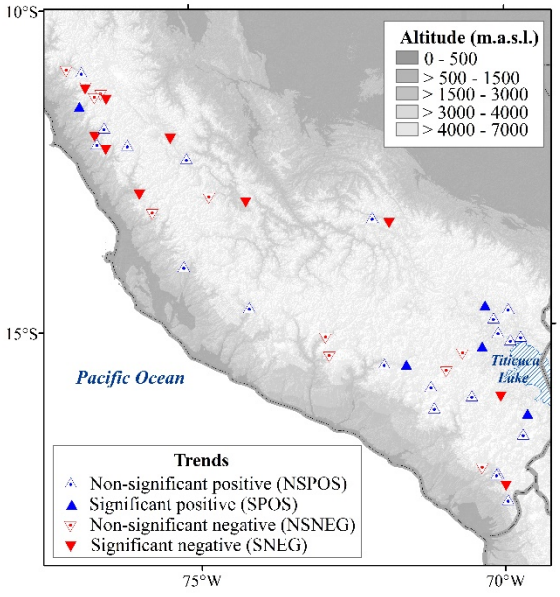

Figure 3.2. As in Figure 3.1, but for: (a) maximum 5-day rainfall (RX5day), (b) annual percentage of wet days (Wdays), (c) 25th percentile, and (d) 75th percentile.

A comparison between trends of six representative rainfall indices obtained by Haylock *et al*. (2006), Skansi *et al*. (2013) and this study at common stations located over CSPA is shown in Table 3.5. Regarding PRCPTOT, a statistically significant decrease in the Amazon basin stations was found in this study, while Haylock *et al*. (2006) and Skansi *et al*. (2013)

found a non-significant negative trend. Both Skansi *et al*. (2013) and this study showed non-significant trends for Progreso station located in the Titicaca basin. With respect to extreme rainfall indices, there is a much larger discrepancy in trends among stations and studies. For instance, Huayao and Marcapomacocha stations in the Amazon basin exhibited statistically significant decrease of RX1day and RX5day in this study in contrast to Haylock *et al*. (2006) and Skansi *et al*. (2013) which found non-statistically significant trends. The possible reasons for these discrepancies are different lengths of time series, the adoption of different calendars to calculate the rainfall indices and the slightly different approaches used to assess trends.

Table 3.5. Comparison between sign and statistical significance of trends obtained for some rainfall indices at common stations analyzed in Haylock *et al.* (2006), Skansi *et al.* (2013) and the present study over Central and Southern Peruvian Andes. The rainfall indices compared are: wet-days annual rainfall (PRCPTOT), consecutive dry days (CDD), very wet day rainfall (R95p), extremely wet day rainfall (R99p), maximum 1-day rainfall (RX1day) and maximum 5-day rainfall (RX5day). The sign and the statistical significance of trends are expressed as: NSNEG (non-statistically significant negative), SNEG (statistically significant negative), NSPOS (non- statistically significant positive), and SPOS (statistically significant positive).

Station	Study	PRCPTOT	CDD	R95p	R99p	RX1day	RX5day
Huayao	Haylock *et al.*, 2006	NSNEG	NSNEG	NSNEG	NSNEG	NSNEG	NSNEG
	Skansi *et al.*, 2013	NSNEG	NSNEG	SNEG	NSPOS	NSNEG	NSNEG
	Current study	SNEG	NSPOS	SNEG	SNEG	SNEG	SNEG
Marcapo-macocha	Skansi *et al.*, 2013	NSNEG	-	NSNEG	NSNEG	-	-
	Current study	SNEG	NSNEG	NSNEG	NSNEG	SNEG	SNEG
Progreso	Skansi *et al.*, 2013	NSNEG	NSNEG	NSPOS	NSPOS	NSPOS	NSPOS
	Current study	NSPOS	NSPOS	NSPOS	NSPOS	NSPOS	NSPOS

D. Conclusions

The use of the hydrological calendar, which adequately characterizes the wet season, was shown to be important to evaluate trends in all forty-seven gauge stations located in Central and Southern Peruvian (CSPA) analyzed in this study, and more remarkably in coastal areas. To assess trends in rainfall indices, Mann-Kendall test and Sen's slope with a correction for time-series autocorrelation were applied to over thirty hydrologic years (1965-2009) of observed rainfall.

Trends in rainfall indices did not show a clear spatial pattern over most subregions of stations, except for a few areas and specific indices. Therefore, the main conclusions were based on statistically significant trends observed in around 30% of stations in each one of the four major regions in CSPA.

Despite the increase in the frequency of wet days, approximately 30-44% of the stations located over the Amazon basin (region A) exhibited negative trends in the yearly rainfall intensity, the number of heavy rainfall days and the maximum 5-days rainfall during 1965-2009. This means that although the number of rainy days has increased, this has not contributed to the increase in the total and mean rainfall indices for this region. Similar negative trends were also detected in the stations located in Central Pacific basin (region B); about 30-43% of the stations in this region showed a decrease in the yearly rainfall intensity, consecutive dry days, the maximum 1-day rainfall and the maximum 5-days rainfall. Despite the indication of consistent negative trends in some indices related to extreme rainfall in this region, about 20% of these stations also showed an increase in the frequency of wet days. In Southern Pacific basin (region C), about 20% of station had a decrease in consecutive dry days and an increase in maximum 1-day rainfall. Finally, one-third of the stations located over the Titicaca basin

(region D) showed an increase in the intensity of rainfall extremes (maximum 1-day rainfall), but these trends did not affect the total annual rainfall in the region.

In summary, important new information on total and extreme rainfall trends in CSPA was generated, which in some cases differ from previous studies because a larger number of quality-controlled stations with longer periods, a more complete number of extreme rainfall indices calculated using hydrologic calendar, and a robust method of trend analysis were used in this study.

CHAPTER IV. MJO-ENSO Influence on Rainfall

A. Introduction

The Madden-Julian Oscillation (MJO) is a couple convective and atmospheric circulation pattern that propagates eastward along the tropics with typical time scales of 20-100 days (Madden and Julian, 1971, 1972, Zhang, 2005, 2013). The typical large-scale pattern of enhanced and suppressed convection during the MJO life cycle shows enhanced convection originating over eastern Africa and suppressed convection over the maritime continent and western Pacific. This dipole of enhanced/suppressed convection slowly propagates eastward (phase speeds ~5 m/s) across the Indian Ocean and western Pacific. Due to the enhanced convective heating and teleconnections, the MJO influences weather variability along the tropical region as well as extratropics of both hemispheres (Jones and Carvalho, 2012; Valadão *et al.*, 2016; Wheeler and Hendon, 2004).

The MJO is recognized to be an important phenomenon bridging weather and climate and depending on its interactions with other phenomena (e.g. El Niño Southern Oscillation, ENSO), the MJO may influence the occurrence of extreme weather events worldwide (Zhang, 2013). On a global scale, around 40 % more extreme precipitation occurs during active MJO than during inactive MJO (Jones *et al.*, 2004b). For instance, impacts of the MJO on rainfall anomalies and extremes are reported in China (Zhang *et al.*, 2009), India (Pai *et al.*, 2011), Australia (Wheeler *et al.*, 2009), Africa (Pohl *et al.*, 2007), United States (Jones and Carvalho, 2012), Brazil (De Souza and Ambrizzi, 2006; Valadão *et al.*, 2015) and Chile (Barrett *et al.*, 2012; Juliá *et al.*, 2012).

The influence of the MJO on rainfall variability in South America has been studied by Nogues-Paegle *et al*. (2000), Carvalho *et al*. (2002, 2004), Liebmann *et al*. (2004), De Souza

and Ambrizzi (2006), Muza *et al*. (2009), Mo *et al*. (2012), and Alvarez *et al*. (2016). However, statistically significant rainfall patterns related to MJO conditions over the Andes are difficult to detect as a result of the sparse density of rainfall gauges in this region (Alvarez *et al.*, 2016). This chapter seeks to fill this gap in the current knowledge of intraseasonal variability of rainfall in the central Andes.

It is important to note that ENSO is the dominant source of interannual climate variability with significant influences on rainfall variability in South America. Roundy *et al*. (2010) and Moon *et al*. (2011) observed enhanced (suppressed) convection over the Maritime Continent and the monsoonal region of South America during La Niña (El Niño). The warm (cold) phase of ENSO is generally associated with below (above) average rainfall over tropical South America (Garreaud, 2009) and the Altiplano (Vuille *et al.*, 2000). In general, easterly (westerly) upper level winds are related to enhanced (suppressed) rainfall on interannual time-scales in the Altiplano resulting from the increased (reduced) moisture influx from east of the Andes (Garreaud and Aceituno, 2001; Vuille, 1999). Furthermore, there is spatially different responses in the central Peruvian Andes (Garreaud *et al.*, 2003) and southern Peruvian Andes (Perry *et al.*, 2014; Vuille and Keimig, 2004). Lagos *et al.* (2008) found weakly positive, neutral and moderately negative correlation coefficients between sea surface temperature (SST) anomalies in the Niño 3.4 region and rainfall in the northern, central and southern Peru, respectively. Lavado and Espinoza (2014) also described the spatial variability of rainfall impacts of ENSO in Peru. During strong La Niña (El Niño) events, they found decreased (increased) rainfall in the Southern Pacific, Titicaca, and Amazon basins (northern Pacific basin).

In regards to the MJO, Zhang (2005; 2013) made a comprehensive review of MJO mechanisms, impacts and its relationship with ENSO. There is lack of consensus on the mechanism explaining the MJO-ENSO interaction (Hendon *et al.*, 2007; Zavala-Garay, 2005). Slingo *et al.* (1999) and Hendon *et al.* (1999) showed MJO indices uncorrelated with ENSO. Kessler (2001), Jones *et al*. (2004a), Pohl and Matthews (2007) and Valadão *et al*. (2016) found no effects on the duration and frequency of MJO phases during different ENSO years. Whereas Deng *et al.* (2016) pointed out that the eastward-propagating MJO tends to strengthen (weaken) in the central equatorial Pacific during the warm (cold) SST episodes. Furthermore, major El Niño are shown to be preceded by strong episodes of the MJO (McPhaden, 2004, 2008). ENSO warming in the eastern Pacific tends to be preceded by enhanced MJO activities (Zavala-Garay, 2005), initiated after persistent Kelvin waves (Zhang and Gottschalck, 2002) and associated with westerly wind bursts (Hendon *et al.*, 2007; Seiki and Takayabu, 2007).

Roundy *et al*. (2010), Moon *et al*. (2011) and Hoell *et al*. (2014) described different rainfall patterns related to MJO-ENSO conditions mainly over the northern hemisphere. Enhanced/suppressed rainfall during MJO-ENSO periods can be expected despite the similar number of days of MJO phases during different ENSO years. ENSO modifies the background state of moist deep convection, wind, and temperature through which the MJO propagates (Roundy *et al.*, 2010). Roundy *et al*. (2010) investigated the modulation of global atmospheric circulation by the MJO and ENSO during 1974-2008 austral summer. They found MJO-ENSO teleconnections across the North Pacific Rim, North America, and North Atlantic.

The interactions between MJO and ENSO and their joint influences on rainfall over the Central and Southern Peruvian Andes (CSPA) have not been investigated in detail. The objective of this chapter is to investigate the following questions: *Does MJO-ENSO*

significantly modulate rainfall in the Peruvian Andes? What are the large-scale circulation and moisture patterns during rainfall events over the CSPA associated with MJO-ENSO? Is the MJO-ENSO influence on CSPA rainfall homogeneous in space?

The MJO influence on rainfall stations is difficult to detect, since large-scale atmospheric circulation related to the MJO is influenced by local topography (Matthews *et al.*, 2013; Valadão *et al.*, 2015). Previous studies used various types of datasets as 20-90 day band-pass filtered rainfall (Valadão *et al.*, 2016), monthly rainfall (Bourrel *et al.*, 2014), and Global Precipitation Climatology Project (GPCP) (Jones *et al.*, 2004b); and applied a variety of methods including the calculation of rainfall anomaly (Valadão *et al.*, 2016; Wheeler *et al.*, 2009) and standardized rainfall anomaly (Barrett *et al.*, 2012), and the test of proportions of rainfall extremes (Jones *et al.*, 2004b) to evaluate MJO effects on rainfall at local scales. Here, unfiltered daily rainfall data is used to characterize intraseasonal variability in stations. Also, an adaptation of the standardized anomaly and frequency of extremes used in Barrett *et al*. (2012) was devised. This adaptation (explained in section C.1) ensures that the statistical assumptions of the dataset are met, thus efficiently detecting MJO-ENSO influence on rainfall.

This chapter examines the relationships between the MJO phases during different ENSO conditions and the occurrence of enhanced rainfall in CSPA. The MJO-ENSO rainfall effects are described for homogeneous regions of stations separately, and the potential relationship between large-scale dynamics generated by MJO-ENSO and local impacts on rainfall is also discussed.

B. Data

1. Gauged stations

November-March 1979-2010 daily rainfall of forty-seven quality-controlled stations located in CSPA. Figure 2.1 shows the location of these stations (same stations used in Chapter 2 and 3) and the regions differentiated are: A (Amazon basin), B (Central Pacific basin), C (Southern Pacific basin), and D (Titicaca basin). It is important to study enhanced rainfall in CSPA, since the forty-seven stations show large contribution (44 to 100%) from rainfall exceeding the 75th percentile to the total Nov-Mar 1979-2010 rainfall.

2. Gridded datasets

To characterize changes in the atmospheric circulation associated with MJO-ENSO and their influence in the distribution of rainfall in Peru, 0.5-deg daily averages of lower (850-hPa, U850) and upper level (200-hPa, U200) winds from the Climate Forecast System Reanalysis (CFSR) were used (Saha *et al.*, 2010). Daily averages of Outgoing Longwave Radiation (OLR) was used as a proxy for tropical convection (Liebmann and Smith 1996). All gridded datasets were obtained for Nov-Mar 1979-2010. Lastly, vertically integrated moisture flux was computed with CFSR data by integrating specific humidity, zonal and meridional winds from the surface up to 200-hPa.

3. MJO index

To identify periods of active and inactive MJO days, the methodology explained in Jones and Carvalho (2014) was followed. First, the daily climatology was removed from OLR, U850 and U200 and a band-pass filter (20-200 day) was applied. A combined Empirical Orthogonal Function (EOF) analysis was performed by averaging the resulting anomalies around the equator (15°S and 15°N). The EOF patterns and phase evolution of the MJO

computed this way is in close agreement with the convention used by Wheeler and Hendon (2004). The primary difference is that Jones and Carvalho (2014) use band-passed anomalies, whereas Wheeler and Hendon (2004) use anomalies from the seasonal cycle. The life cycle of the MJO starts with enhanced convection in the western Indian Ocean (phase 1) and progressively moves eastward to the central Pacific (phase 8). MJO events were defined here when: 1) the phase angle between the first two time coefficients (PC1 and PC2) systematically rotated counterclockwise, indicating eastward propagation at least to the Maritime Continent; 2) the normalized amplitude ($\sqrt{PC1^2 + PC2^2}$) was always larger than 0.35; 3) the mean amplitude during the event was larger than 0.9; and 4) the entire duration of the event lasted between 30 and 90 days. When those conditions were not satisfied, the MJO was considered to be in a quiescent (inactive) phase. Figure 2 of Jones and Carvalho (2012) shows the characteristic dipole pattern of enhanced/suppressed convection during active MJO phases.

According to ONI, eleven El Niño (EN), eight La Niña (LN) and thirteen ENSO-neutral (NT) years occurred during 1979-2010. Table 4.1 shows the percentage of MJO days during Nov-Mar 1979-2010 and the percentage of EN, LN and NT days for each MJO phase. MJO active days occurred during 62% of the period analyzed here (4689 days). The percentage of days during each MJO phase occurred almost equally distributed among ENSO conditions, as noted in Valadão *et al*. (2016).

C. Methods

1. Rainfall patterns

The distribution of rainfall variance during Nov-Mar 1979-2010 was examined using power spectrum analysis. Forty CSPA stations, out of the forty-seven, were chosen to perform the power spectrum analysis since they had complete time-series. Before computing the power

Table 4.1. Percentage of MJO days from the entire period analyzed (Nov-Mar 1979-2010, 4689 days) and percentage of El Niño (EN), La Niña (LN) and ENSO-neutral (NT) days for each MJO phase. MJO activity refers to inactive (INA) and active (MJO) MJO conditions.

MJO activity	**MJO phase**	**Days out of the entire period (%)**	**EN days out of each MJO phase (%)**	**LN days out of each MJO phase (%)**	**NT days out of each MJO phase (%)**
INA	0	38	25	45	30
MJO	1	7	40	20	41
	2	9	42	23	35
	3	8	48	26	26
	4	7	43	23	34
	5	8	41	26	32
	6	8	33	26	41
	7	9	35	26	39
	8	6	38	27	35

spectrum, the long-term mean, linear trend and semi-annual cycle were removed from the time-series. The computation of the power spectrum followed the methodology described in Carvalho *et al.* (2012). For a given station, the power spectrum was first computed for each time series separately by applying 10% tapering at each end of the time series and raw spectral estimates computed with Fast Fourier Transform. The raw spectral estimates were then averaged using a moving average of length L=3. The smoothed spectra were normalized by the total variance and averaged together to obtain a 30-yr ensemble mean. The red-noise background spectrum was estimated with a first-order auto-regressive process. The 95% significance level of the ensemble spectrum was estimated with χ^2 distribution with the degrees of freedom adjusted by tapering.

To evaluate variations of rainfall during MJO-ENSO conditions at each station, the standardized anomaly of rainfall (*StAnom*) and the frequency of extreme rainfall (*FrqEx*)

during twenty-seven conditions of MJO-ENSO were calculated. The MJO-ENSO conditions are a combination of eight MJO phases, inactive MJO, and three ENSO conditions (EN, LN and NT). An extreme rainfall event was considered when the daily rainfall exceeded the 75th percentile during Nov-Mar 1979-2010. *StAnom* and *FrqEx* were calculated only for the CSPA stations that showed statistically significant intraseasonal variability.

StAnom was calculated based on the median rainfall during each MJO-ENSO condition ($M_{MJO-ENSO}$), and the median (M) and interquartile range (IQR) of rainfall during Nov-Mar 1979-2010. *StAnom* was calculated as in Junker *et al.* (2008) and Barrett *et al.* (2012), but using median and interquartile range instead of mean and standard deviation, respectively, since the data did not follow a normal distribution. Therefore, *StAnom* = $(M_{MJO-ENSO} - M)/IQR$.

FrqEx was calculated based on the number of extreme rainfall events ($NumEx_{MJO-ENSO}$) and the total number of days ($NumTot_{MJO-ENSO}$) per each MJO-ENSO condition. *FrqEx* was calculated as Barrett *et al.* (2012), but here the threshold to define extreme rainfall was the 75th percentile instead of one standard deviation. *FrqEx* (in %) was calculated as $\left(NumEx_{MJO-ENSO}\right) * 100/NumTot_{MJO-ENSO}$.

2. Atmospheric circulation

The climatology of vertically integrated moisture flux during Nov-Mar 1979-2010 was calculated to understand mean atmospheric circulation patterns. Composites of moisture flux anomalies (deviations from daily climatology) during MJO-ENSO conditions were used to evaluate atmospheric circulation patterns associated during those conditions. To assess the statistical significance of mean anomalies, the Student's t-test was applied. The test statistic (*t*) was $t = (X_{anom} * \sqrt{n' - 1})/S_{anom}$ (Wilks, 2011). Where the mean of the anomalies is X_{anom} s, n' is the number of MJO events, and S_{anom} is the standard deviation of anomalies. The

composite was statistically significant if t was greater-than, less-than or equal to the table critical value of two-tailed t-test with 95% confidence level and $n' - 1$ degrees of freedom. Note that n' was the number of MJO events; this was a more restrictive (robust) approach to test the statistical significance of anomalies than using the total number of days during each MJO-ENSO. An MJO event is defined as the period of consecutive days from the start to the end of the event.

D. Results

1. Rainfall patterns

Inspection of individual ensemble power spectrum of rainfall shows important intraseasonal variability in most CSPA stations. Thirty-three stations, out of the forty stations analyzed, showed statistically significant peaks between 20 to 100 days. To illustrate intraseasonal variability, Figure 4.1 shows the power spectrum over selected CSPA stations, while Figure 4.2 indicates the locations that exhibit intraseasonal and non-intraseasonal rainfall variability. From the forty CSPA stations analyzed, 75%, 83%, 92% and 75% of stations in regions A (Amazon basin), B (Central Pacific basin), C (Southern Pacific basin) and D (Titicaca basin), respectively, show intraseasonal rainfall variability. Despite the high altitude and complex terrain of CSPA stations, the four regions show significant intraseasonal variability. The stations located in the coastal Pacific basin (regions A and B), western side of the Andes, are the most sensitive; while the stations located in the eastern side of the Andes (Amazon basin or region C) and in the high-Andean plateau (Titicaca basin or region D) are slightly less sensitive. These results motivate further explanation of the effects of the MJO, the main source of intraseasonal rainfall variability in the tropics, on CSPA and its variations during different ENSO conditions.

MJO-ENSO rainfall patterns were studied using standardized anomaly (*StAnom*) and frequency of enhanced rainfall (*FrqEx*) during each MJO-ENSO condition. The location of stations and its geographic features determined if MJO-ENSO imprints an effect on rainfall at local scales. Suppressed rainfall (*StAnom* less than -0.5), enhanced rainfall (*StAnom* greater than 0.5) and the frequency of extreme rainfall (*FrqEx*) greater than 20% varied greatly depending on the location of CSPA region, the MJO phase and the ENSO condition.

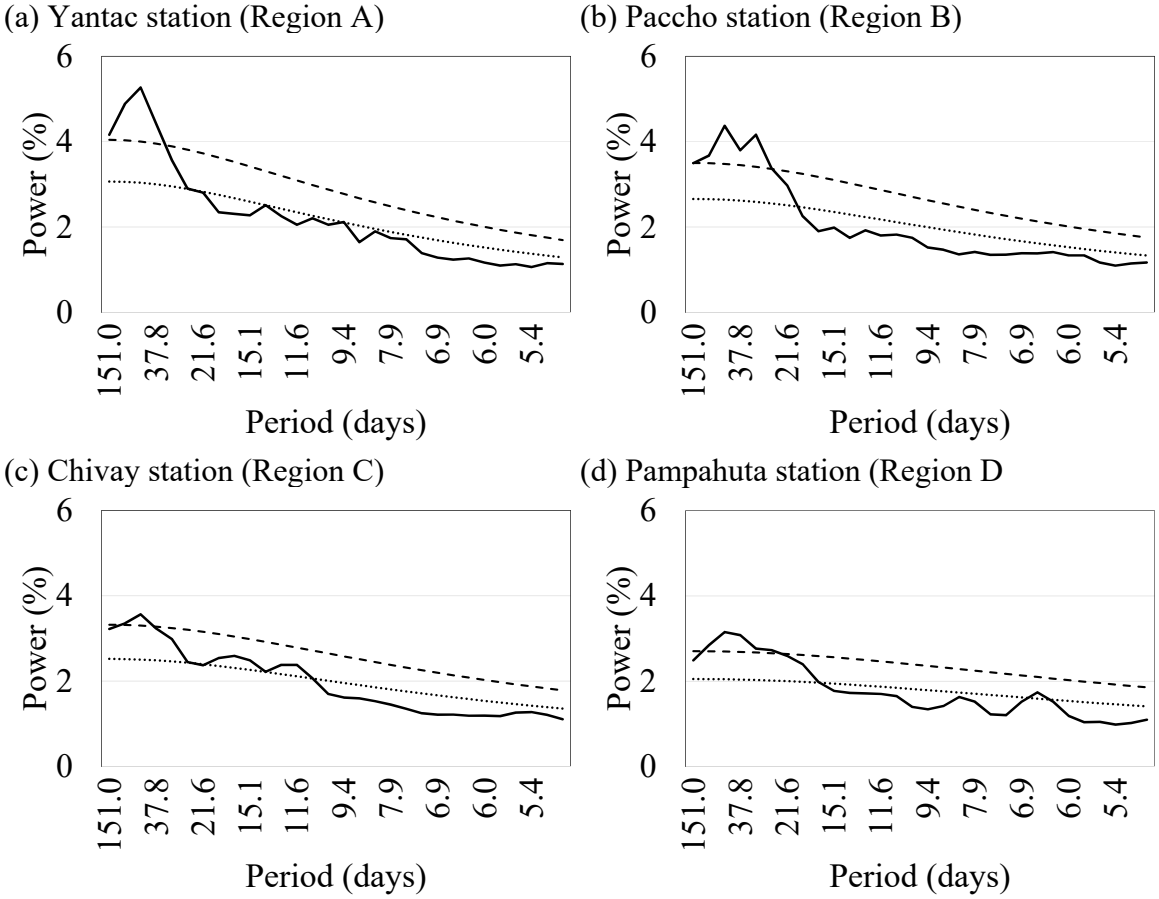

Figure 4.1. Power spectrum of some Central and Southern Peruvian Andes stations during Nov-Mar 1979-2010: (a) Yantac station (located in region A), (b) Paccho station (located in region B), (c) Chivay station (located in region C), and (d) Pampahuta station (located in region D). Continuous, dotted and dashed line represent power spectrum, background red-noise spectrum and 95 % significance level, respectively.

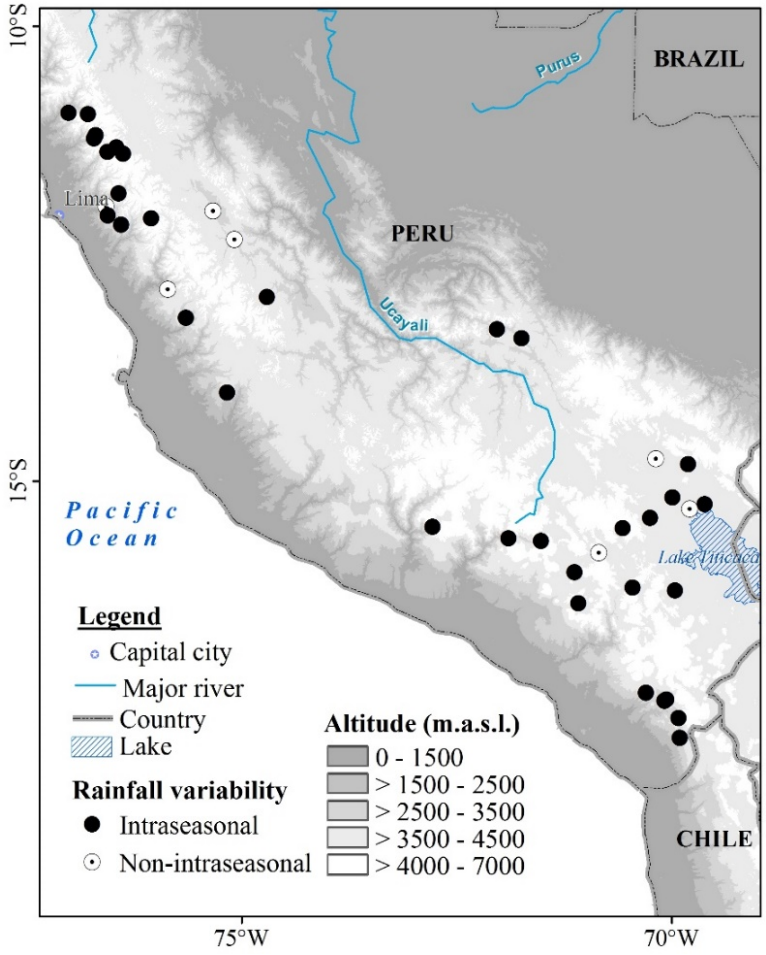

Figure 4.2. Stations with intraseasonal or non-intraseasonal rainfall variability during Nov-Mar 1979-2010.

The percentage of stations from each CSPA region that experienced suppressed rainfall during different MJO and ENSO phases is shown in Figure 4.3. 70-80% of stations in region A showed *StAnom* less than -0.5 during MJO1-EN, MJO2-EN, MJO5-EN, MJO8-EN and MJO2-LN (Figure 4.3 a). About 70% of the stations located in region B have suppressed rainfall during MJO4-EN (Figure 4.3 b). About 60% of the stations located in region C show suppressed rainfall during MJO8-EN and MJO4-LN (Figure 4.3 c). About 80% of stations in region D have suppressed rainfall during MJO1-EN, MJO3-EN, MJO5-EN and MJO2-NT (Figure 4.3 d).

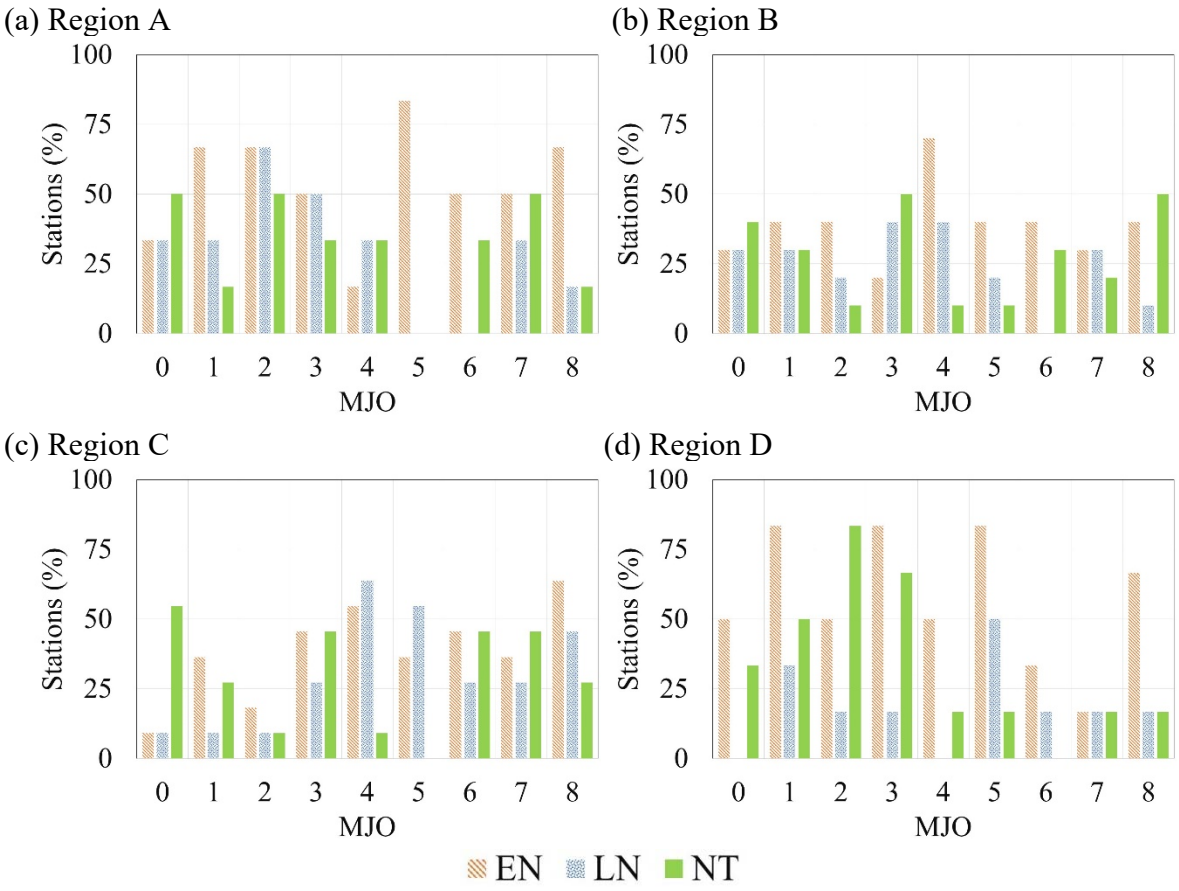

Figure 4.3. Percentage of Central and Southern Peruvian Andes (CSPA) stations with suppressed rainfall (*StAnom* < -0.5) for different MJO-ENSO conditions during Nov-Mar 1979-2010. CSPA regions of stations: (a) A (Amazon basin), (b) B (Central Pacific basin), (c) C (Southern Pacific basin) and (d) D (Titicaca basin).

Figure 4.4 shows the percentage of stations from each CSPA region that experienced enhanced rainfall during different MJO-ENSO phases. 70-80% of the stations located in region A showed *StAnom* greater than 0.5 during MJO5-LN, MJO6-LN, MJO8-LN, MJO4-NT, MJO5-NT and MJO8-NT (Figure 4.4 a). 60-70% of stations in region B showed enhanced rainfall during MJO5-LN, MJO6-LN, MJO8-LN, MJO4-NT and MJO5-NT (Figure 4.4 b). 60-70% of stations in region C had enhanced rainfall during MJO1-LN, MJO3-LN, MJO6-LN and MJO2-NT (Figure 4.4 c). 70-80% of stations in region D had enhanced rainfall during

MJO2-LN, MJO4-LN, MJO7-LN, MJO8-LN, MJO6-NT, MJO7-NT and MJO8-NT (Figure 4.4 d).

The percentage of stations from each CSPA region that experienced frequencies of extreme rainfall (*FrqEx*) greater than 20% during different MJO-ENSO conditions is shown in Figure 4.5. This percentage of stations is about 70% only during MJO3-LN in region A (Figure 4.5 a) and C (Figure 4.5 c). The frequency of enhanced rainfall greater than 20% is not observed in more than half the stations in all regions during EN or NT conditions.

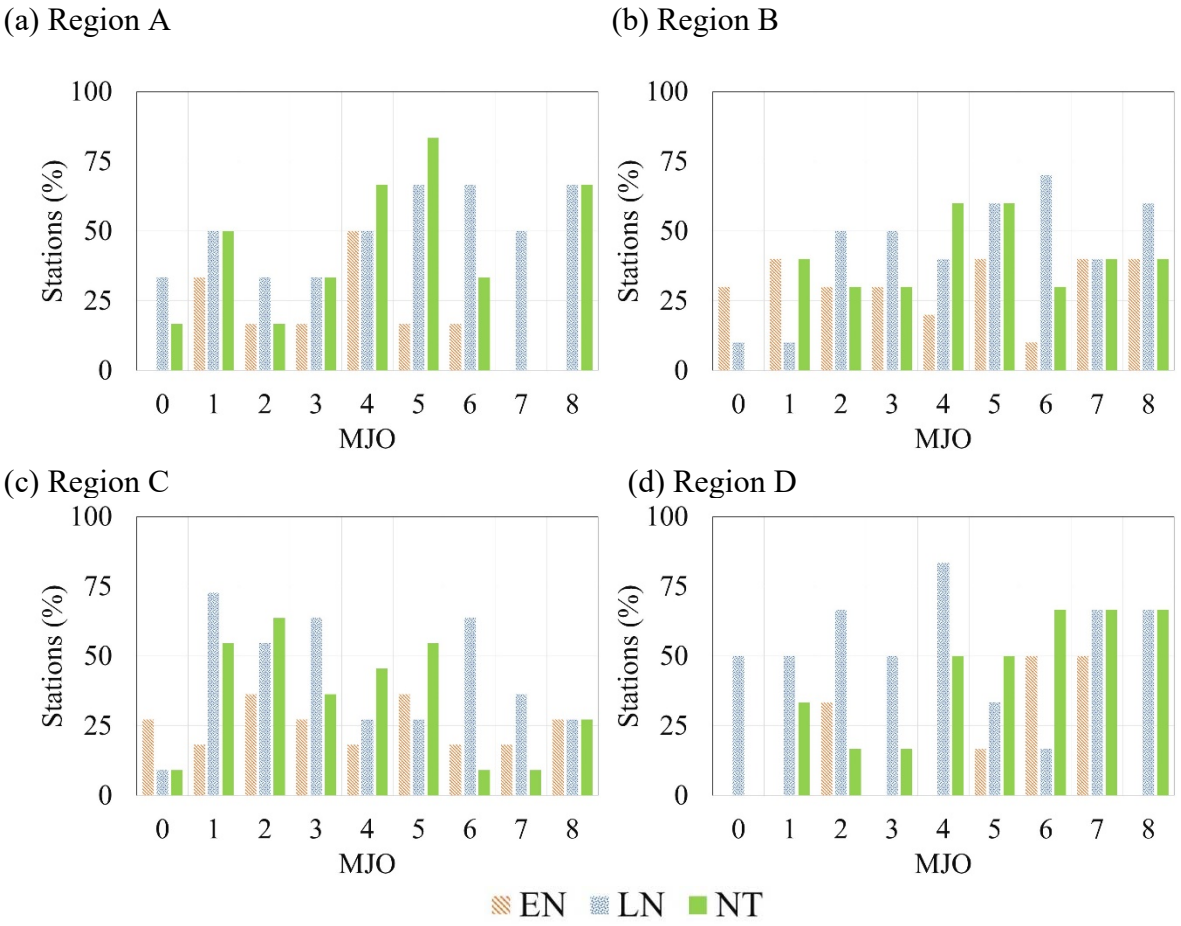

Figure 4.4. As Figure 4.3, but for enhanced rainfall (*StAnom* > 0.5).

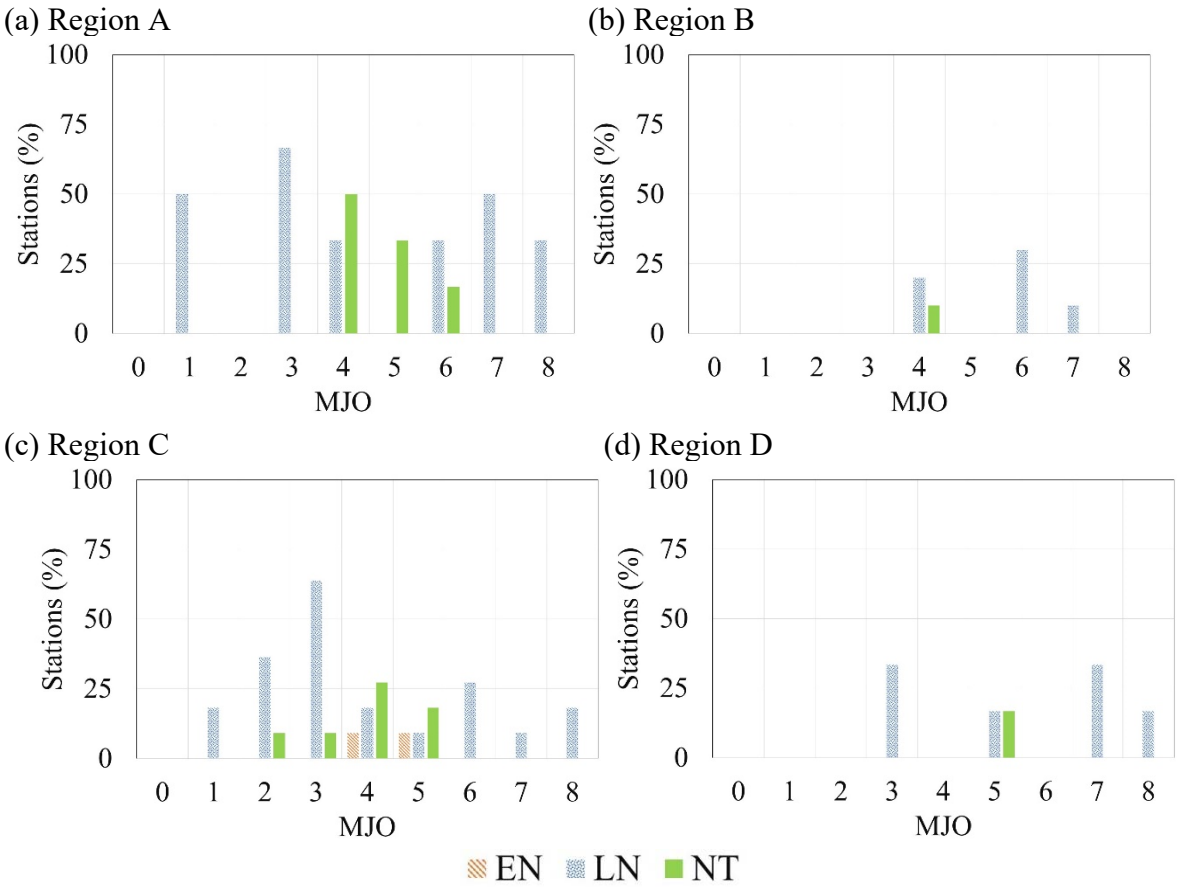

Figure 4.5. As Figure 4.4, but for frequencies of extreme rainfall events greater than 20% (*FrqEx* > 20%).

2. Atmospheric circulation

To relate the above-mentioned changes in gauged rainfall with moisture flux patterns, both the climatology and anomalies of moisture flux were calculated. The climatology of moisture flux over South America is presented in Figure 4.6. It shows the typical easterly moisture flux transport near the equator. On the eastern slopes of the Andes, moisture flux circulation progressively has a northerly component due to the topographic barrier. Moisture is then transported toward subtropical South America. The general features of integrated moisture transport obtained with CFSR reanalysis agrees with other studies that analyzed daily low-level winds from NCEP-NCAR reanalysis (e.g. Carvalho *et al.* (2002), Jones and Carvalho

(2002) and Marengo *et al.* (2012)). The low-level moisture transport is a key ingredient for the maintenance of strong convective activity over the Amazon basin and the associated upper-level circulation characterized by the Bolivian High.

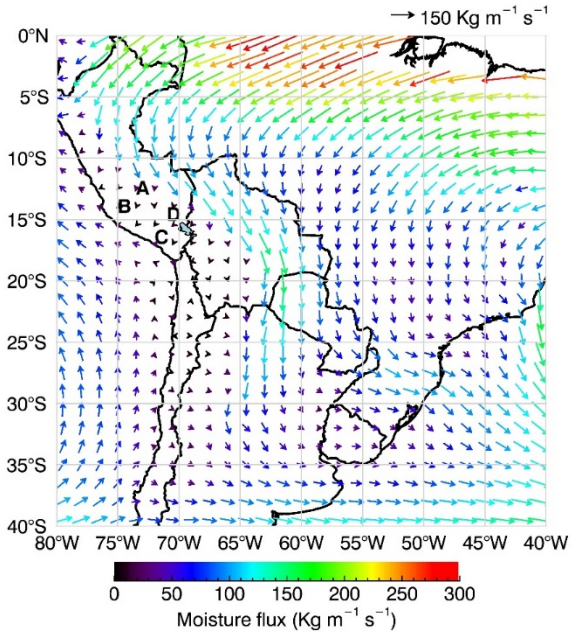

Figure 4.6. Climatology of vertically integrated moisture flux over most of South America during Nov-Mar 1979-2010. Central and Southern Peruvian Andes regions are denoted as A (Amazon basin), B (Central Pacific basin), C (Southern Pacific basin), and D (Titicaca basin).

The atmospheric circulation during MJO-ENSO conditions is described with composites of intraseasonal moisture flux anomalies, which are presented in Figure 4.7 (MJO phases 1 to 4) and Figure 4.8 (MJO phases 5 to 8) for EN conditions, in Figure 4.9 (MJO phases 1 to 4) and Figure 4.10 (MJO phases 5 to 8) for LN conditions, and in Figure 4.11 (MJO phases 1 to 4) and Figure 4.12 (MJO phases 5 to 8) for NT conditions. The predominant direction of statistically significant moisture flux anomalies during different MJO-ENSO conditions over each CSPA region is summarized in Table 4.2 based on Figures 4.7 to 4.12. During MJO phase 1, moisture flux direction has easterly or southerly components in all CSPA regions during all ENSO conditions. During MJO phase 2, southerly moisture flux is seen in region C (A and B)

during EN (LN). During MJO phase 3, easterly or northeasterly directions are predominant in all CSPA regions during EN and NT, while southeasterly directions are seen in region B during LN. During MJO phase 4, northerly (easterly) moisture flux anomalies are evident in all (most) CSPA regions during EN (LN). During MJO phase 5, moisture flux direction has easterly or southeasterly components in all (most) CSPA regions during EN (LN and NT). During MJO phase 6, moisture flux has easterly components in most CSPA regions during NT. During MJO phase 7, westerly or northwesterly moisture flux anomalies are evident in all (most) CSPA regions during EN (NT). During MJO phase 8, westerly or northwesterly anomalies are seen in all CSPA regions (regions A and D) during EN (NT), and in region A and B during LN.

Likewise, the predominant direction of statistically significant moisture flux anomalies during different MJO-ENSO conditions over two contrasting locations in South America (outside CSPA) is summarized in Table 4.3 based on Figures 4.7 to 4.12. These two locations which showed spatially consistent moisture flux anomalies are the western Amazon (centered approximately in 5°S and 65°W) and the east of the Andes region (centered between 12.5°S and 17.5°S, to the east of the Andes). Westerly (easterly) moisture flux anomalies are seen over western Amazon associated with southeasterly (northwesterly) anomalies over the east of the Andes region during certain MJO-ENSO. Statistically significant westerly (southeasterly) anomalies of moisture flux are seen over western Amazon (east of the Andes) during MJO1-EN, MJO4-LN, MJO5-LN and MJO1-NT. Statistically significant easterly (northwesterly) anomalies of moisture flux are seen over western Amazon (east of the Andes) during MJO6-EN, MJO8-EN, MJO5-NT, MJO7-NT and MJO8-NT.

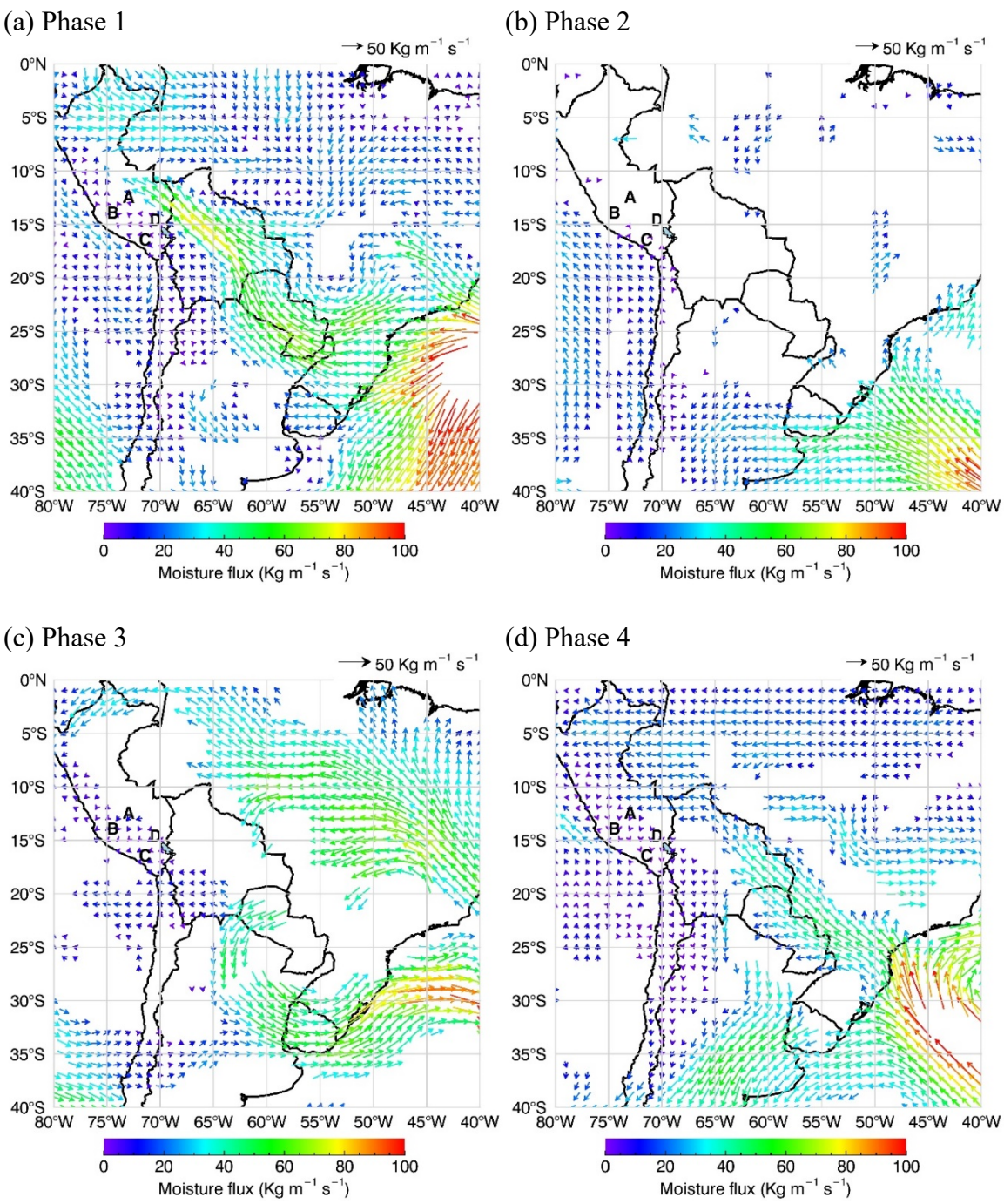

Figure 4.7. Composites of 20-100 days filtered anomalies of vertically integrated moisture flux during El Niño years and different MJO phases of the period Nov-Mar 1979-2010; where the different MJO phases are (a) Phase 1, (b) Phase 2, (c) Phase 3, and (d) Phase 4. Central and Southern Peruvian Andes regions are denoted as A (Amazon basin), B (central Pacific basin), C (southern Pacific basin), and D (Titicaca basin). Only statistically significant mean filtered anomalies were mapped, based on a 2-tailed t-test with 95% level of confidence.

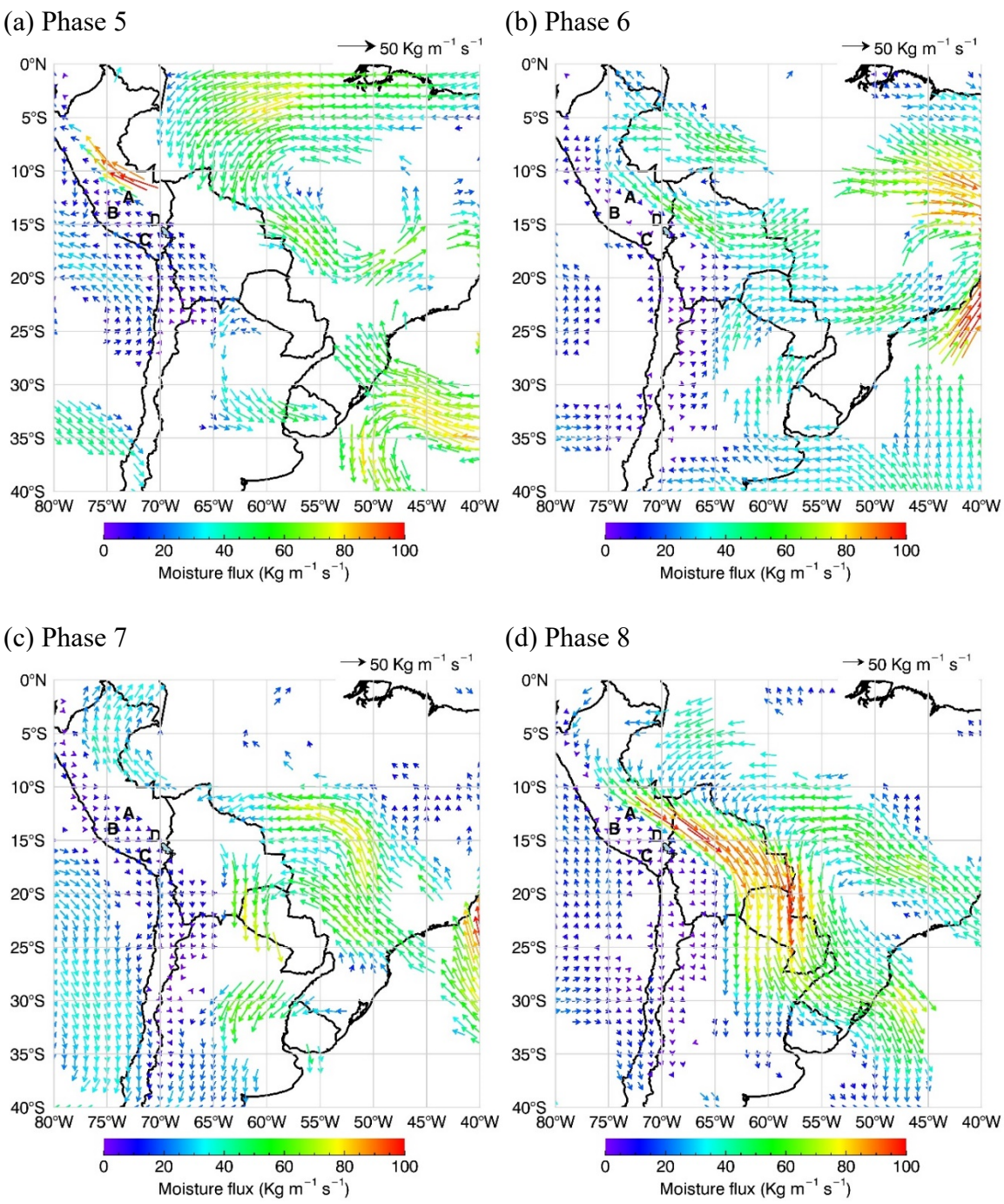

Figure 4.8. As Figure 4.7, but for MJO (a) Phase 5, (b) Phase 6, (c) Phase 7 and (d) Phase 8.

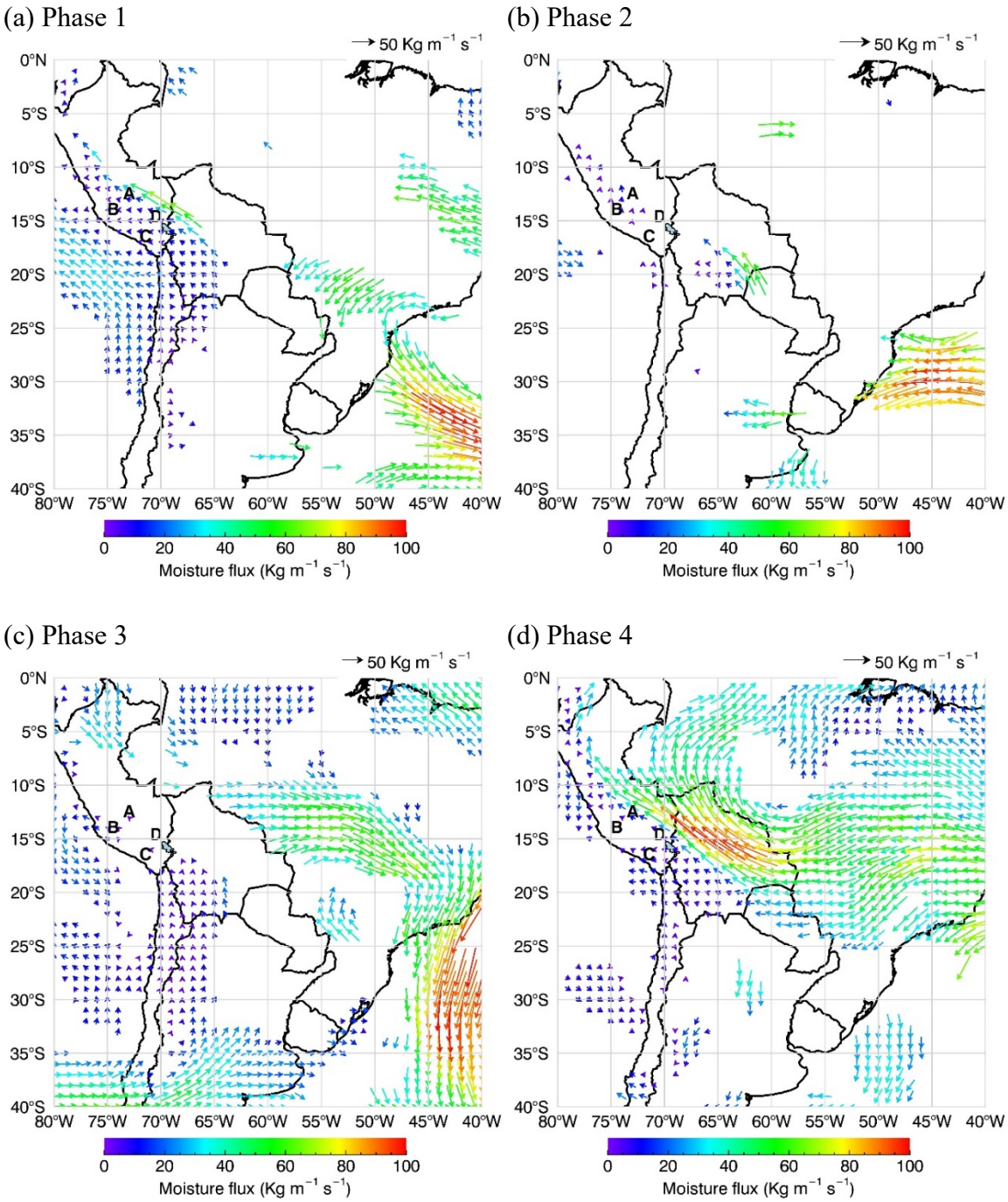

Figure 4.9. Composites of 20-100 days filtered anomalies of vertically integrated moisture flux during La Niña years and different MJO phases of the period Nov-Mar 1979-2010; where the different MJO phases are (a) Phase 1, (b) Phase 2, (c) Phase 3, and (d) Phase 4. Central and Southern Peruvian Andes regions are denoted as A (Amazon basin), B (central Pacific basin), C (southern Pacific basin), and D (Titicaca basin). Only statistically significant mean filtered anomalies were mapped, based on a 2-tailed t-test with 95% level of confidence.

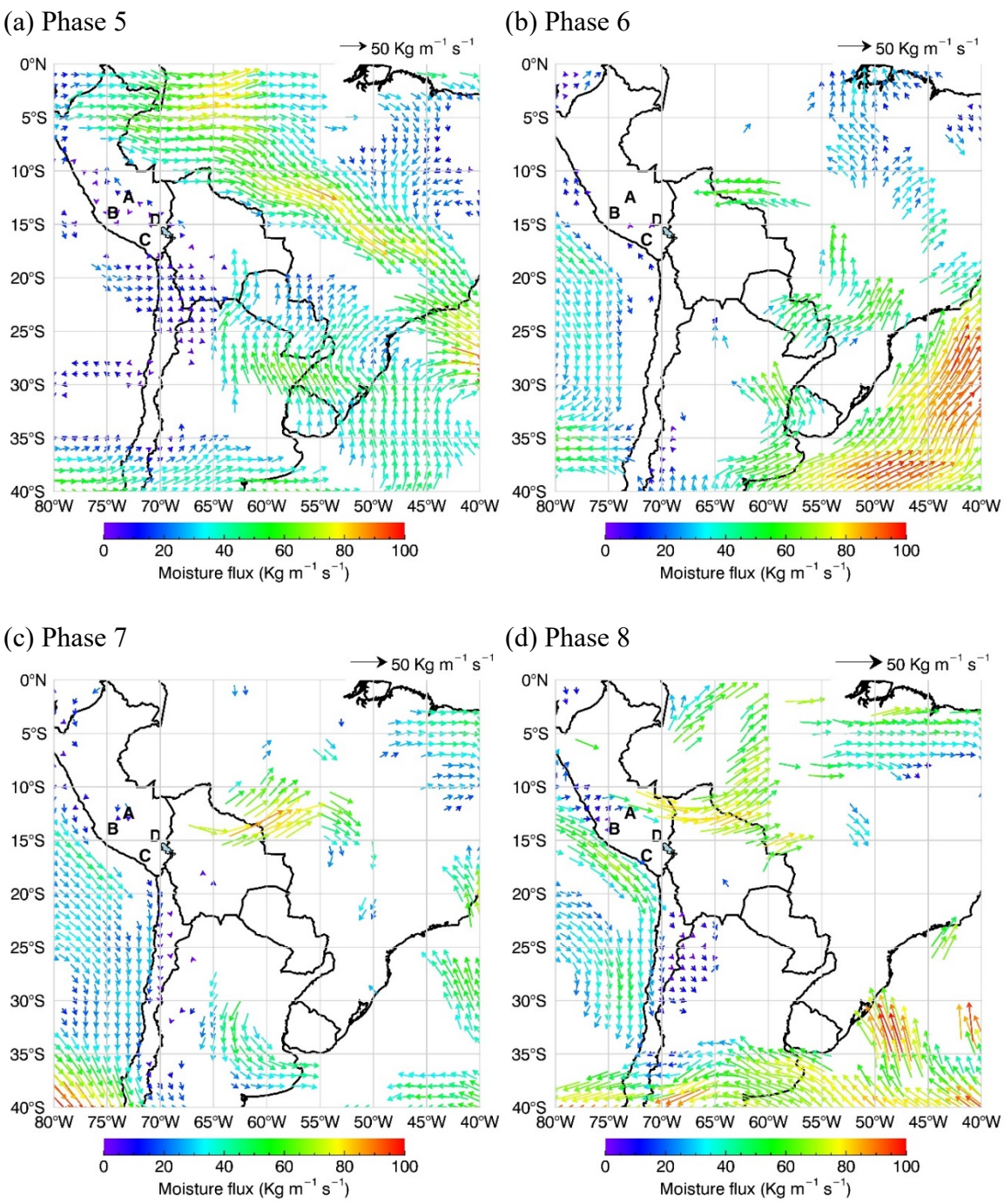

Figure 4.10. As Figure 4.9, but for MJO (a) Phase 5, (b) Phase 6, (c) Phase 7 and (d) Phase 8.

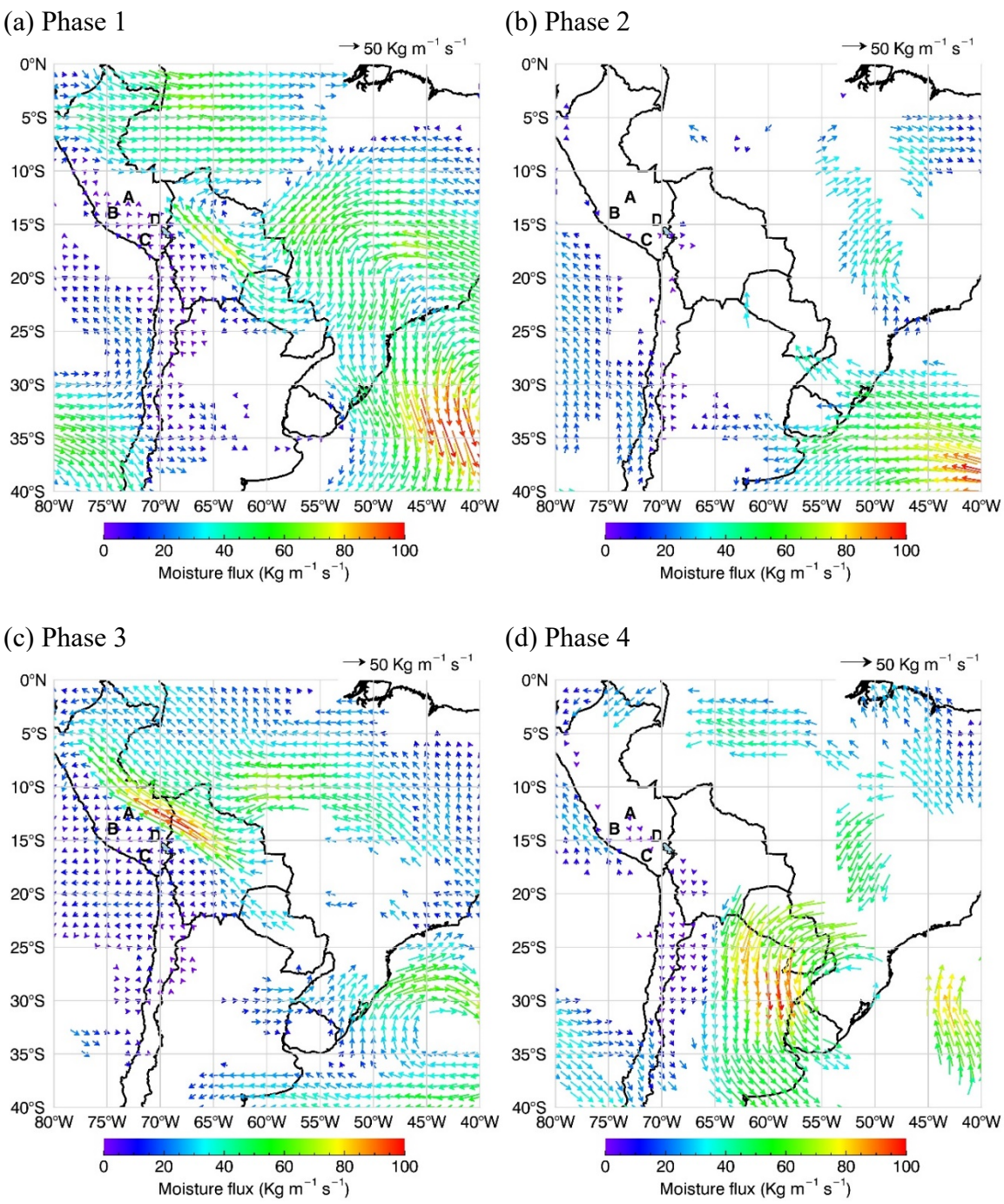

Figure 4.11. Composites of 20-100 days filtered anomalies of vertically integrated moisture flux during ENSO-neutral years and different MJO phases of the period Nov-Mar 1979-2010; where the different MJO phases are (a) Phase 1, (b) Phase 2, (c) Phase 3, and (d) Phase 4. Central and Southern Peruvian Andes regions are denoted as A (Amazon basin), B (central Pacific basin), C (southern Pacific basin), and D (Titicaca basin). Only statistically significant mean filtered anomalies were mapped, based on a 2-tailed t-test with 95% level of confidence.

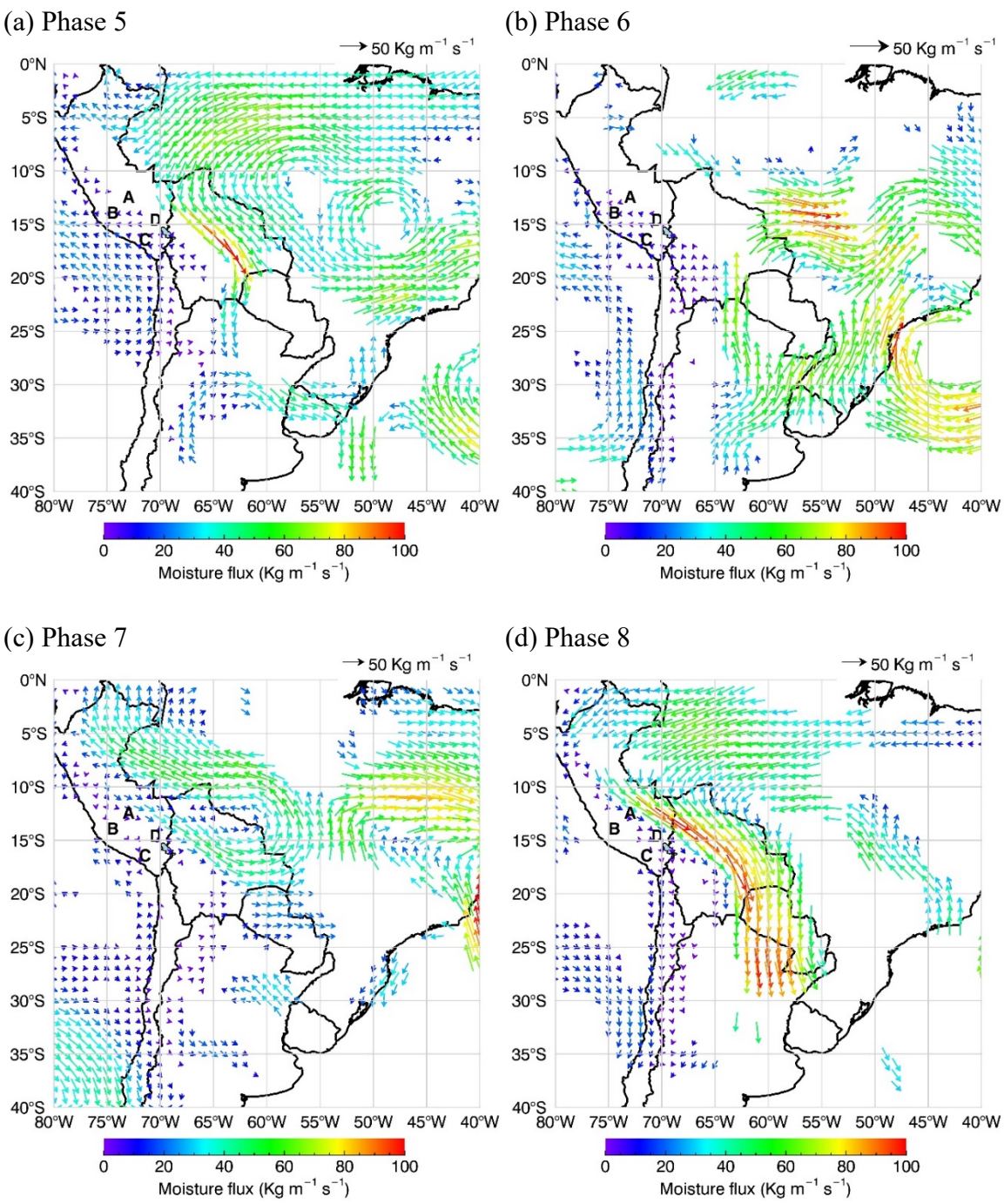

Figure 4.12. As Figure 4.11, but for MJO (a) Phase 5, (b) Phase 6, (c) Phase 7 and (d) Phase 8.

Table 4.2. Prevailing directions of statistically significant moisture flux anomalies during MJO active phases (1 to 8) and different ENSO conditions (EN, LN and NT) of the period Nov-Mar 1979-2010 over each Central and Southern Peruvian Andes (CSPA) region. CSPA regions are A (Amazon basin), B (Central Pacific basin), C (Southern Pacific basin) and D (Titicaca basin). The directions of anomalies are northerly (↓), easterly (←), southerly (↑), westerly (→), northeasterly (↙), northwesterly (↘) and southeasterly (↖).

MJO	Region	ENSO		
		EN	LN	NT
1	A	↖	↖	↑
	B	↖	←	↑
	C	←	←	↖
	D	↖	↖	↖
2	A	-	↑	-
	B	-	↑	-
	C	↑	-	-
	D	-	-	-
3	A	↙	-	←
	B	↙	↖	←
	C	←	-	←
	D	←	-	←
4	A	↓	↖	↓
	B	↓	-	-
	C	↓	←	-
	D	↓	←	-
5	A	↖	↖	-
	B	←	↓	←
	C	←	-	←
	D	←	↖	←
6	A	↘	-	-
	B	-	-	←
	C	-	-	←
	D	-	-	↖
7	A	→	↓	↘
	B	→	-	-
	C	↘	-	↓
	D	↘	-	→
8	A	↘	→	↘
	B	→	→	-
	C	→	-	-
	D	→	-	↘

Table 4.3. As Table 4.2, but over two contrasting locations in South America: western Amazon and east of the Andes.

MJO	Location	ENSO		
		EN	LN	NT
1	Western Amazon	→	-	→
	East of the Andes	↖	↖	↖
2	Western Amazon	-	-	-
	East of the Andes	-	-	-
3	Western Amazon	-	-	←
	East of the Andes	-	-	↖
4	Western Amazon	←	→	←
	East of the Andes	-	↖	-
5	Western Amazon	←	→	←
	East of the Andes	↖	↖	↘
6	Western Amazon	←	-	-
	East of the Andes	↘	-	-
7	Western Amazon	-	-	←
	East of the Andes	-	-	↘
8	Western Amazon	←	-	←
	East of the Andes	↘	-	↘

E. Discussion

To describe the atmospheric patterns potentially related to the MJO-ENSO effects on rainfall over each CSPA region, we compared the outstanding features of suppressed rainfall, enhanced rainfall and enhanced frequency of extreme events (shown in Figures 4.3 to 4.5) with moisture flux anomalies (shown in Figures 4.7 to 4.12). This comparison is summarized in Table 4.4. More than 55% of stations in each CSPA region experience suppressed rainfall mainly during EN conditions and certain MJO phases, and this effect is associated with different directions of moisture flux anomalies. In region A, the suppressed rainfall that occurs during MJO1-EN, MJO5-EN, MJO8-EN and MJO2-LN is associated with statistically significant moisture flux anomalies with southeasterly, southeasterly, northwesterly and southerly directions in region A, respectively. In region B, suppressed rainfall is evident

Table 4.4. Summary of suppressed rainfall (SupR), enhanced rainfall (EnhR), enhanced frequencies of extreme rainfall events (FrqEx) and direction of statistically significant moisture flux anomalies (Mflux) during different MJO-ENSO conditions for each CSPA region. SupR, EnhR and FrqEx show an 'X' ('-') when more (less) than 55% of stations per each region reported suppressed rainfall, enhanced rainfall and enhanced rainfall extremes, respectively. Mflux shows the direction of spatially coherent moisture flux anomalies: northerly (↓), easterly (←), southerly (↑), westerly (→), northeasterly (↙), northwesterly (↘) and southeasterly (↖). 'X' is colored in red (blue) to highlight the MJO-ENSO conditions when rainfall is suppressed (enhanced) and a spatially coherent moisture flux in the region is present.

Region	MJO	SupR			EnhR			FrqEx			Mflux		
		EN	LN	NT	EN	LN	NT	EN	LN	NT	EN	LN	NT
A	1	X	-	-	-	-	-	-	-	-	↖	↖	↑
	2	X	X	-	-	-	-	-	-	-	-	↑	-
	3	-	-	-	-	-	-	-	X	-	↙	-	←
	4	-	-	-	-	-	X	-	-	-	↓	↖	↓
	5	X	-	-	-	X	X	-	-	-	↖	↖	-
	6	-	-	-	-	X	-	-	-	-	↘	-	-
	7	-	-	-	-	-	-	-	-	-	→	↓	↘
	8	X	-	-	-	X	X	-	-	-	↘	→	↘
B	1	-	-	-	-	-	-	-	-	-	↖	←	↑
	2	-	-	-	-	-	-	-	-	-	-	↑	-
	3	-	-	-	-	-	-	-	-	-	↙	↖	←
	4	X	-	-	-	-	X	-	-	-	↓	-	-
	5	-	-	-	-	X	X	-	-	-	←	↓	←
	6	-	-	-	-	X	-	-	-	-	-	-	←
	7	-	-	-	-	-	-	-	-	-	→	-	-
	8	-	-	-	-	X	-	-	-	-	→	→	-
C	1	-	-	-	-	X	X	-	-	-	←	←	↖
	2	-	-	-	-	X	X	-	-	-	↑	-	-
	3	-	-	-	-	X	-	-	X	-	←	-	←
	4	X	X	-	-	-	-	-	-	-	↓	←	-
	5	-	X	-	-	-	X	-	-	-	←	-	←
	6	-	-	-	-	X	-	-	-	-	-	-	←
	7	-	-	-	-	-	-	-	-	-	↘	-	↓
	8	X	-	-	-	-	-	-	-	-	→	-	-
D	1	X	-	-	-	-	-	-	-	-	↖	↖	↖
	2	-	-	X	-	X	-	-	-	-	-	-	-
	3	X	-	X	-	-	-	-	-	-	←	-	←
	4	-	-	-	-	X	-	-	-	-	↓	←	-
	5	X	-	-	-	-	-	-	-	-	←	↖	←
	6	-	-	-	-	-	X	-	-	-	-	-	↖
	7	-	-	-	-	X	X	-	-	-	↘	-	→
	8	X	-	-	-	X	X	-	-	-	→	-	↘

during MJO4-EN; a condition that shows statistically significant northerly moisture flux anomalies in region B. In region C, suppressed rainfall occurs during MJO4-EN, MJO8-EN and MJO4-LN; these conditions show statistically significant northerly, westerly and easterly moisture flux anomalies in region C, respectively. In region D, suppressed rainfall is evident during MJO1-EN, MJO3-EN, MJO5-EN, MJO8-EN and MJO3-NT; conditions that are associated with statistically significant southeasterly, easterly, easterly, westerly and easterly moisture flux anomalies in region D, respectively.

MJO-ENSO generated spatially-dependent enhanced rainfall associated with different atmospheric circulation patterns over CSPA (Table 4.4). In general, more than 55% of stations in each CSPA region experience enhanced rainfall mainly during LN and NT conditions and certain MJO phases. In region A, the enhanced rainfall that occurs during MJO5-LN, MJO8-LN, MJO4-NT and MJO8-NT show statistically significant moisture flux anomalies with southerly, westerly, northerly and northwesterly directions, respectively. In region B, enhanced rainfall during MJO5-LN, MJO8-LN and MJO5-NT show statistically significant northerly, westerly and easterly moisture flux anomalies in region B, respectively. In region C, enhanced rainfall during MJO1-LN, MJO1-NT and MJO5-NT show easterly, southeasterly and easterly directions in region C, respectively. In region D, enhanced rainfall during MJO4-LN, MJO6-NT, MJO7-NT and MJO8-LN show statistically significant moisture flux anomalies with easterly, southeasterly, westerly and northwesterly directions in region D, respectively. Finally, the percentage of FrqEx greater than 20% occurs in regions A and C during MJO3-LN; a condition that shows non-statistically significant moisture flux anomaly over regions A and C.

The easterly (westerly) patterns found here (Table 4.3) over the western Amazon during certain MJO-ENSO conditions are consistent with the intraseasonal wind patterns shown in Carvalho *et al.* (2002) and Jones and Carvalho (2002) during break (active) phases of the South American Monsoon System or SAMS. They examined intraseasonal variations (10-70 days) in low-level wind circulation and OLR and found evidence of enhanced convection over southeast Brazil (centered in 15°S and 50°W), suppressed convection over the Altiplano (centered in 20°S and 65°W), and suppressed convection over northern South America (centered in 4°N and 65°W) during westerly regimes or active phase of SAMS; while opposite patterns occurred during easterly regimes or the break phase of SAMS.

Lastly, the transport of moisture from the Amazon to the Andean region is a well-known condition that generates rainfall over CSPA (Garreaud *et al.* 2009; Giovannettone and Barros 2009; Perry *et al.* 2014; among others). Here, this pattern (transport of moisture from the east) is seen during certain MJO-ENSO conditions and is related to enhanced rainfall in some CSPA regions; as during (a) MJO5-LN in region A, (b) MJO5-NT in region B, (c) MJO1-LN, MJO1-NT and MJO5-NT in region C, and (d) MJO4-LN and MJO6-NT in region D. Nevertheless, rainfall modulation solely by MJO-ENSO conditions can be difficult to observe due to possible existence of complex terrain (Giovannettone and Barros, 2009) and local forcings (Gonzalez *et al.*, 2008) acting simultaneously (and/or remotely) in the study region. Therefore, adding space-time variability to the moist atmospheric processes. Future analysis, most likely by using climate modeling approaches, would be needed to further explain the following complex processes simultaneously: MJO-ENSO modulation of rainfall, local forcing of mesoscale convective activity and topographic modulation of rainfall and moisture flux.

F. Conclusions

Daily gauged rainfall during November-March 1979-2010 was used to evaluate the effects of MJO-ENSO in the Central and Southern Peruvian Andes (CSPA). The CSPA stations analyzed in this study are located in four main regions: A (Amazon basin), B (Central Pacific basin), C (Southern Pacific basin) and D (Titicaca basin). Most stations in each CSPA region are sensitive to intraseasonal rainfall variability since they exhibit statistically significant power spectrum peaks on 20-100 time-scales. Only these stations, with evident intraseasonal rainfall variability, were used to evaluate MJO-ENSO effects on rainfall. The MJO-ENSO effects on gauged rainfall are described for each CSPA region based on standardized rainfall anomalies and frequency of rainfall extremes.

In general, none of the regions shows clear patterns of rainfall suppression or enhancement during inactive MJO for all ENSO conditions. During El Niño or EN (La Niña or LN and ENSO-neutral or NT), rainfall is suppressed (enhanced) in most CSPA stations depending on the MJO phase and the location of the stations. Suppressed rainfall is evident during MJO phases 1, 2, 5 and 8 with EN conditions in region A, during MJO phase 4 with EN conditions in region B, during MJO phase 4 with LN conditions or MJO phase 8 with EN conditions in region C, and during MJO phases 1, 3 and 5 with EN conditions or MJO phase 2 with NT conditions in region D.

Enhanced rainfall is experienced during MJO phases 4, 5 and 8 with NT conditions or MJO phases 5, 6 and 8 with LN conditions in region A, during MJO phases 4 and 5 with NT conditions or MJO phases 5, 6 and 8 with LN conditions in region B, during MJO phase 2 with NT conditions or MJO phases 1, 3 and 6 with LN conditions in region C, during MJO phases 6, 7 and 8 with NT or during MJO phases 2, 4, 7 and 8 with LN conditions in region D. Lastly,

most stations in regions A and C show frequencies of extreme rainfall greater than 20% during MJO phase 3 with LN conditions.

The MJO-ENSO conditions that generates positive or negative anomalies of CSPA rainfall are associated with different patterns of moisture flux anomalies in each CSPA region. The enhanced (suppressed) rainfall seen in region A during MJO5-LN, MJO8-LN, MJO4-NT and MJO8-NT (MJO1-EN, MJO5-EN, MJO8-EN and MJO2-LN) is associated with southerly, westerly, northerly and northwesterly (southeasterly, southeasterly, northwesterly and southerly) anomalies, respectively. In region B, the enhanced (suppressed) rainfall that occurs during MJO5-LN, MJO8-LN and MJO5-NT (MJO4-EN) is related to northerly, westerly and easterly (northerly) anomalies, respectively. In region C, the enhanced (suppressed) rainfall observed during MJO1-LN, MJO1-NT and MJO5-NT (MJO4-EN, MJO8-EN and MJO4-LN) is associated to easterly, southeasterly and easterly (northerly, westerly and easterly) anomalies, respectively. In region D, the enhanced (suppressed) rainfall seen during MJO4-LN, MJO6-NT, MJO7-NT and MJO8-NT (MJO1-EN, MJO3-EN, MJO5-EN, MJO8-EN and MJO3-NT) is related to easterly, southeasterly, westerly and northwesterly (southeasterly, easterly, easterly, westerly and easterly) anomalies, respectively.

CHAPTER V. Final conclusions and recommendations

The regionalization of CSPA rainfall stations proposed in this study not only proved to be useful to describe trends over homogeneous regions, but also to better differentiate ENSO, PDO and MJO-ENSO location-dependent effects on rainfall. For each region, the mean and standard deviation of rainfall indices, geographic features and rainfall anomalies among stations were presented. In future studies, a greater number of stations with longer time-series should be used to test if the regionalization proposed here for CSPA is consistent over time. Moreover, this regionalization method could be applied in other mountainous regions.

ENSO and PDO effects in CSPA rainfall were described according to each region and subregion. All CSPA regions showed statistically significant positive (negative) anomalies of total and extreme rainfall indices (consecutive dry days) during La Niña (El Niño) years. Titicaca basin showed statistically significant positive (negative) anomalies of total annual rainfall during positive (negative) PDO. Except for the Central Pacific basin, all CSPA regions exhibited statistically significant positive (negative) anomalies of consecutive dry days during positive (negative) PDO. In addition to ENSO and PDO, other coupled climatic modes such as the North Atlantic Oscillation (NAO), the Atlantic Dipole (AD), and the Atlantic Multidecadal Oscillation (AMO), among others, may have played important role in rainfall patterns over the region. The independent influence of ENSO, PDO, NAO, AD, and AMO should be explored in future research, as long as the impacts of the diversity of ENSO (e.g strong, moderate, Central Pacific or Eastern Pacific El Niño) on regional rainfall.

Most CSPA stations showed non-statistically significant trends in rainfall indices during 1965-2009 hydrologic years. Stations with statistically significant trends at each CSPA region were identified and regions with at least one-third of their stations having statistically

significant trends were considered as exhibiting trends for a particular rainfall index. In the Amazon basin, the following trends were identified: decreased yearly rainfall intensity, number of heavy rainfall days and maximum 5-days rainfall, and increased number of rainy days. In the Central Pacific basin, the following trends were observed: decreased yearly rainfall intensity, consecutive dry days, maximum 1-day rainfall and maximum 5-days rainfall, and increased frequency of wet days. In the Southern Pacific basin, we observed decreased consecutive dry days and increased maximum 1-day rainfall. The Titicaca basin showed an increase in the intensity of rainfall extremes that did not affect the total annual rainfall.

The predominant absence of long term trends of rainfall indices over CSPA apparently resulted from the decade-dependent variability of the ENSO-rainfall relationship. Nevertheless, numerous factors may be important for the low-frequency variability in CSPA rainfall. Modeling studies could help to further investigate mechanisms causing rainfall variations and changes in CSPA and proxies could help to improve our understanding about low-frequency variability in the region. Upcoming modeling approaches should focus on evaluating the mesoscale-to-large atmospheric circulation and thermodynamics that could cause changes in the South American Monsoon System and orographic rainfall in CSPA.

This study demonstrated the impacts of MJO-ENSO (Nov-Mar 1979-2010) on rainfall over CSPA, and how the MJO influence varied according to the location of stations. During ENSO-neutral years, enhanced rainfall in stations located over upper Amazon and Central Pacific basins was evident during MJO phases 4 and 5, whereas MJO phase 2 (phases 6, 7 and 8) modulated enhanced rainfall in stations located over Southern Pacific (Titicaca) basin. During La Niña years, enhanced rainfall was evident during MJO phases 5, 6 and 8 in the Amazon and Central Pacific basins, whereas MJO phases 1, 3 and 6 (phases 2, 4, 7 and 8)

generated enhanced rainfall in Southern Pacific (Titicaca) basin. During El Niño years, suppressed rainfall was evident in MJO phases 1, 2, 5 and 8 in the Amazon basin, in phase 4 in the Central Pacific basin, in MJO phase 8 in the Southern Pacific basin, and in MJO phases 1, 3 and 5 in the Titicaca basin. The following interesting questions arise from this study, and should be addressed in the future: *Do MJO-ENSO effects on rainfall varies seasonally? Does the relationship between MJO-ENSO and rainfall depend on the evaluated decade? More importantly, what is the cause of MJO-ENSO impacts on rainfall?* This last question is challenging and there is no consensus in the literature yet. Therefore, a holistic overview of the interactions between the MJO and ENSO and consequent effects on circulation and thermodynamics is necessary to improve our understanding about the combined effect of these modes on rainfall in the Peruvian Andes.

In this study, total and extreme rainfall trends and intraseasonal-to-interannual rainfall variability were evaluated using point-wise data, which provided details of the local rainfall conditions. Nevertheless, mapping the spatial patterns of rainfall variability could be improved by using gridded data such as the obtained from satellite or model estimations. Satellite-derived rainfall (Tropical Rainfall Measurement Mission 3B42 or TRMM) and modeled rainfall (Weather Research and Forecasting or WRF) time-series were compared with gauged stations during Nov-Mar 1998-2010 over CSPA. Mean and total rainfall variability were well captured by TRMM and WRF. Nevertheless, the detection of rainfall extremes was difficult for both gridded sources. TRMM captured well the intraseasonal variability when compared with gauged data, showing a statistically significant peak of rainfall variability at 37 days in most locations. Future studies would benefit from the spatial information given by TRMM (or by the current Global Precipitation Measurement, also known as GPM) and WRF after being

improved by applying a suitable correction technique (e.g. wavelet-based merging of gridded and gauged datasets) or a downscaling process.

People living in Peru largely rely on rain falling in the Andean region for water consumption, agriculture, industry, and hydropower generation. Understanding well the rainfall variability and change in CSPA will improve the sustainable management of water resources in the region. This study, generated invaluable information regarding interannual-to-decadal variability and long-term rainfall changes based on observed data. Notwithstanding, two important questions remain to be answered in future studies: *Is there any long-term trend in water resources, economic activities and weather-related disasters potentially correlated to rainfall changes in CSPA? Are ENSO, PDO and MJO-ENSO impacts on CSPA rainfall also translated into impacts on streamflow, runoff, erosion, crop productivity and the occurrence of droughts, floods and landslides?* Finally, more crucial is to work on how to increase the preparedness and adaptation of local people to upcoming climate-related variability and change, as well as on how to improve the climate literacy of stakeholders so that they can achieve science-based strategies to cope with climate change in CSPA.

References

1. Alexander L V., Zhang X, Peterson TC, Caesar J, Gleason B, Klein Tank a. MG, Haylock M, Collins D, Trewin B, Rahimzadeh F, Tagipour A, Rupa Kumar K, Revadekar J, Griffiths G, Vincent L, Stephenson DB, Burn J, Aguilar E, Brunet M, Taylor M, New M, Zhai P, Rusticucci M, Vazquez-Aguirre JL. 2006. Global observed changes in daily climate extremes of temperature and precipitation. *Journal of Geophysical Research* **111**(D5): D05109. DOI: 10.1029/2005JD006290.
2. Alvarez MS, Vera CS, Kiladis GN, Liebmann B. 2016. Influence of the Madden Julian Oscillation on precipitation and surface air temperature in South America. *Climate Dynamics*. Springer Berlin Heidelberg **46**(1–2): 245–262. DOI: 10.1007/s00382-015-2581-6.
3. ANA (Autoridad Nacional del Agua). 2015. *Plan Nacional de Recursos Hídricos*. Ministerio de Agricultura y Riego: Lima.
4. Arias P a., Fu R, Vera C, Rojas M. 2015. A correlated shortening of the North and South American monsoon seasons in the past few decades. *Climate Dynamics*. DOI: 10.1007/s00382-015-2533-1.
5. Barrett BS, Carrasco JF, Testino AP. 2012. Madden-Julian oscillation (MJO) modulation of atmospheric circulation and chilean winter precipitation. *Journal of Climate* **25**(5): 1678–1688. DOI: 10.1175/JCLI-D-11-00216.1.
6. Beck C, Grieser J, Rudolf B, Schneider U. 2005. A new monthly precipitation climatology for the global land areas for the period 1951 to 2000. *Geophys. Res. Abstr* **7**: 181–190.
7. Bourrel L, Rau P, Dewitte B, Labat D, Lavado W, Coutaud A, Vera A, Alvarado A, Ordoñez J. 2014. Low-frequency modulation and trend of the relationship between ENSO and precipitation along the northern to centre Peruvian Pacific coast. *Hydrological Processes*. DOI: 10.1002/hyp.10247.
8. Carvalho L, Cavalcanti I. 2016. The South American Monsoon System (SAMS). In: Carvalho L and Jones C (eds) *The Monsoons and Climate Change: observations and modeling*. Springer, 262.
9. Carvalho LM V., Jones C. 2013. CMIP5 Simulations of Low-Level Tropospheric Temperature and Moisture over the Tropical Americas. *Journal of Climate* **26**(17): 6257–6286. DOI: 10.1175/JCLI-D-12-00532.1.
10. Carvalho LM V., Jones C, Posadas AND, Quiroz R, Bookhagen B, Liebmann B. 2012. Precipitation characteristics of the South American Monsoon System derived from multiple datasets. *Journal of Climate* **25**(13): 4600–4620. DOI: 10.1175/JCLI-D-11-00335.1.
11. Carvalho LM V., Jones C, Silva AE, Liebmann B, Silva Dias PL. 2011a. The South American Monsoon System and the 1970s climate transition. *International Journal of Climatology* **31**(8): 1248–1256. DOI: 10.1002/joc.2147.
12. Carvalho LM V., Silva AE, Jones C, Liebmann B, Silva Dias PL, Rocha HR. 2011b. Moisture transport and intraseasonal variability in the South America monsoon system. *Climate Dynamics* **36**(9–10): 1865–1880. DOI: 10.1007/s00382-010-0806-2.
13. Carvalho LM V, Jones C, Liebmann B. 2004. The South Atlantic Convergence Zone: Intensity, form, persistence, and relationships with intraseasonal to interannual activity and extreme rainfall. *Journal of Climate* **17**(1): 88–108.
14. Carvalho LM V, Jones C, Silva Dias M a F. 2002. Intraseasonal large-scale circulations and mesoscale convective activity in tropical South America during the TRMM-LBA campaign. *Journal of Geophysical Research: Atmospheres* **107**(20): 1–20. DOI: 10.1029/2001JD000745.
15. Comrie AC, Glenn EC. 1998. Principal components-based regionalization of

precipitation regimes across the southwest United States and northern Mexico, with an application to monsoon precipitation variability. *Climate Research* **10**(3): 201–215. DOI: 10.3354/cr010201.
16. De Souza EB, Ambrizzi T. 2006. Modulation of the intraseasonal rainfall over tropical Brazil by the Madden–Julian oscillation. *International Journal of Climatology* **26**(13): 1759–1776. DOI: 10.1002/joc.1331.
17. Deng L, Li T, Liu J, Peng M. 2016. Factors controlling the interannual variations of MJO intensity. *Journal of Meteorological Research* **30**(9620): 328–340. DOI: 10.1007/s13351-016-5113-3.1.
18. Donat MG, Alexander L V., Yang H, Durre I, Vose R, Dunn RJH, Willett KM, Aguilar E, Brunet M, Caesar J, Hewitson B, Jack C, Klein Tank a. MG, Kruger a. C, Marengo J, Peterson TC, Renom M, Oria Rojas C, Rusticucci M, Salinger J, Elrayah a. S, Sekele SS, Srivastava a. K, Trewin B, Villarroel C, Vincent L a., Zhai P, Zhang X, Kitching S. 2013. Updated analyses of temperature and precipitation extreme indices since the beginning of the twentieth century: The HadEX2 dataset. *Journal of Geophysical Research: Atmospheres* **118**(5): 2098–2118. DOI: 10.1002/jgrd.50150.
19. Donat MG, Sillmann J, Wild S, Alexander L V., Lippmann T, Zwiers FW. 2014. Consistency of temperature and precipitation extremes across various global gridded in situ and reanalysis datasets. *Journal of Climate* **27**(13): 5019–5035. DOI: 10.1175/JCLI-D-13-00405.1.
20. Espinoza JC, Ronchail J, Guyot JL, Junquas C, Vauchel P, Lavado W, Drapeau G, Pombosa R. 2011. Climate variability and extreme drought in the upper Solimoes River (western Amazon Basin): Understanding the exceptional 2010 drought. *Geophysical Research Letters* **38**(13): 1–6. DOI: 10.1029/2011GL047862.
21. Farr TG, Rosen PA, Caro E, Crippen R, Duren R, Hensley S, Kobrick M, Paller M, Rodriguez E, Roth L, Seal D, Shaffer S, Shimada J, Umland J, Werner M, Oskin M, Burbank D, Alsdorf D. 2007. The Shuttle Radar Topography Mission. *Reviews of geophysics* (2005): 1–33. DOI: 10.1029/2005RG000183.
22. Folland CK, Miller C, Bader D, Crowe M, Jones P, Plummer N, Richman M, Parker DE, Rogers J, Scholefield P. 1999. Workshop on indices and indicators for climate extremes, Asheville, NC, USA 3-6 June 1997. Breakout group C: Temperature indices for climate extremes. *Climate Change* **42**: 31–43.
23. Garreaud RD. 2009. The Andes climate and weather. *Advances in Geosciences*, 3–11. DOI: 10.5194/adgeo-22-3-2009.
24. Garreaud RD, Aceituno P. 2001. Interannual rainfall variability over the South American Altiplano. *J Climate* **14**(1987): 2779–2789.
25. Garreaud RD, Vuille M, Clement AC. 2003. The climate of the Altiplano: observed current conditions and mechanisms of past changes. *Palaeogeography, Palaeoclimatology, Palaeoecology* **194**(1–3): 5–22. DOI: 10.1016/S0031-0182(03)00269-4.
26. Garreaud RD, Vuille M, Compagnucci R, Marengo J. 2009. Present-day South American climate. *Palaeogeography, Palaeoclimatology, Palaeoecology*. Elsevier B.V. **281**(3–4): 180–195. DOI: 10.1016/j.palaeo.2007.10.032.
27. Gilbert RO. 1987. *Statistical methods for environmental pollution monitoring*. John Wiley & Sons: New York.
28. Giovannettone JP, Barros AP. 2009. Probing regional orographic controls of precipitation and cloudiness in the Central Andes using satellite data. *Journal of Hydrometeorology* **10**(1): 167–182. DOI: 10.1175/2008JHM973.1.
29. Gocic M, Trajkovic S. 2013. Analysis of changes in meteorological variables using Mann-Kendall and Sen's slope estimator statistical tests in Serbia. *Global and Planetary Change*. Elsevier B.V. **100**: 172–182. DOI:

10.1016/j.gloplacha.2012.10.014.
30. Gonzalez PLM, Vera CS, Liebmann B, Kiladis G. 2008. Intraseasonal variability in subtropical South America as depicted by precipitation data. *Climate Dynamics* **30**(7–8): 727–744. DOI: 10.1007/s00382-007-0319-9.
31. Hamed KH, Rao AR. 1998. A modified Mann-Kendall trend test for autocorrelated data. *Journal of Hydrology* **204**(1–4): 182–196. DOI: 10.1016/S0022-1694(97)00125-X.
32. Haylock MR, Peterson TC, Alves LM, Ambrizzi T, Anunciação YMT, Baez J, Barros VR, Berlato M a, Bidegain M, Coronel G, Corradi V, Garcia VJ, Grimm AM, Karoly D, Marengo J a, Marino MB, Moncunill DF, Nechet D, Quintana J, Rebello E, Rusticucci M, Santos JL, Trebejo I, Vincent L a. 2006. Trends in total and extreme South American rainfall in 1960–2000 and links with sea surface temperature. *Journal of Climate* **19**(8): 1490–1512. DOI: 10.1175/JCLI3695.1.
33. Hendon HH, Wheeler MC, Zhang C (Miami). 2007. Seasonal Dependence of the MJO – ENSO Relationship. *Journal of Climate* **20**(Lau 2005): 531–544. DOI: 10.1175/JCLI4003.1.
34. Hendon HH, Zhang C, Glick JD. 1999. Interannual variation of the Madden – Julian Oscillation during austral summer. *Journal of Climate* **12**: 2538–2550.
35. Hoell A, Barlow M, Wheeler MC, Funk C. 2014. Disruptions of El Niño-Southern Oscillation teleconnections by the Madden-Julian Oscillation. *Geophysical Research Letters* **41**(3): 998–1004. DOI: 10.1002/2013GL058648.
36. Hollander M, Wolfe DA. 1973. *Nonparametric statistical methods*. New York.
37. Huggel C, Scheel M, Albrecht F, Andres N, Calanca P, Jurt C, Khabarov N, Mira-Salama D, Rohrer M, Salzmann N, Silva Y, Silvestre E, Vicuña L, Zappa M. 2015. A framework for the science contribution in climate adaptation: Experiences from science-policy processes in the Andes. *Environmental Science & Policy* **47**: 80–94. DOI: 10.1016/j.envsci.2014.11.007.
38. Jones C, Carvalho L, Higgins W, Waliser D, Schemm JKE. 2004a. Climatology of tropical intraseasonal convective anomalies : 1979 – 2002. *Journal of Climate* **17**(3): 523–539.
39. Jones C, Carvalho LMV. 2014. Sensitivity to Madden–Julian Oscillation variations on heavy precipitation over the contiguous United States. *Atmospheric Research*. The Authors **147**–**148**: 10–26. DOI: 10.1016/j.atmosres.2014.05.002.
40. Jones C, Carvalho LM V. 2013. Climate Change in the South American Monsoon System: Present Climate and CMIP5 Projections. *Journal of Climate* **26**(17): 6660–6678. DOI: 10.1175/JCLI-D-12-00412.1.
41. Jones C, Carvalho LM V. 2002. Active and break phases in the South American monsoon system. *Journal of Climate* **15**(8): 905–914.
42. Jones C, Carvalho LM V. 2012. Spatial-intensity variations in extreme precipitation in the contiguous United States and the Madden-Julian Oscillation. *Journal of Climate* **25**(14): 4898–4913. DOI: 10.1175/JCLI-D-11-00278.1.
43. Jones C, Waliser DE, Lau KM, Stern W. 2004b. Global occurrences of extreme precipitation and the Madden-Julian Oscillation: Observations and predictability. *Journal of Climate* **17**(23): 4575–4589. DOI: 10.1175/3238.1.
44. Juliá C, Rahn DA, Rutllant JA. 2012. Assessing the influence of the MJO on strong precipitation events in subtropical, semi-arid north-central Chile (30°S). *Journal of Climate* **25**(20): 7003–7013. DOI: 10.1175/JCLI-D-11-00679.1.
45. Junker NW, Grumm RH, Hart R, Bosart LF, Bell KM, Pereira FJ. 2008. Use of normalized anomaly fields to anticipate extreme rainfall in the mountains of northern California. *Wea. Forecasting* **23**(Faber 2003): 336–356. DOI: 10.1175/2007WAF2007013.1.

46. Kendall MG. 1975. *Rank correlation methods*. Griffin & Co: London, UK.
47. Kessler WS. 2001. Representations of the Madden – Julian Oscillation and its connection with ENSO. *Journal of Climate* **14**(13): 3055–3061.
48. Lagos P, Silva Y, Nickl E, Mosquera K. 2008. El Niño - related precipitation variability in Peru. *Advances In Geosciences* **14**(3): 231–237.
49. Lavado W, Espinoza JC. 2014. Impactos de El Niño y La Niña en las lluvias del Perú (1965-2007). *Revista Brasileira de Meteorologia* **29**(2): 171–182. DOI: 10.1590/S0102-77862014000200003.
50. Lavado WS, Labat D, Ronchail J, Espinoza JC, Guyot JL. 2013. Trends in rainfall and temperature in the Peruvian Amazon-Andes basin over the last 40 years (1965-2007). *Hydrological Processes* **27**(20): 2944–2957. DOI: 10.1002/hyp.9418.
51. Lavado Casimiro WS, Ronchail J, Labat D, Espinoza JC, Guyot JL. 2012. Basin-scale analysis of rainfall and runoff in Peru (1969–2004): Pacific, Titicaca and Amazonas drainages. *Hydrological Sciences Journal* **57**(4): 625–642. DOI: 10.1080/02626667.2012.672985.
52. Liebmann B, Kiladis GN, Vera CS, Saulo AC, Carvalho LM V. 2004. Subseasonal variations of rainfall in South America in the vicinity of the low-level jet east of the Andes and comparison to those in the South Atlantic convergence zone. *Journal of Climate* **17**(19): 3829–3842.
53. Liebmann B, Mechoso CR. 2011. The South American Monsoon System. In: Chang C-P, Ding Y and Lau N-C (eds) *The Global Monsoon System: Research and Forecast*. World Scientific: Singapore, 137–157.
54. Madden RA, Julian PR. 1971. Detection of a 40-50 day oscillation in the zonal wind in the tropical Pacific. *Journal of the Atmospheric Sciences* **28**(5): 702–708.
55. Madden RA, Julian PR. 1972. Description of global-scale circulation cells in the Tropics with a 40–50 day period. *Journal of the Atmospheric Sciences*, 1109–1123.
56. Mann HB. 1945. Non-parametric tests against trend. *Econometrica* **13**: 245–259.
57. Mantua NJ, Hare SR. 2002. The Pacific Decadal Oscillation. *Journal of Oceanography* **58**: 35–44.
58. Marengo J a. 2004. Interdecadal variability and trends of rainfall across the Amazon basin. *Theoretical and Applied Climatology* **78**(1–3): 79–96. DOI: 10.1007/s00704-004-0045-8.
59. Marengo J a., Liebmann B, Grimm a. M, Misra V, Silva Dias PL, Cavalcanti IF a., Carvalho LM V., Berbery EH, Ambrizzi T, Vera CS, Saulo a. C, Nogues-Paegle J, Zipser E, Seth A, Alves LM. 2012. Recent developments on the South American monsoon system. *International Journal of Climatology* **32**(1): 1–21. DOI: 10.1002/joc.2254.
60. Marengo J a., Rusticucci M, Penalba O, Renom M. 2009. An intercomparison of observed and simulated extreme rainfall and temperature events during the last half of the twentieth century: Part 2: Historical trends. *Climatic Change* **98**(3): 509–529. DOI: 10.1007/s10584-009-9743-7.
61. Marengo JA, Tomasella J, Alves LM, Soares WR, Rodriguez DA. 2011. The drought of 2010 in the context of historical droughts in the Amazon region. *Geophysical Research Letters* **38**(12): 1–5. DOI: 10.1029/2011GL047436.
62. Matthews AJ, Pickup G, Peatman SC, Clews P, Martin J. 2013. The effect of the Madden-Julian Oscillation on station rainfall and river level in the Fly River system, Papua New Guinea. *Journal of Geophysical Research Atmospheres* **118**(19): 10926–10935. DOI: 10.1002/jgrd.50865.
63. McPhaden MJ. 2004. Evolution of the 2002/03 El Niño. *Bulletin of the American Meteorological Society* **85**(5): 677–695. DOI: 10.1175/BAMS-85-5-677.
64. McPhaden MJ. 2008. Evolution of the 2006 – 2007 El Niño: the role of intraseasonal

to interannual time scale dynamics. *Advances in Geosciences* **14**: 219–230.
65. MINAM (Ministerio del Ambiente). 2011. *Mapa de vulnerabilidad física del Perú. Herramienta para la gestión del riesgo.* Ministerio del Ambiente: Lima.
66. Minvielle M, Garreaud RD. 2011. Projecting Rainfall Changes over the South American Altiplano. *Journal of Climate* **24**(17): 4577–4583. DOI: 10.1175/JCLI-D-11-00051.1.
67. Mo K, Jones C, Nogués-Paegle J. 2012. Pan America. In: Lau K and Waliser D (eds) *Intraseasonal variability in the atmosphere–ocean climate system*. Springer-Verlag: Berlin, 613.
68. Moon JY, Wang B, Ha KJ. 2011. ENSO regulation of MJO teleconnection. *Climate Dynamics* **37**(5): 1133–1149. DOI: 10.1007/s00382-010-0902-3.
69. Morin E. 2011. To know what we cannot know: Global mapping of minimal detectable absolute trends in annual precipitation. *Water Resources Research* **47**(7): 1–9. DOI: 10.1029/2010WR009798.
70. Muza MN, Carvalho LM V, Jones C, Liebmann B. 2009. Intraseasonal and interannual variability of extreme dry and wet events over southeastern South America and the subtropical Atlantic during austral summer. *Journal of Climate* **22**(7): 1682–1699. DOI: 10.1175/2008JCLI2257.1.
71. Neukom R, Rohrer M, Calanca P, Salzmann N, Huggel C, Acuña D, Christie DA, Morales MS. 2015. Facing unprecedented drying of the Central Andes? Precipitation variability over the period AD 1000–2100. *Environ. Res. Lett. Environ. Res. Lett*. IOP Publishing **10**(10): 84017–84017. DOI: 10.1088/1748-9326/10/8/084017.
72. Newman M, Alexander MA, Ault TR, Cobb KM, Deser C, Di Lorenzo E, Mantua NJ, Miller AJ, Minobe S, Nakamura H, Schneider N, Vimont DJ, Phillips AS, Scott JD, Smith CA. 2016. The Pacific decadal oscillation, revisited. *Journal of Climate* **29**(12): 4399–4427. DOI: 10.1175/JCLI-D-15-0508.1.
73. Nicholls N, Murray W. 1999. Workshop on Indices and Indicators for Climate Extremes, Breakout Group B: Precipitation. *Climatic Change*, 23–29. DOI: 10.1023/A:1005495627778.
74. Nogués-Paegle J, Byerle LA, Mo KC. 2000. Intraseasonal modulation of South American summer precipitation. *Monthly Weather Review* **128**: 837–850.
75. North GR, Bell TL, Cahalan RF, Moeng FJ. 1982. Sampling errors in the estimation of empirical orthogonal functions.pdf. *Monthly Weather Review* **110**(7): 699–706.
76. Pai DS, Bhate J, Sreejith OP, Hatwar HR. 2011. Impact of MJO on the intraseasonal variation of summer monsoon rainfall over India. *Climate Dynamics* **36**(1–2): 41–55. DOI: 10.1007/s00382-009-0634-4.
77. Perry LB, Seimon A, Kelly GM. 2014. Precipitation delivery in the tropical high Andes of southern Peru: New findings and paleoclimatic implications. *International Journal of Climatology* **34**(1): 197–215. DOI: 10.1002/joc.3679.
78. Pohl B, Matthews AJ. 2007. Observed changes in the lifetime and amplitude of the Madden-Julian oscillation associated with interannual ENSO sea surface temperature anomalies. *Journal of Climate* **20**(11): 2659–2674. DOI: 10.1175/JCLI4230.1.
79. Pohl B, Richard Y, Fauchereau N. 2007. Influence of the Madden–Julian Oscillation on southern African summer rainfall. *Journal of Climate* **20**(16): 4227–4242. DOI: 10.1175/JCLI4231.1.
80. Rau P, Bourrel L, Labat D, Melo P, Dewitte B, Frappart F. 2016. Regionalization of rainfall over the Peruvian Pacific slope and coast. . DOI: 10.1002/joc.4693.
81. Romatschke U, Houze R a. 2010. Extreme summer convection in South America. *Journal of Climate* **23**(14): 3761–3791. DOI: 10.1175/2010JCLI3465.1.
82. Romatschke U, Houze R a. 2013. Characteristics of precipitating convective systems accounting for the summer rainfall of tropical and subtropical South America.

Journal of Hydrometeorology **14**(1): 25–46. DOI: 10.1175/JHM-D-12-060.1.
83. Roundy PE, MacRitchie K, Asuma J, Melino T. 2010. Modulation of the global atmospheric circulation by combined activity in the Madden-Julian oscillation and the El Nino-southern oscillation during boreal winter. *Journal of Climate* **23**(15): 4045–4059. DOI: 10.1175/2010JCLI3446.1.
84. Rousseeuw PJ. 1987. Silhouettes: A graphical aid to the interpretation and validation of cluster analysis. *Journal of Computational and Applied Mathematics* **20**: 53–65. DOI: 10.1016/0377-0427(87)90125-7.
85. Saha S, Moorthi S, Pan H-L, Wu X, Wang J, Nadiga S, Tripp P, Kistler R, Woollen J, Behringer D, Liu H, Stokes D, Grumbine R, Gayno G, Wang J, Hou Y-T, Chuang H-Y, Juang H-MH, Sela J, Iredell M, Treadon R, Kleist D, Van Delst P, Keyser D, Derber J, Ek M, Meng J, Wei H, Yang R, Lord S, Van Den Dool H, Kumar A, Wang W, Long C, Chelliah M, Xue Y, Huang B, Schemm J-K, Ebisuzaki W, Lin R, Xie P, Chen M, Zhou S, Higgins W, Zou C-Z, Liu Q, Chen Y, Han Y, Cucurull L, Reynolds RW, Rutledge G, Goldberg M. 2010. The NCEP Climate Forecast System Reanalysis. *Bulletin of the American Meteorological Society* **91**(8): 1015–1057. DOI: 10.1175/2010BAMS3001.1.
86. Segura H, Espinoza JC, Junquas C, Takahashi K. 2016. Evidencing decadal and interdecadal hydroclimatic variability over the Central Andes. *Environmental Research Letters*. IOP Publishing **11**(9): 94016. DOI: 10.1088/1748-9326/11/9/094016.
87. Seiki A, Takayabu Y. 2007. Westerly wind bursts and their relationship with intraseasonal variations and ENSO. Part I : Statistics. *American Meteorological Society* **135**: 3325–3345. DOI: 10.1175/MWR3477.1.
88. Seiler C, Hutjes RW a, Kabat P. 2013. Climate variability and trends in Bolivia. *Journal of Applied Meteorology and Climatology* **52**(1): 130–146. DOI: 10.1175/JAMC-D-12-0105.1.
89. Sen PK. 1968. Estimates of the regression coefficient based on Kendall's tau. *Journal of the American Statistical Association* **63**(324): 1379–1389. DOI: 10.2307/2285891.
90. Skansi MDLM, Brunet M, Sigró J, Aguilar E, Arevalo Groening JA, Bentancur OJ, Castellón Geier YR, Correa Amaya RL, Jácome H, Malheiros Ramos A, Oria Rojas C, Pasten AM, Sallons Mitro S, Villaroel Jiménez C, Martínez R, Alexander L V., Jones PD. 2013. Warming and wetting signals emerging from analysis of changes in climate extreme indices over South America. *Global and Planetary Change*. Elsevier B.V. **100**: 295–307. DOI: 10.1016/j.gloplacha.2012.11.004.
91. Slingo JM, Rowell DP, Sperber K., Nortley F. 1999. On the predictability of the interannual behaviour of the Madden-Julian Oscillation and its relationship with El Niiio. *Quarterly Journal of the Royal Meteorological Society* **125**: 583–609.
92. Takahashi K, Montecinos A, Goubanova K, Dewitte B. 2011. ENSO regimes: Reinterpreting the canonical and Modoki El Nio. *Geophysical Research Letters* **38**(10): 1–5. DOI: 10.1029/2011GL047364.
93. Tomaziello ACN, Carvalho LM V., Gandu AW. 2015. Intraseasonal variability of the Atlantic Intertropical Convergence Zone during austral summer and winter. *Climate Dynamics*. Springer Berlin Heidelberg. DOI: 10.1007/s00382-015-2929-y.
94. Valadão CEA, Carvalho LM V., Lucio PS, Chaves RR. 2016. Impacts of the Madden-Julian oscillation on intraseasonal precipitation over Northeast Brazil. *International Journal of Climatology*. DOI: 10.1002/joc.4818.
95. Valadão CEA, Lucio PS, Chaves RR, Carvalho LM V, Valadão CEA. 2015. MJO modulation of station rainfall in the semiarid Seridó, northeast Brazil. *Atmospheric and Climate Sciences* **5**(5): 408–417. DOI: 10.4236/acs.2015.54032.
96. Vera C, Higgins W, Amador J, Ambrizzi T, Garreaud R, Gochis D, Zhang C. 2006.

Towards a unified view of the American Monsoon System. *Journal of Climate* **19**(4977): 5000.
97. Vuille M. 1999. Atmospheric circulation over the Bolivian Altiplano during dry and wet periods and extreme phases of the Southern Oscillation. *International Journal of Climatology* **19**(14): 1579–1600.
98. Vuille M, Bradley R, Keimig F. 2000. Interannual climate variability in the Central Andes and its relation to tropical Pacific and Atlantic forcing. *Journal of Geophysical research* **105**(12): 447–460. DOI: 10.1029/2000JD900134.
99. Vuille M, Bradley R, Werner M, Keimig F. 2003. 20th century climate change in the tropical Andes: observations and model results. *Climate Variability and Change …* **59**(1): 75–99. DOI: 10.1023/a:1024406427519.
100. Vuille M, Keimig F. 2004. Interannual variability of summertime convective cloudiness and precipitation in the central Andes derived from ISCCP-B3 data. *Journal of Climate* **17**(17): 3334–3348.
101. Wang XL. 2008a. Penalized maximal F test for detecting undocumented mean shift without trend change. *Journal of Atmospheric and Oceanic Technology* **25**(3): 368–384. DOI: 10.1175/2007JTECHA982.1.
102. Wang XL. 2008b. Accounting for autocorrelation in detecting mean shifts in climate data series using the penalized maximal t or F test. *Journal of Applied Meteorology and Climatology* **47**(9): 2423–2444. DOI: 10.1175/2008JAMC1741.1.
103. Wang XL, Wen QH, Wu Y. 2007. Penalized maximal T test for detecting undocumented mean change in climate data series. *Journal of Applied Meteorology and Climatology* **46**(6): 916–931. DOI: 10.1175/JAM2504.1.
104. Wheeler MC, Hendon HH. 2004. An all-season real-time multivariate MJO index: Development of an index for monitoring and prediction. *Monthly Weather Review* **132**(8): 1917–1932. DOI: 10.1175/1520-0493(2004)132<1917:AARMMI>2.0.CO;2.
105. Wheeler MC, Hendon HH, Cleland S, Meinke H, Donald A. 2009. Impacts of the Madden-Julian Oscillation on Australian rainfall and circulation. *Journal of Climate* **22**(6): 1482–1498. DOI: 10.1175/2008JCLI2595.1.
106. Wilks DS. 2011. *Statistical methods in the atmospheric sciences*. Academic press.
107. Yoon JH, Zeng N. 2010. An Atlantic influence on Amazon rainfall. *Climate Dynamics* **34**(2): 249–264. DOI: 10.1007/s00382-009-0551-6.
108. Yue S, Wang C. 2004. The Mann-Kendall test modified by effective sample size to detect trend in serially correlated hydrological series. *Water Resources Management* **18**(3): 201–218. DOI: 10.1023/B:WARM.0000043140.61082.60.
109. Zavala-Garay J. 2005. The Linear Response of ENSO to the Madden – Julian Oscillation. *New York* (1996): 2441–2459.
110. Zhang C. 2005. Madden-Julian Oscillation. *Reviews of Geophysics*, 1–36. DOI: 10.1029/2004RG000158.
111. Zhang C. 2013. Madden–Julian Oscillation: Bridging weather and climate. *Bulletin of the American Meteorological Society* **94**(12): 1849–1870. DOI: 10.1175/BAMS-D-12-00026.1.
112. Zhang C, Gottschalck J. 2002. SST anomalies of ENSO and the Madden-Julian oscillation in the equatorial Pacific. *Journal of Climate* **15**(17): 2429–2445. DOI: 10.1175/1520-0442(2002)015<2429:SAOEAT>2.0.CO;2.
113. Zhang L, Wang B, Zeng Q. 2009. Impact of the Madden–Julian Oscillation on summer rainfall in southeast China. *Journal of Climate* **22**(2): 201–216. DOI: 10.1175/2008JCLI1959.1.
114. Zhang X, Alexander L, Hegerl GC, Jones P, Tank AK, Peterson TC, Trewin B, Zwiers FW. 2011. Indices for monitoring changes in extremes based on daily temperature and precipitation data. *Wiley Interdisciplinary Reviews: Climate Change*

2(6): 851–870. DOI: 10.1002/wcc.147.
115. Zhang Y, Wallace JM, Battisti DS. 1997. ENSO-like interdecadal variability: 1900-93. *Journal of Climate* **10**(5): 1004–1020. DOI: 10.1175/1520-0442(1997)010<1004:ELIV>2.0.CO;2.
116. Zilli MT, Carvalho LM V., Liebmann B, Silva Dias MA. 2016. A comprehensive analysis of trends in extreme precipitation over southeastern coast of Brazil. *International Journal of Climatology*. DOI: 10.1002/joc.4840.